Analysis of Evaporating Flows of a Gas from its Condensed Phase on the Basis of Kinetic Theory

Hiroshi Sugimoto

1991

Analysis of Evaporating Flows of a Gas from its Condensed Phase on the Basis of Kinetic Theory

Hiroshi Sugimoto

1991

CONTENTS

CHAPTER I

INTRODUCTION

Gas flows around a condensed phase, where evaporation or condensation is taking place, have been investigated by many authors on the basis of kinetic theory, and various interesting and important results of the flow have been presented.[1-28] The approach by kinetic theory is required, on one hand, by the fact that many important engineering problems that involve evaporation or condensation, such as isotope separation with laser[29], occur in a low density state and, on the other hand, in order to derive the fundamental law concerning evaporation and condensation in hydrodynamics, which is outside of the continuum mechanics.

One of the most important problems in the latter category is derivation of the boundary condition for the hydrodynamic equation on the interface between a vapor gas and its condensed phase. The problem has been studied by analyzing the asymptotic behavior of the small mean free path limit of the boundary-value problem of the kinetic equation for a general domain.[10,12,23,30,31] From the analysis, the hydrodynamic equation, which describes the over-all behavior of the gas, is derived and the problem determining the boundary condition for the hydrodynamic equation on the interface is reduced to the problem of evaporation or condensation on an infinite plane condensed phase. The solution of the half-space problem over the plane boundary gives not only the boundary condition for the hydrodynamic equation but also the local correction, called Knudsen layer correction, to the solution of the hydrodynamic equation.

Because of this importance besides its simplicity and intrinsic physical interest, the evaporation and condensation problem on a plane condensed phase has been extensively

studied.[1-6,9-22] For weak evaporation or condensation, the problem is clarified theoretically and numerically. The relation between the rate of evaporation or condensation, the parameters of the condensed phase and those of the gas at infinity is established, and the behavior of the gas in the nonequilibrium region from the condensed phase to the equilibrium state at infinity is obtained. The case of strong condensation is also clarified.[18,21] Owing to the combination of a Knudsen layer and a shock wave resulting from the nonlinearity of the problem, an interesting feature not found in the case of weak condensation is seen.

In the present study, we first study the strong evaporation from a plane condensed phase and clarify the relation between the evaporation rate, the parameters of the condensed phase and those of the gas at infinity together with the behavior of the gas in the transition region from the condensed phase to the equilibrium state at infinity (Chapter II). Thus, we establish the boundary condition for the hydrodynamic equation on the interface where strong evaporation is taking place. In order to avoid missing any possible stable solution in the nonlinear problem where no mathematical theorem is available, we analyze the problem by the time-dependent approach which is successfully applied to the study of strong condensation.[18,21] As the by-product of the time-dependent study, we find various important features of wave propagation in a rarefied gas, especially the propagation of discontinuity of the velocity distribution function of the molecules into a gas.

The plane condensed phase problem, where there is no geometric reference length, does not provide information about evaporating flows from a finite body, i.e., the effect of the gas rarefaction (Knudsen number effect) on the flows. Thus, in Chapter III, the problem of steady flows evaporating from its cylindrical condensed phase in an

infinite expanse of the gas is considered. We analyze the problem numerically for a wide range of gas rarefaction and strength of evaporation and obtain the flow field from the condensed phase to infinity as well as the relation among the mass and energy flow rates, the parameters of the condensed phase and those of the surrounding gas. Thus, we clarify the effect of the gas rarefaction on the evaporation flow from a finite body. In the analysis we point out the existence of discontinuity of the velocity distribution function of the molecules in a gas around a convex body and propose a general method of analyzing rarefied gas flow problems with this type of discontinuity.

CHAPTER II

STRONG EVAPORATION

FROM A PLANE CONDENSED PHASE[32-35]

I. INTRODUCTION

Consider a semi-infinite expanse of an initially uniform gas bounded by its plane condensed phase. Depending on the conditions of the gas and the condensed phase, condensation or evaporation will take place on the condensed phase; the disturbance induced by their interaction will propagate in the gas; and after a long time a steady condensation or evaporation flow will be established. In Refs. 18 and 21, the problem is considered on the basis of kinetic theory when condensation takes place, and the behavior of the gas is analyzed numerically by a finite difference method for a large number of initial situations, from which the transient behavior to a final steady state is classified and the steady behavior, especially the relation satisfied among the parameters at infinity and of the condensed phase in a condensation flow, is clarified.

In this chapter we consider the problem when evaporation takes place from the condensed phase and investigate the time development of the disturbance, especially the propagation and decay of the discontinuity of the velocity distribution function, and the steady behavior of the evaporation from a plane condensed phase. The relations among the variables at infinity and of the condensed phase in the steady evaporation serve as the boundary condition for the macroscopic gas dynamic equations on the interface of a gas and its condensed phase. Thus we also investigate the effect of different microscopic boundary conditions on the steady evaporation.

II. PROBLEM AND ASSUMPTION

Consider a semi-infinite expanse of a rarefied gas bounded by its plane condensed phase with a uniform and constant surface temperature T_w. Let the gas occupy $x_1 > 0$, where x_i is the Cartesian coordinate system. At time t=0, the gas is in a uniform equilibrium state with pressure p_∞, temperature T_∞, and velocity $u_{i\infty} = (u_\infty, 0, 0)$, which is not in equilibrium with the condensed phase. We investigate the time development of the disturbance produced by the interaction of the gas with the condensed phase on the basis of kinetic theory and clarify the behavior of the steady evaporation in the half space from the long time behavior of the transient solution.

We analyze the problem under the following assumptions:

(i) The behavior of the gas is described by the Boltzmann-Krook-Welander (BKW) equation[36,37].

(ii) In Sec. IV we consider the problem under the conventional boundary condition on the condensed phase. That is, the gas molecules leaving the condensed phase constitute the corresponding part of the Maxwellian distribution pertaining to the saturated gas at rest and with temperature of the condensed phase. In Sec. V we discuss the effect of different boundary conditions at the condensed phase on the steady solution. The explicit forms of the condition to be considered are given there.

III. BASIC EQUATION AND BOUNDARY CONDITION

The Boltzmann-Krook-Welander equation in the present one dimensional case is written in the following form:

$$\frac{\partial f}{\partial t} + \xi_1 \frac{\partial f}{\partial x_1} = A_{col}\rho(f_e - f), \qquad (2-1)$$

$$f_e = \frac{\rho}{(2\pi RT)^{3/2}} \exp\left(-\frac{(\xi_i - u_i)^2}{2RT}\right), \qquad (2-2)$$

$$\rho = \iiint f d\xi_1 d\xi_2 d\xi_3, \qquad (2-3a)$$

$$u_1 = \frac{1}{\rho} \iiint \xi_1 f d\xi_1 d\xi_2 d\xi_3, \qquad (2-3b)$$

$$T = \frac{1}{3R\rho} \iiint (\xi_i - u_i)^2 f d\xi_1 d\xi_2 d\xi_3, \qquad (2-3c)$$

$$p = R\rho T. \qquad (2-3d)$$

where $f(t, x_1, \xi_i)$ is the velocity distribution function, ξ_i is the molecular velocity, ρ is the density of the gas, $u_i = (u_1, 0, 0)$ is its velocity, T is its temperature, p is its pressure, R is the specific gas constant, A_{col} is a constant ($A_{col}\rho$ is the collision frequency of the gas molecules), and the domain of integration in Eq. (3) is the whole space of ξ_i.

The conventional boundary condition on the condensed phase is

$$f = \frac{\rho_w}{(2\pi RT_w)^{3/2}} \exp\left(-\frac{\xi_i^2}{2RT_w}\right), \qquad (\text{for } \xi_1 > 0, \text{at } x_1 = 0), \qquad (2-4a)$$

where ρ_w is given by p_w, the saturation gas pressure at temperature T_w, and T_w with

$$\rho_w = p_w (RT_w)^{-1}. \qquad (2-4b)$$

In the present study, however, the relation between p_w and T_w (Clausius-Clapeyron relation[38]) is never used, thus they can be chosen freely in the results. The boundary condition at infinity and the initial condition are

$$f = \frac{\rho_\infty}{(2\pi RT_\infty)^{3/2}} \exp\left(-\frac{(\xi_i - u_{i\infty})^2}{2RT_\infty}\right),$$

$$(\text{for } \xi_1 < 0, \text{at } x_1 \to \infty \text{ and for all } \xi_i, \text{at } t = 0), \qquad (2-5a)$$

where

$$\rho_\infty = p_\infty (RT_\infty)^{-1}. \qquad (2-5b)$$

According to Ref. 39, we can eliminate the two molecular velocity components, ξ_2 and ξ_3 from our system, Eqs. (1)–(5). That is, multiplying Eqs. (1), (4), and (5) by 1 and $\xi_2^2 + \xi_3^2$ and integrating the results over the whole ξ_2–ξ_3 space, we obtain the system for the reduced distribution functions g and h defined by

$$\Phi = \begin{bmatrix} g \\ h \end{bmatrix} = \frac{1}{\rho_w (2RT_w)^{1/2}} \iint_{-\infty}^{\infty} \begin{bmatrix} 2RT_w \\ \xi_2^2 + \xi_3^2 \end{bmatrix} f \, d\xi_2 d\xi_3. \qquad (2-6)$$

The equations derived from Eq. (1) are as follows:

$$\frac{\partial \Phi}{\partial \tilde{t}} + \zeta \frac{\partial \Phi}{\partial x} = \frac{2}{\sqrt{\pi}} \tilde{\rho} (\Phi_e - \Phi), \qquad (2-7)$$

$$\Phi_e(\tilde{t}, x, \zeta) = \Psi(\tilde{\rho}(\tilde{t}, x), \tilde{u}(\tilde{t}, x), \tilde{T}(\tilde{t}, x), \zeta), \qquad (2-8a)$$

$$\Psi(\tilde{\rho}, \tilde{u}, \tilde{T}, \zeta) = \frac{\tilde{\rho}}{\sqrt{\pi \tilde{T}}} \begin{bmatrix} 1 \\ \tilde{T} \end{bmatrix} \exp\left(-\frac{(\zeta - \tilde{u})^2}{\tilde{T}} \right), \qquad (2-8b)$$

$$\tilde{\rho} = \int_{-\infty}^{\infty} g \, d\zeta, \qquad (2-9a)$$

$$\tilde{u} = \frac{1}{\tilde{\rho}} \int_{-\infty}^{\infty} \zeta g \, d\zeta, \qquad (2-9b)$$

$$\tilde{T} = \frac{2}{3\tilde{\rho}} \left(\int_{-\infty}^{\infty} \zeta^2 g + h \, d\zeta - \tilde{\rho} \tilde{u}^2 \right), \qquad (2-9c)$$

$$\tilde{p} = \tilde{\rho} \tilde{T}. \qquad (2-9d)$$

The boundary and inital conditions derived from Eqs. (4) and (5) are as follows:

$$\Phi(\tilde{t}, x, \zeta) = \Psi(1, 0, 1, \zeta), \quad (\text{for } \zeta > 0, \text{at } x = 0), \tag{2-10}$$

$$\Phi(\tilde{t}, x, \zeta) = \Psi\left(\frac{p_\infty}{p_w}\frac{T_w}{T_\infty}, M_\infty\left(\frac{5}{3}RT_\infty\right)^{1/2}, \frac{T_\infty}{T_w}, \zeta\right),$$

$$(\text{for } \zeta < 0, \text{at } x \to \infty \text{ and for all } \zeta, \text{at } \tilde{t} = 0), \tag{2-11}$$

where

$$\left.\begin{aligned} x &= \ell_w^{-1} x_1, \\ \zeta &= (2RT_w)^{-1/2}\xi_1, \\ \tilde{t} &= t_w^{-1} t, \\ \tilde{\rho}(\tilde{t}, x) &= \rho_w^{-1}\rho(t_w\tilde{t}, \ell_w x), \\ \tilde{u}(\tilde{t}, x) &= (2RT_w)^{-1/2}u(t_w\tilde{t}, \ell_w x), \\ \tilde{T}(\tilde{t}, x) &= T_w^{-1}T(t_w\tilde{t}, \ell_w x), \end{aligned}\right\} \tag{2-12a}$$

$$\left.\begin{aligned} \ell_w &= \frac{(2RT_w)^{1/2}}{A_{col}\rho_w}\frac{2}{\sqrt{\pi}}, \\ t_w &= \frac{\ell_w}{(2RT_w)^{1/2}}. \end{aligned}\right\} \tag{2-12b}$$

The system arranged in the nondimensional variables contains three parameters $M_\infty[= u_\infty/(5RT_\infty/3)^{1/2}]$, p_∞/p_w, T_∞/T_w, for various sets of which we analyze the problem numerically.

IV. BEHAVIOR OF THE GAS

A. Transient behavior

For $\zeta > 0$, the velocity distribution function Φ is discontinuous at $(\tilde{t}, x) = (0, 0)$, i.e., $\lim_{\tilde{t}\to 0} \Phi(\tilde{t}, 0, \zeta) \neq \lim_{x\to 0} \Phi(0, x, \zeta)$, from the boundary and initial data, Eqs. (10), (11). This discontinuity propagates into the gas along each characteristic line $x = \zeta\tilde{t}$ of Eq. (7), depending on ζ, as time goes on. Therefore, Φ is discontinuous on the surface $x = \zeta\tilde{t}$ $(\zeta > 0)$ in the $(\tilde{t}, x, \zeta)$ space. On the other hand, Φ is continuous for $\zeta < 0$. The macroscopic variables, $\tilde{\rho}, \tilde{u}, \tilde{T}$, are continuous in the $(\tilde{t}, x)$ plane. The discontinuity in Φ is expected to decay rapidly with time (exponentially in $\tilde{t}$) owing to molecular collisions. Since the standard finite difference method can not describe this discontinuity accurately, we rewrite the system in the characteristic variables $(\tilde{t}, x-\zeta\tilde{t}, \zeta)$ and integrate this system until the discontinuities of g and h decay sufficiently. After that, we analyzed the original system by a finite difference method.[21]

The transient behavior for $M_\infty = 0$, $p_\infty/p_w = 1/4$, and $T_\infty/T_w = 1$ is shown in Figs. 1–3. Fig. 1 shows the development of the disturbance at initial stage, and Fig. 2 shows the separation process of the disturbance into a shock wave, a contact layer, and a Knudsen layer, accompanying the development of uniform regions between these wave or layers. Fig. 3 shows the decay of the discontinuity of the reduced velocity distribution function g, where the discontinuity is invisible at $t = 50t_w$.

Figs. 4 and 5 show the case with $M_\infty = 0.75$, $p_\infty/p_w = 1$, and $T_\infty/T_w = 1$. Since the gas is initially receding from the condensed phase, a rarefaction region develops near the condensed phase, from which an expansion wave, a contact layer, and a Knudsen layer are separated and uniform regions develop between the wave or layers.

The long time behavior of the case $M_\infty = 1.0924$, $p_\infty/p_w = 0.1850$, and $T_\infty/T_w =$

0.6152 in Figs. 6 and 7 is an example to demonstrate that a supersonic region in the gas, if any, moves away up to infinity. In the figures, $c = (5RT/3)^{1/2}$ is the local sound speed, and X^c is the point where $(u_1 - c)/(2RT_w)^{1/2}$ takes a given value and thus a function of $(u_1 - c)/(2RT_w)^{1/2}$ and t/t_w. In Fig. 6 the supersonic region is shifting toward infinity. In Fig. 7 the shifting velocity dX^c/dt of the point X^c of a given $(u_1 - c)/(2RT_w)^{1/2}$ versus $u_1 - c$ is plotted for various large t, where the curve $t \to \infty$ is estimated by extrapolating the approximate behavior $\beta t^{-\alpha}$ of d^2X^c/dt^2 around $t = 20000t_w$ up to $t = \infty$. The dX^c/dt approaches $u_1 - c$ in the supersonic region and 0 in the subsonic region. This suggests that an expansion wave in the classical gas dynamics is propagating toward the condensed phase relative to the gas motion. Since any supersonic X_c point moves away from the condensed phase with a speed larger than $u_1 - c$, the supersonic region finally disappears from the flow field to infinity.

B. Steady behavior

Making use of the preceding transient behavior, we construct a large number of steady solutions, from which the behavior of steady evaporation is clarified. That is, we pursue the time development until a uniform state ahead of the Knudsen layer develops enough and confirm that g and h there correspond to those of the Maxwellian; if necessary, we introduce the following cut and patch process several times: replace the contact layer etc. ahead of the nearly uniform region by a uniform state and pursue the time development. Since we are interested only in a steady solution, we don't have to follow the time development accurately, and the time consuming characteristic coordinate method is unnecessary. Instead, in order to avoid to miss any possible stable steady solution, we try various nonuniform initial conditions.

From a large number of steady solutions, we find that p_∞/p_w and T_∞/T_w are

determined by M_∞, where p_∞, T_∞, and M_∞ are the data at infinity in the steady solution (but not those of the initial data). They are tabulated in Table 1. No steady solution exists for $M_\infty > 1$. Three examples of the transition region or Knudsen layer ($M_\infty = 0.1$, 0.5001, and 0.9897) are shown in Fig. 8, where $\times$ denotes the value at $x_1 = 0$. For $M_\infty = 0.9897$ the transition region extends over about $100\ell_w$ or $40\ell_\infty$, where $\ell_\infty [= (p_w/p_\infty)(T_\infty/T_w)^{3/2}\ell_w]$ is the mean free path of the equilibrium state at rest with pressure p_∞ and temperature T_∞. In contrast to the case of condensation,[18,21] the thickness of the transition region depends much on M_∞.

When $M_\infty \simeq 1$, convergence to its steady state is very slow. In order to confirm the convergence, we examine the decay of the shifting velocity dX^M/dt of the point X^M with a given local Mach number $M[= u_1(5RT/3)^{-1/2}]$. If the slope of the curve $\log_{10}(dX^M/dt)(2RT_w)^{-1/2}$ versus $\log_{10} t/t_w$ is less than -1, the point X^M converges to a finite point from the condensed phase. Fig. 9 shows the curves for various M in a case, where the flow converges to the steady state with $M_\infty = 0.9897$. From the decay curve of dX^M/dt, we can also estimate the error of the steady profiles. This method is also applied in Ref. 21.

C. Asymptotic behavior

From about 70 examples of the numerical solution as shown in Sec. IV A, we induce that the long time behavior of our system (1)-(5) is classified in the following cases.

1 : Knudsen layer + contact layer + shock wave,

2 : Knudsen layer + contact layer + expansion wave R,

3 : Knudsen layer + expansion wave L + contact layer + shock wave,

4 : Knudsen layer + expansion wave L + contact layer + expansion wave R,

where each element is arranged in order of the position from the condensed phase. The shock wave and the expansion wave R are propagating away from the condensed phase relative to the gas motion. The expansion wave L is propagating toward the condensed phase relative to the gas motion, and its front is at sonic condition. The contact layer corresponds to the contact discontinuity in the classical gas dynamics.

After each element is separated enough from each other, the Knudsen layer, practically steady, corresponds to the steady solution in Sec. IV B, and the uniform regions on both sides of shock wave or expansion wave or contact layer are confirmed numerically to be related by the classical gas dynamic relation of shock wave or simple wave or contact discontinuity. This is reasonable from the asymptotic theory.[40] With the aid of these relations we can derive, by a simple calculation, which asymptotic behavior $\boxed{1}$, $\boxed{2}$, $\boxed{3}$, or $\boxed{4}$ occurs from a given initial condition. The map of the asymptotic behavior on the initial data $u_\infty - p_\infty$ plane for $T_\infty = T_w$ is given in Fig. 10, where the framed number except $\boxed{5}$ corresponds to the number of the preceding classification. In the region $\boxed{5}$ condensation takes place, which is discussed in detail in Refs. 18 and 21. As the shock or expansion (R) wave vanishes with the approach of the initial condition to the boundary of $\boxed{1}$ and $\boxed{2}$ or $\boxed{3}$ and $\boxed{4}$ regions, a weak pulse propagating with attenuation as Fig. 4(e) of Ref. 18 dominates in the microstructure.

V. EFFECT OF BOUNDARY CONDITION

So far we discussed the problem under the conventional boundary condition on the condensed phase, where the velocity distribution function of the molecules leaving the condensed phase is independent of the velocity distribution of the molecules incident on the condensed phase and its shape is the half of a stationary Maxwellian. Now we

investigate the effect of different boundary conditions at the condensed phase on the steady evaporation.

A. Effect of the condensation factor

First we consider the effect of the incident molecules. The generalized boundary condition suggested by Woetberg's experiment[20] on a solid surface is given as follows. The velocity distribution of the leaving molecules is given by the sum of two terms: α_c times of the distribution of the conventional boundary condition (Sec. IV) and $(1-\alpha_c)$ times of the diffuse reflection distribution, where $\alpha_c (0 < \alpha_c \leq 1)$ is a constant called condensation factor. That is, the distribution of the leaving molecules is given by replacing p_w in the conventional boundary condition (4) by the following $\widehat{p}_w$:

$$\widehat{p}_w = \alpha_c p_w - (1-\alpha_c)(2\pi R T_w)^{1/2} \int_{\xi_1<0} \xi_1 f(t,0,\xi_i) d\xi_1 d\xi_2 d\xi_3. \qquad (2-13)$$

Comparing the conventional condition (4) and the generalized condition, we find a simple relation between the steady solutions of the two types of the boundary condition. Let $f_\alpha(x_1, \xi_i, p_w^G, T_w^G)$ be the steady solution under the generalized boundary condition with $p_w = p_w^G$ and $T_w = T_w^G$, and let $f(x_1, \xi_i, p_w^C, T_w^C)$ be the steady solution under the conventional boundary condition (4) with $p_w = p_w^C$ and $T_w = T_w^C$, where p_∞, T_∞, and M_∞ are assumed to be common. Then the following relations hold between the two solutions:

$$f_\alpha(x_1, \xi_i, p_w^G, T_w^G) = f(x_1, \xi_i, p_w^C, T_w^C), \qquad (2-14a)$$

$$p_w^G = [1 + (1-\alpha_c) K(M_\infty)] \alpha_c^{-1} p_w^C, \qquad (2-14b)$$

$$T_w^G = T_w^C, \qquad (2-14c)$$

where

$$K(M_\infty) = (10\pi/3)^{1/2}(p_\infty/p_w^C)(T_\infty/T_w^C)^{-1/2}M_\infty - 1. \qquad (2-15)$$

The p_∞/p_w^C and T_∞/T_w^C, the pressure and temperature ratios for the conventional boundary condition, are the functions of M_∞ given in Table 1 with p_w and T_w replaced by p_w^C and T_w^C respectively. The $K(M_\infty)$ versus M_∞ is plotted in Fig. 11, and p_∞/p_w^G versus M_∞ for various α_c in Fig. 12.

B. Effect of the form of the distribution function of the molecules

Next we consider the effect of the shape of the velocity distribution of the leaving molecules on the steady evaporation. Let the velocity distribution of the molecules leaving the condensed phase be the corresponding part of the Maxwellian $\bar{f}$ with pressure $\bar{p}$, temperature $\bar{T}$, and velocity $(\bar{u}, 0, 0)$, and put

$$p_w^S = 2\int_{\xi_1>0} \xi_1^2 \bar{f} d\xi_1 d\xi_2 d\xi_3, \qquad (2-16a)$$

$$T_w^S = \frac{1}{3R}\int_{\xi_1>0} \xi_i^2 \bar{f} d\xi_1 d\xi_2 d\xi_3 \left(\int_{\xi_1>0} \bar{f} d\xi_1 d\xi_2 d\xi_3\right)^{-1}. \qquad (2-16b)$$

Taking $\bar{M}[= \bar{u}(5R\bar{T}/3)^{-1/2}]$ as the shape factor, we consider the cases $\bar{M} = -0.5$, 0.5, 1.0, and 1.5 [$\bar{M} = 0$ corresponds to the conventional boundary condition (4)]. For each $\bar{M}$, we look for the possible steady solutions as in Sec. IV B and find the relations among p_∞/p_w^S, T_∞/T_w^S and M_∞ that allow a steady solution. The p_∞/p_w^S and T_∞/T_w^S are the functions of M_∞ plotted in Figs. 13 and 14. When $\bar{M} < 1$, the steady solution exists for $M_\infty < 1$; when $\bar{M} > 1$, the steady solution exists for $M_\infty < M_L$, where $M_L = [(\bar{M}^2 + 3)/(5\bar{M}^2 - 1)]^{1/2}$ (the standing shock wave relation between upstream and downstream Mach numbers, $\bar{M}$ and M_L), besides an obvious isolated solution, Maxwellian with pressure $\bar{p}$, temperature $\bar{T}$, and gas velocity $(\bar{u}, 0, 0)$, for $p_\infty = \bar{p}$, $T_\infty = \bar{T}$, and $u_\infty = \bar{u}$ (thus $M_\infty > 1$). Finally, the distributions of the leaving molecules considered here are compared in Fig. 15.

CHAPTER III

STEADY FLOWS OF A GAS EVAPORATING FROM ITS CYLINDRICAL CONDENSED PHASE[41,42]

I. INTRODUCTION

In Chapter II, the steady transient process of flows evaporating from a plane condensed phase to a uniform state at infinity was extensively studied as the limiting solution of a time-dependent problem. The problem contains three parameters: the pressure ratio (the pressure at infinity divided by the saturation pressure at the temperature of the condensed phase), the temperature ratio (the temperature at infinity divided by the temperature of the condensed phase), and the Mach number at infinity. In the steady flow these parameters are not independent and only one of them can be chosen. As the pressure ratio is decreased, the Mach number increases, but the flow with the pressure ratio less than a certain constant (0.2075 for the Boltzmann-Krook-Welander equation[36,37] and the conventional boundary condition) is not realized. The flow is accelerated as going downstream from the condensed phase and reaches a uniform state, but it cannot be supersonic anywhere in the gas for any pressure ratio. It is important both theoretically and practically to study how these fundamental flow properties are different in evaporation flows from a condensed phase of a finite size and to clarify the effect of gas rarefaction (or Knudsen number), which has degenerated in the preceding one-dimensional problem of a semi-infinite domain. In this chapter we investigate a steady flow evaporating from a cylindrical condensed phase to a uniform state at infinity for a wide range of the pressure ratio and the Knudsen number and

clarify the flow field from the condensed phase to infinity as well as the relations among the mass flow rate, the energy flow rate, the pressure ratio, and the temperature ratio.

Another important point which we discuss in this chapter is a discontinuity of the velocity distribution function in the gas. In Sec. III C, we point out that there is a discontinuity of the velocity distribution function in a gas around a convex body (with or without evaporation or condensation) and discuss its behavior. Then we propose a scheme to analyze a gas flow problem with this discontinuity accurately and efficiently. For small Knudsen numbers the discontinuity is in a thin layer with thickness of the order of the mean free path squared over the radius of the curvature of the boundary. This is the S-layer at the bottom of the Knudsen layer, pointed out in Ref. 43.

In the two dimensional problem, approach to the uniform state at infinity is slow. Some technique is required for numerical computation of the problem. In Sec III B we discuss the analytical asymptotic solution far from the cylinder and, on the basis of this, present a method which is generally applicable to an infinite domain problem.

II. PROBLEM AND BASIC EQUATION

Consider a cylindrical condensed phase (radius L and surface temperature T_w) in an infinite expanse of its vapor gas at rest (pressure p_∞ and temperature T_∞). Let p_w be the saturation gas pressure at temperature T_w. If $p_\infty \neq p_w$, evaporation or condensation takes place on the condensed phase. In this chapter we investigate the steady evaporation flow induced around the cylinder for a wide range of the pressure ratio p_∞/p_w and the Knudsen number Kn_w (the mean free path at the stationary equilibrium state with pressure p_w and temperature T_w divided by the radius of the cylinder) under the following assumptions: (i) the behavior of the gas is described by the Boltzmann-Krook-Welander (BKW or BGK) equation[36,37]; (ii) the gas molecules leaving the condensed

phase constitute the corresponding part of the stationary Maxwellian distribution with pressure p_w and temperature T_w (the conventional boundary condition for evaporation-condensation). The extension of the results to more general boundary condition will be discussed in Sec. VI.

The Boltzmann-Krook-Welander equation for a steady flow is

$$\xi_i \frac{\partial f}{\partial x_i} = A_{col}\rho(f_e - f), \tag{3-1}$$

$$f_e = \frac{\rho}{(2\pi RT)^{3/2}} \exp\left(-\frac{(\xi_i - u_i)^2}{2RT}\right), \tag{3-2}$$

$$\rho = \iiint f d\xi_1 d\xi_2 d\xi_3, \tag{3-3a}$$

$$u_i = \frac{1}{\rho} \iiint \xi_i f d\xi_1 d\xi_2 d\xi_3, \tag{3-3b}$$

$$T = \frac{1}{3R\rho} \iiint (\xi_i - u_i)^2 f d\xi_1 d\xi_2 d\xi_3, \tag{3-3c}$$

$$p = R\rho T, \tag{3-3d}$$

where x_i is the Cartesian coordinate system with the x_3 axis on the axis of the cylinder; ξ_i is the molecular velocity; f is the velocity distribution function of the gas molecules; ρ is the density of the gas; u_i is the flow velocity; T is the gas temperature; p is the gas pressure; A_{col} is a constant; R is the specific gas constant (per unit mass); the integrations are carried out over the whole space of ξ_i. The $A_{col}\rho$ is the collision frequency of a gas molecule, which is independent of molecular velocity for the BKW equation.

The boundary condition on the condensed phase (at $r = L$, where $r = (x_1^2+x_2^2)^{1/2}$) is

$$f = \frac{\rho_w}{(2\pi RT_w)^{3/2}} \exp\left(-\frac{\xi_i^2}{2RT_w}\right), \qquad (\xi_1 x_1 + \xi_2 x_2 > 0), \tag{3-4a}$$

where

$$\rho_w = p_w / RT_w. \tag{3-4b}$$

The condition at infinity ($r \to \infty$) is

$$f = \frac{\rho_\infty}{(2\pi RT_\infty)^{3/2}} \exp\left(-\frac{\xi_i^2}{2RT_\infty}\right), \qquad (\xi_1 x_1 + \xi_2 x_2 < 0), \tag{3-5a}$$

where

$$\rho_\infty = p_\infty / RT_\infty. \tag{3-5b}$$

In view of the cylindrical symmetry and independence from x_3 of the problem, we introduce the following nondimensional variables:

$$x_1 = L\tilde{r}\cos\theta, \qquad x_2 = L\tilde{r}\sin\theta, \tag{3-6a}$$

$$\xi_1 = V_w \zeta \cos(\theta + \theta_\zeta), \qquad \xi_2 = V_w \zeta \sin(\theta + \theta_\zeta), \qquad \xi_3 = V_w \zeta_z, \tag{3-6b}$$

$$f = \frac{\rho_w}{2V_w{}^3} \tilde{f}(\tilde{r}, \zeta, \theta_\zeta, \zeta_z), \tag{3-6c}$$

$$\left.\begin{aligned} &\rho = \rho_w \tilde{\rho}(\tilde{r}), \qquad T = T_w \tilde{T}(\tilde{r}), \qquad p = p_w \tilde{p}(\tilde{r}), \\ &u_1 = V_w \tilde{u}(\tilde{r})\cos\theta, \qquad u_2 = V_w \tilde{u}(\tilde{r})\sin\theta, \qquad u_3 = 0, \end{aligned}\right\} \tag{3-6d}$$

where

$$V_w = (2RT_w)^{1/2}. \tag{3-6e}$$

The variables $(L\tilde{r}, \theta, x_3)$, where $\tilde{r} = r/L$, are cylindrical coordinates for the physical space, and the variables $(V_w\zeta, \theta_\zeta, V_w\zeta_z)$ are local cylindrical coordinates for the molecular velocity (Fig. 1). The gas flow has only the radial component u:

$$u = V_w \tilde{u}(\tilde{r}). \tag{3 - 6f}$$

The velocity distribution function $\tilde{f}$ is an even function of θ_ζ:

$$\tilde{f}(\tilde{r}, \zeta, \theta_\zeta, \zeta_z) = \tilde{f}(\tilde{r}, \zeta, -\theta_\zeta, \zeta_z), \tag{3 - 6g}$$

and therefore will be considered over the domain $(1 \le \tilde{r} < \infty,\ 0 \le \zeta < \infty,\ 0 \le \theta_\zeta \le \pi,\ -\infty < \zeta_z < \infty)$.

With these new variables, the BKW equation is reduced to

$$D\tilde{f} = \frac{2}{\sqrt{\pi} Kn_w} \tilde{\rho}(\tilde{f}_e - \tilde{f}), \tag{3 - 7}$$

where

$$D = \zeta \cos\theta_\zeta \frac{\partial}{\partial \tilde{r}} - \frac{\zeta \sin\theta_\zeta}{\tilde{r}} \frac{\partial}{\partial \theta_\zeta}, \tag{3 - 8a}$$

$$Kn_w = \frac{\ell_w}{L}, \qquad \ell_w = \frac{(8RT_w/\pi)^{1/2}}{A_{col}\rho_w}, \tag{3 - 8b}$$

$$\tilde{f}_e = \frac{2\tilde{\rho}}{(\pi\tilde{T})^{3/2}} \exp\left(-\frac{\zeta^2 + \tilde{u}^2 - 2\tilde{u}\zeta\cos\theta_\zeta + \zeta_z^2}{\tilde{T}}\right). \tag{3 - 8c}$$

The parameter ℓ_w is the mean free path at the equilibrium state at rest with pressure p_w and temperature T_w, and Kn_w is called Knudsen number at the state. The nondimensional macroscopic variables $\tilde{\rho}$, $\tilde{u}$, $\tilde{T}$, and $\tilde{p}$ are related to $\tilde{f}$ as

$$\tilde{\rho} = \iiint \zeta \tilde{f}\, d\zeta d\theta_\zeta d\zeta_z, \tag{3 - 9a}$$

$$\tilde{u} = \frac{1}{\tilde{\rho}} \iiint \zeta^2 \cos\theta_\zeta \tilde{f}\, d\zeta d\theta_\zeta d\zeta_z, \qquad (3-9b)$$

$$\tilde{T} = \frac{2}{3\tilde{\rho}} \left(\iiint \zeta(\zeta^2 + \zeta_z^2) \tilde{f}\, d\zeta d\theta_\zeta d\zeta_z - \tilde{\rho}\tilde{u}^2 \right), \qquad (3-9c)$$

$$\tilde{p} = \tilde{\rho}\tilde{T}. \qquad (3-9d)$$

The three fold integrations with respect to ζ, θ_ζ, and ζ_z in Eqs. (9a)–(9c) and the following are carried out over the domain ($0 \le \zeta < \infty$, $0 \le \theta_\zeta \le \pi$, $-\infty < \zeta_z < \infty$), unless otherwise stated.

The nondimensional form of the boundary conditions are , at $\tilde{r} = 1$,

$$\tilde{f} = \frac{2}{\pi^{3/2}} \exp\left(-(\zeta^2 + \zeta_z^2)\right), \quad (0 \le \theta_\zeta < \pi/2), \qquad (3-10)$$

and, at infinity,

$$\tilde{f} = \frac{2\tilde{\rho}_\infty}{(\pi\tilde{T}_\infty)^{3/2}} \exp\left(-\frac{\zeta^2 + \zeta_z^2}{\tilde{T}_\infty}\right), \quad (\pi/2 < \theta_\zeta \le \pi), \qquad (3-11)$$

where

$$\tilde{\rho}_\infty = \rho_\infty/\rho_w, \qquad \tilde{T}_\infty = T_\infty/T_w. \qquad (3-12)$$

We can eliminate the molecular velocity ζ_z from the boundary-value problem, Eqs. (7)–(11). That is, multiplying Eqs. (7), (10), and (11) by 1 or ζ_z^2 and integrating them over $-\infty < \zeta_z < \infty$, we obtain the system for the marginal velocity distribution functions g and h defined by

$$\begin{bmatrix} g \\ h \end{bmatrix} = \int_{-\infty}^{\infty} \begin{bmatrix} 1 \\ \zeta_z^2 \end{bmatrix} \tilde{f}\, d\zeta_z. \qquad (3-13)$$

The equations for g and h are

$$D\begin{bmatrix} g \\ h \end{bmatrix} = \frac{2}{\sqrt{\pi} Kn_w} \tilde{\rho} \left(\begin{bmatrix} g_e \\ h_e \end{bmatrix} - \begin{bmatrix} g \\ h \end{bmatrix} \right), \tag{3-14}$$

$$\begin{bmatrix} g_e \\ h_e \end{bmatrix} = \frac{\tilde{\rho}}{\pi} \begin{bmatrix} 2/\tilde{T} \\ 1 \end{bmatrix} \exp\left(-\frac{\zeta^2 + \tilde{u}^2 - 2\tilde{u}\zeta\cos\theta_\zeta}{\tilde{T}} \right). \tag{3-15}$$

The variables $\tilde{\rho}$, $\tilde{u}$, and $\tilde{T}$ are expressed by g and h as

$$\tilde{\rho} = \iint \zeta g \, d\zeta d\theta_\zeta, \tag{3-16a}$$

$$\tilde{u} = \frac{1}{\tilde{\rho}} \iint \zeta^2 \cos\theta_\zeta g \, d\zeta d\theta_\zeta, \tag{3-16b}$$

$$\tilde{T} = \frac{2}{3\tilde{\rho}} \left(\iint \zeta(\zeta^2 g + h) \, d\zeta d\theta_\zeta - \tilde{\rho}\tilde{u}^2 \right). \tag{3-16c}$$

The two fold integrations with respect to ζ and θ_ζ in Eqs. (16a)–(16c) and the following are carried out over the domain $(0 \le \zeta < \infty, 0 \le \theta_\zeta \le \pi)$, unless otherwise stated. The boundary conditions are, at $\tilde{r} = 1$,

$$\begin{bmatrix} g \\ h \end{bmatrix} = \frac{1}{\pi} \begin{bmatrix} 2 \\ 1 \end{bmatrix} \exp\left(-\zeta^2\right), \quad (0 \le \theta_\zeta < \pi/2), \tag{3-17}$$

and, as $\tilde{r} \to \infty$,

$$\begin{bmatrix} g \\ h \end{bmatrix} = \frac{\tilde{p}_\infty}{\pi \tilde{T}_\infty} \begin{bmatrix} 2/\tilde{T}_\infty \\ 1 \end{bmatrix} \exp\left(-\frac{\zeta^2}{\tilde{T}_\infty} \right), \quad (\pi/2 < \theta_\zeta \le \pi). \tag{3-18}$$

The boundary value problem, Eqs. (7)–(11) or Eqs. (14)–(18), contains the two parameters, the pressure ratio $\tilde{p}_\infty (= p_\infty / p_w)$ and the temperature ratio $\tilde{T}_\infty (= T_\infty / T_w)$, besides the Knudsen number Kn_w. The solution of the problem exists only when these

parameters satisfy a relation, i.e., $\tilde{T}_\infty = F_T(\tilde{p}_\infty,\ Kn_w)$. In this chapter we analyze the problem numerically by a finite difference method and obtain the accurate solution over the whole field, as well as the relations among $\tilde{p}_\infty$, $\tilde{T}_\infty$, Kn_w, and the rate of evaporation, for a wide range of $\tilde{p}_\infty$ and Kn_w.

From the equation obtained by integrating Eq. (7) multiplied by 1 or $\zeta^2 + \zeta_z^2$ over the whole space of $(\zeta,\ \theta_\zeta,\ \zeta_z)$, we obtain the following integrals of Eq. (7):

$$\tilde{\rho}\tilde{u}\tilde{r} = Q/(2\pi\rho_w V_w L), \tag{3-19}$$

$$\tilde{w}\tilde{r} = W/(2\pi p_w V_w L), \tag{3-20}$$

$$\tilde{w} = \iint \zeta^2(\zeta^2 g + h)\cos\theta_\zeta d\zeta d\theta_\zeta, \tag{3-21}$$

where Q and W are the mass flow rate and the energy flow rate from the cylinder (per its unit length and per unit time) respectively. The relations (19) and (20) are used in the accuracy test of computation (Sec. V D).

The saturation gas pressure p_w is a function of T_w given by the Clausius-Clapeyron relation[38]. In the following analysis, however, the relation between p_w and T_w is never used, and thus p_w and T_w can be chosen freely in the results.

III. METHOD OF ANALYSIS

A. Outline of numerical analysis

In the following numerical analysis of the boundary-value problem, Eqs. (14)–(18), by a finite difference method, we consider the problem over a finite domain ($1 \le \tilde{r} \le \tilde{r}_D$, $0 \le \zeta \le \zeta_D$, $0 \le \theta_\zeta \le \pi$), where $\tilde{r}_D$ and ζ_D are chosen properly depending on the situations. The process of reduction to the finite domain will be discussed in Sec. III B.

Let $(\tilde{r}^{(i)}, \zeta^{(j)}, \theta_\zeta^{(k)})$ be the lattice points in the domain, where $i = 0, 1, \ldots, I$ ($\tilde{r}^{(0)} = 1$, $\tilde{r}^{(I)} = \tilde{r}_D$), $j = 0, 1, \ldots, J$ ($\zeta^{(0)} = 0$, $\zeta^{(J)} = \zeta_D$), and $k = 0, 1, \ldots, \hat{K}, \ldots, K$ ($\theta_\zeta^{(0)} = 0$, $\theta_\zeta^{(\hat{K})} = \pi/2$, $\theta_\zeta^{(K)} = \pi$). For the convenience of analysis, the points $\tilde{r}^{(i)}$, $\zeta^{(j)}$, and $\theta_\zeta^{(k)}$ are taken as the values of smooth functions $\tilde{r}(s)$, $\zeta(s)$, and $\theta_\zeta(s)$ of a continuous variable s evaluated at integer points $s = i, j$, and k :

$$\tilde{r}^{(i)} = \tilde{r}(i), \qquad \zeta^{(j)} = \zeta(j), \qquad \theta_\zeta^{(k)} = \theta_\zeta(k). \tag{3-22}$$

The variables g, h, $\tilde{\rho}$, etc. at a lattice point are denoted by the superscripts corresponding to the lattice point:

$$g^{(i,j,k)} = g(\tilde{r}^{(i)}, \zeta^{(j)}, \theta_\zeta^{(k)}), \qquad \tilde{\rho}^{(i)} = \tilde{\rho}(\tilde{r}^{(i)}). \tag{3-23}$$

The notations Φ and Φ_e are introduced for simplicity:

$$\Phi = \begin{bmatrix} g \\ h \end{bmatrix}, \qquad \Phi_e = \begin{bmatrix} g_e \\ h_e \end{bmatrix}. \tag{3-24}$$

Then

$$\Phi^{(i,j,k)} = \begin{bmatrix} g^{(i,j,k)} \\ h^{(i,j,k)} \end{bmatrix}, \qquad {\Phi_e}^{(i,j,k)} = \begin{bmatrix} g_e^{(i,j,k)} \\ h_e^{(i,j,k)} \end{bmatrix}. \tag{3-25}$$

Note that ${\Phi_e}^{(i,j,k)}$ depends on $\tilde{r}^{(i)}$ only through $\tilde{\rho}^{(i)}$, $\tilde{u}^{(i)}$, and $\tilde{T}^{(i)}$ (see Eq. (15)).

We construct the discrete solution $\Phi^{(i,j,k)}$ of Eqs. (14)–(18) as the limit of the series $\Phi_{(n)}^{(i,j,k)} (n = 0, 1, 2, \ldots)$ obtained by the iteration process described below. Corresponding to Eq. (14), the following finite difference equation for $\Phi_{(n)}^{(i,j,k)}$ is adopted:

$$\zeta^{(j)} \cos\theta_\zeta^{(k)} \frac{\Delta_1^{(i,j,k)} \Phi_{(n)}}{(d\tilde{r}/di)} - \frac{\zeta^{(j)} \sin\theta_\zeta^{(k)}}{\tilde{r}^{(i)}} \frac{\Delta_2^{(i,j,k)} \Phi_{(n)}}{(d\theta_\zeta/dk)}$$

$$= \frac{2}{\sqrt{\pi} K n_w} \tilde{\rho}_{(n-1)}^{(i)} ({\Phi_e}_{(n-1)}^{(i,j,k)} - \Phi_{(n)}^{(i,j,k)}), \tag{3-26}$$

where

$$\Delta_1^{(i,j,k)}\Phi_{(n)} = \begin{cases} \frac{3}{2}\Phi_{(n)}^{(i,j,k)} - 2\Phi_{(n)}^{(i-1,j,k)} + \frac{1}{2}\Phi_{(n)}^{(i-2,j,k)}, & \\ \qquad (2 \le i \le I,\ 0 \le k \le \hat{K}-1), & (3-27\text{a}) \\ \Phi_{(n)}^{(1,j,k)} - \Phi_{(n)}^{(0,j,k)}, \qquad (0 \le k \le \hat{K}-1), & (3-27\text{b}) \\ -\frac{3}{2}\Phi_{(n)}^{(i,j,k)} + 2\Phi_{(n)}^{(i+1,j,k)} - \frac{1}{2}\Phi_{(n)}^{(i+2,j,k)}, & \\ \qquad (0 \le i \le I-1,\ \hat{K} \le k \le K), & (3-27\text{c}) \end{cases}$$

$$\Delta_2^{(i,j,k)}\Phi_{(n)} = -\frac{3}{2}\Phi_{(n)}^{(i,j,k)} + 2\Phi_{(n)}^{(i,j,k+1)} - \frac{1}{2}\Phi_{(n)}^{(i,j,k+2)}, \qquad (3-27\text{d})$$

$$(d\tilde{r}/di) = (d\tilde{r}/ds)_{s=i}, \qquad (d\theta_\zeta/dk) = (d\theta_\zeta/ds)_{s=k}, \qquad (3-27\text{e})$$

$$\Phi_{(n)}^{(i,j,K+1)} = \Phi_{(n)}^{(i,j,K-1)}, \qquad (3-27\text{f})$$

and $\Phi_{e_{(n-1)}}^{(i,j,k)}$ is defined by Eqs. (15) and (25) where $\tilde{\rho}_{(n-1)}^{(i)}$, $\tilde{u}_{(n-1)}^{(i)}$, and $\tilde{T}_{(n-1)}^{(i)}$ are substituted for $\tilde{\rho}^{(i)}$, $\tilde{u}^{(i)}$, and $\tilde{T}^{(i)}$ respectively. Equation (27f) corresponds to the symmetry relation with respect to θ_ζ around $\theta_\zeta = \pi$ (Eq. (6g)). The variable $\Phi_{(n)}^{(I+1,j,k)}$ outside the domain is specified as a part of boundary conditions (Sec. III B). The $\Phi_{(n)}^{(i,j,K+2)}$ does not appear since $\sin\theta_\zeta^{(K)} = 0$.

Corresponding to the boundary condition (17), we impose the condition:

$$\Phi_{(n)}^{(0,j,k)} = \frac{1}{\pi}\begin{bmatrix}2\\1\end{bmatrix}\exp(-(\zeta^{(j)})^2), \qquad (k = 0, 1, \ldots, \hat{K}-1), \qquad (3-28)$$

which is independent of k. As the condition at $\tilde{r} = \tilde{r}_D$, we assume

$$\Phi_{(n)}^{(I,j,k)} = \Psi_{a(n)}^{(j,k)}, \quad (k = \hat{K}, \ldots, K), \qquad (3-29\text{a})$$

$$\Phi^{(I+1,j,k)}_{(n)} = \Psi^{(j,k)}_{b(n)}, \quad (k = \hat{K}, \ldots, K). \tag{3-29b}$$

Two conditions are required since the second order difference scheme, Eq. (27c), is used in Eq. (26). The explicit forms of $\Psi^{(j,k)}_{a(n)}$ and $\Psi^{(j,k)}_{b(n)}$ and the reason of their choice are given in Sec. III B.

We construct the series $\Phi^{(i,j,k)}_{(n)}$ $(n = 0, 1, 2, \ldots)$ by the following process (see Fig. 2a). Let $\Phi^{(i,j,k)}_{(n-1)}$, thus $\tilde{\rho}^{(i)}_{(n-1)}$, $\tilde{u}^{(i)}_{(n-1)}$, and $\tilde{T}^{(i)}_{(n-1)}$, be known.

(i) For $\hat{K} \leq k \leq K$, starting from $\Phi^{(I-1,j,k)}_{(n)}$, compute $\Phi^{(i,j,k)}_{(n)}$ using Eqs. (26), (29a), and (29b) in descending order of i down to $\Phi^{(0,j,k)}_{(n)}$. The step $i = i+1$ to $i = i$ is as follows. Let $\Phi^{(i',j,k)}_{(n)}$ $(i' > i)$ be given. Starting from $\Phi^{(i,j,K)}_{(n)}$, compute $\Phi^{(i,j,k)}_{(n)}$ using Eqs. (26), (27c), and (27d) (and Eqs. (29a) and (29b) for $i = I-1, I-2$) in descending order of k down to $\Phi^{(i,j,\hat{K})}_{(n)}$. Carry out this step for every j.

(ii) For $0 \leq k \leq \hat{K} - 1$, starting from $\Phi^{(1,j,k)}_{(n)}$, compute $\Phi^{(i,j,k)}_{(n)}$ using Eqs. (26), (28) in ascending order of i up to $\Phi^{(I,j,k)}_{(n)}$. The step $i = i-1$ to $i = i$ is as follows. Let $\Phi^{(i',j,k)}_{(n)}$ $(i' < i)$ be given. Starting from $\Phi^{(i,j,\hat{K}-1)}_{(n)}$, compute $\Phi^{(i,j,k)}_{(n)}$ using Eqs. (26)–(27b) and (27d) (and Eq. (28) for $i = 1$ and 2) in descending order of k down to $\Phi^{(i,j,0)}_{(n)}$. Carry out this step for every j.

(iii) Applying the Simpson formula to Eqs. (16a)–(16c), compute $\tilde{\rho}^{(i)}_{(n)}$, $\tilde{u}^{(i)}_{(n)}$, and $\tilde{T}^{(i)}_{(n)}$ from $\Phi^{(i,j,k)}_{(n)}$.

(iv) Repeat the process of (i)–(iii) with shift of the subscript (n to $n+1$) until $\Phi^{(i,j,k)}_{(n)}$ converges. We take the limit as the solution $\Phi^{(i,j,k)}$.

The order of computation in the preceding process is consistent with the natural course of integration of Eq. (14) along its characteristics in the direction of molecular velocity.

B. Asymptotic behavior for large $\tilde{r}$ and the condition at $\tilde{r} = \tilde{r}_D$

We have limited the original infinite domain ($1 \leq \tilde{r} < \infty,\ 0 \leq \zeta < \infty,\ 0 \leq \theta_\zeta \leq \pi$) to the finite domain ($1 \leq \tilde{r} \leq \tilde{r}_D,\ 0 \leq \zeta \leq \zeta_D,\ 0 \leq \theta_\zeta \leq \pi$). It does not introduce any problem to limit the range of ζ. As is easily checked by computation, Φ decays very rapidly as $\zeta \to \infty$, and therefore the accurate computation of the problem can be carried out with a reasonable size of ζ_D.

The problem is not so simple for the case of the $\tilde{r}$ variable. Obviously from Eq. (19), $\tilde{u}(\tilde{r})$ decays very slowly ($\sim\ \tilde{r}^{-1}$) as $\tilde{r} \to \infty$. Because of the slow decay to the uniform state at infinity, a very large $\tilde{r}_D$ is required to obtain an accurate result by simple application of the boundary condition (18). We therefore introduce a method to make use of the asymptotic solution for large $\tilde{r}$.

Let the deviation $\delta\Phi(= \Phi(\tilde{r}, \zeta, \theta_\zeta) - \Phi(\infty, \zeta, \theta_\zeta))$ from the equilibrium state at infinity be $O(\tilde{r}^{-1})$ for large $\tilde{r}$. Then $\partial\delta\Phi/\partial\tilde{r} = \tilde{r}^{-1}O(\delta\Phi)$. That is, for $\tilde{r} > \tilde{r}_A$ the characteristic length scale of variation of $\delta\Phi$ is larger than $\tilde{r}_A$, and therefore the effective Knudsen number Kn_{eff} ($= \ell_\infty/L\tilde{r}_A = Kn_\infty/\tilde{r}_A$, where ℓ_∞ is the mean free path at infinity ($u = 0,\ p = p_\infty,\ T = T_\infty$)) is small for large $\tilde{r}_A$. Then we can make use of the asymptotic theory developed in Refs. 24, 30, 31, and 44. In $\tilde{r} > \tilde{r}_A$, the deviation $\delta\Phi$ is $O(\tilde{r}_A^{-1})$, and therefore $\delta\Phi = O(Kn_{eff})$. This is the case to which the weakly nonlinear theory in Refs. 24, 31, and 44 applies. The asymptotic solution Φ_a of the diverging radial flow, accurate up to the 2nd order of Kn_{eff} or $\delta\Phi$, is expressed as follows:

$$\Phi_a = \frac{\tilde{p}_a}{\pi\tilde{T}_a}\begin{bmatrix} 2/\tilde{T}_a \\ 1 \end{bmatrix} \exp\left(-\frac{\zeta^2 + \tilde{u}_a^2 - 2\tilde{u}_a\zeta\cos\theta_\zeta - \chi\zeta^2\cos 2\theta_\zeta}{\tilde{T}_a}\right), \qquad (3-30)$$

$$\tilde{u}_a = \frac{\tilde{Q}}{\tilde{\rho}_a\tilde{r}}, \quad \tilde{p}_a = \tilde{p}_\infty(1 - \frac{X^2}{\tilde{r}^2}), \quad \tilde{T}_a = \tilde{T}_\infty(1 - \frac{Y}{\tilde{r}^2}), \quad \tilde{\rho}_a = \frac{\tilde{p}_a}{\tilde{T}_a}, \qquad (3-31a)$$

$$Y = \frac{2(2k+X)X^2}{5(k+X)}, \qquad \chi = \frac{2kX}{\tilde{r}^2}, \qquad (3-31b)$$

$$k = \frac{\sqrt{\pi}}{2}\frac{\tilde{T}_\infty^{3/2}}{\tilde{p}_\infty} Kn_w = \frac{\sqrt{\pi}}{2} Kn_\infty, \qquad \tilde{Q} = \frac{Q}{2\pi\rho_w V_w L}, \tag{3-31c}$$

where Q (the mass flow rate) and X are undetermined constants, which enter in Eqs. (30) and (31a) since the condition of the upstream is not imposed. In these equations some higher-order terms of Kn_{eff} such as $(k/\tilde{r})^3$ are included so that Eq. (30) can be arranged in an exponential form.

If $\tilde{r}_D$ is taken larger than $\tilde{r}_A$, Eq. (30) can be used to evaluate Φ at $\tilde{r} = \tilde{r}^{(I)}$ and $\tilde{r}^{(I+1)}$. † That is, let $\tilde{p}_\infty$ be fixed and let $\tilde{T}_\infty$ be left free in Eqs. (31a)–(31c). We connect $\tilde{u}_a$, $\tilde{p}_a$, and $\tilde{T}_a$ in Eq. (31a), respectively, with $\tilde{u}_{(n)}^{(I)}$, $\tilde{p}_{(n)}^{(I)} (= \tilde{\rho}_{(n)}^{(I)} \tilde{T}_{(n)}^{(I)})$, and $\tilde{T}_{(n)}^{(I)}$, determined by the step (iii) in Sec. III A, at $\tilde{r} = \tilde{r}_D$ by adjusting the three free parameters $\tilde{T}_\infty$, $\tilde{Q}$, and X. Let the asymptotic solution Φ_a thus connected be $\Phi_{a(n)}$. Then we take $\Phi_{a(n)}$ at $(\tilde{r}^{(I)}, \zeta^{(j)}, \theta_\zeta^{(k)})$ and at $(\tilde{r}^{(I+1)}, \zeta^{(j)}, \theta_\zeta^{(k)})$ as $\Psi_{a(n+1)}^{(j,k)}$ (Eq. (29a)) and $\Psi_{b(n+1)}^{(j,k)}$ (Eq. (29b)), respectively. Thus the boundary condition (29a) and (29b) for the finite difference system is completed (see Fig. 2a). Incidentally, it may be noted that $\tilde{T}_\infty$ finally obtained depends on $\tilde{p}_\infty$ and Kn_w.

Two practical points to improve the accuracy of numerical computation are added here. For a rather wide range of $\tilde{r}$ (say $\tilde{r}_d < \tilde{r} < \tilde{r}_D$), the difference between the solution Φ and the asymptotic solution Φ_a is fairly small. We, therefore, take the difference:

$$\Phi' = \Phi - \Phi_a, \tag{3-32}$$

and analyze the equation for Φ':

$$D\Phi' = \frac{2}{\sqrt{\pi} Kn_w}\tilde{\rho}(-\Phi' + \Phi_e - \Phi_a) - D\Phi_a, \tag{3-33}$$

† Let the lattice points on $\tilde{r}$ be extended to $\tilde{r}^{(I+1)}$.

numerically in the range $\tilde{r}_d < \tilde{r} < \tilde{r}_D$ instead of Eq. (14). By this approach, we can avoid the error introduced to form the more slowly decaying dominant part Φ_a by the direct analysis of Eq. (14). † In fact, the accuracy of conservation relations (19) and (20) are considerably improved in our numerical test. Another point is also related to errors in numerical integration. For rather large $\tilde{r}$, the solution Φ is not far from the equilibrium distribution Φ_e. Then for the step (iii) in Sec. III A, we put

$$\Phi_{(n)} = (\Phi_{(n)} - \Phi_{e(n-1)}) + \Phi_{e(n-1)}, \qquad (3-34)$$

and compute the integral (16a)–(16c). The contribution of the last term, which is the dominant part for large $\tilde{r}$, can be computed rigorously and is expressed by $\tilde{\rho}_{(n-1)}$, $\tilde{u}_{(n-1)}$, and $\tilde{T}_{(n-1)}$. Thus the error of integration is considerably reduced.

C. Discontinuity of the velocity distribution function and an appropriate difference scheme

Discontinuity of the velocity distribution function in a gas is one of the typical features of the behavior of the gas around a convex body. On a boundary the velocity distribution of the molecules incident on the boundary is determined by the behavior of the surrounding gas, but that of the molecules leaving the boundary is determined by the condition of the boundary. Their nature is different, and the velocity distribution function of the molecules has discontinuity at the molecular velocities whose normal components to the boundary vanish. This discontinuity propagates into the gas in the

† The effect of this method is easily examined by a simple equation $dy/dx + 3y/x = 2/x^2$ (*). The accurate asymptotic behavior of y for $x \gg 1$ is obtained more efficiently by the equation for $\bar{y}(= y - 1/x)$, $d\bar{y}/dx + 3\bar{y}/x = 0$, than by Eq. (*) (e.g., solve Eq. (*) for $x \geq 10$ under $y(10) = 1$).

direction of the velocity at this discontinuity, which is the characteristic of Eq. (1), when the boundary is convex. Such discontinuity does not exist in a gas over a concave boundary since the corresponding characteristic does not enter into the gas.

The discontinuity decays with distance from the boundary owing to molecular collision and is appreciable only over the distance of the order of the mean free path ℓ along the characteristic. When the Knudsen number ℓ/L_r, where L_r is the radius of the curvature of the boundary and thus $L_r = L$ in our cylinder problem, is of the order of unity or larger, the discontinuity extends to the region of the order of ℓ from the boundary (Fig. 3a). When the Knudsen number ℓ/L_r is small, the discontinuity decays in a short distance compared with L_r (Fig. 3b), where the line of discontinuity is still nearly parallel to the boundary and its distance δ from the boundary is of the order of ℓ^2/L_r since $(L_r + \delta)^2 = L_r^2 + O(\ell^2)$ and $\ell/L_r \ll 1$. Therefore, the discontinuity is confined in a thin layer with thickness of the order of ℓ^2/L_r adjacent to the boundary. This thin layer corresponds to the S-layer[43] at the bottom of the Knudsen layer with thickness of the order of ℓ. Thus, the correction to the Knudsen layer is required over a convex boundary (see Ref. 45 for details). It may be worth repeating that there is a decisive difference between the velocity distribution function over a convex boundary and that over a concave boundary.

The difference scheme, Eqs. (26)–(27d), is not appropriate to describe the discontinuity of Φ around the cylinder because the difference formulae (27a)–(27d) for $\partial\Phi/\partial\tilde{r}$ and $\partial\Phi/\partial\theta_\zeta$ contain the values at the lattice points on both sides of the discontinuity. It may be a natural way to integrate Eq. (14) along the characteristics until the discontinuity vanishes practically and to use the standard scheme, (26)–(27d), as was done in Chapter II for a time-dependent problem. The method, however, is time-consuming.

Fortunately, since the discontinuity is only on a single characteristic, $\tilde{r}\sin\theta_\zeta = 1$, fixed in $(\tilde{r}, \theta_\zeta, \zeta)$ space in the present problem, we can introduce a more effective method, similar to that used in Ref. 46 for a time-dependent problem over a plane wall, to describe the discontinuity accurately.

In our problem the discontinuity is only on the characteristic of leaving molecules tangent to the cylinder, i.e., $\tilde{r}\sin\theta_\zeta = 1$ $(0 \leq \theta_\zeta \leq \pi/2)$, which extends from $\tilde{r} = 1$, $\theta_\zeta = \pi/2$ to $\tilde{r} \to \infty$, $\theta_\zeta = 0$. No correction, therefore, is required for the formulae for $\pi/2 \leq \theta_\zeta \leq \pi$ or $k = \hat{K}$ to K. For $0 \leq \theta_\zeta < \pi/2$ or $k = 0$ to $\hat{K} - 1$, we introduce the following corrections to the difference formulae for $\partial\Phi/\partial\tilde{r}$ and $\partial\Phi/\partial\theta_\zeta$ at some neighboring points (i, j, k) of the discontinuity (Fig. 4):

(i.a) Let the characteristic pass the line $\theta_\zeta = \theta_\zeta^{(k)}$ between $\tilde{r} = \tilde{r}^{(i-2)}$ and $\tilde{r} = \tilde{r}^{(i-1)}$. Then replace $\Delta_1^{(i,j,k)}\Phi_{(n)}$ in Eq. (27a) by

$$\Delta_1^{(i,j,k)}\Phi_{(n)} = A_1\Phi_{(n)}^{(i,j,k)} - A_2\Phi_{(n)}^{(i-1,j,k)} + A_3\Phi_{+(n)}^{(j,k)}, \qquad (3-35)$$

where

$$\Phi_{+(n)}^{(j,k)} = \Phi_{(n)}(1/\sin\theta_\zeta^{(k)} + 0, \zeta^{(j)}, \theta_\zeta^{(k)}), \qquad (3-36)$$

and A_1, A_2, and A_3 are chosen in such a way that the present $\Delta_1^{(i,j,k)}\Phi/(d\tilde{r}/di)$ is a difference expression of the 2nd order accuracy for $\partial\Phi/\partial\tilde{r}$ at $(\tilde{r}^{(i)}, \zeta^{(j)}, \theta_\zeta^{(k)})$.

(i.b) Let the characteristic pass the line $\theta_\zeta = \theta_\zeta^{(k)}$ between $\tilde{r} = \tilde{r}^{(i-1)}$ and $\tilde{r} = \tilde{r}^{(i)}$. Then replace $\Delta_1^{(i,j,k)}\Phi_{(n)}$ in Eq. (27a) and (27b) by

$$\Delta_1^{(i,j,k)}\Phi_{(n)} = A_4(\Phi_{(n)}^{(i,j,k)} - \Phi_{+(n)}^{(j,k)}), \qquad (3-37)$$

where A_4 is chosen in such a way that this $\Delta_1^{(i,j,k)}\Phi/(d\tilde{r}/di)$ is a difference expression of the 1st order accuracy for $\partial\Phi/\partial\tilde{r}$ at $(\tilde{r}^{(i)}, \zeta^{(j)}, \theta_\zeta^{(k)})$.

(ii.a) Let the characteristic pass $\tilde{r} = \tilde{r}^{(i)}$ between $\theta_\zeta = \theta_\zeta^{(k+2)}$ and $\theta_\zeta = \theta_\zeta^{(k+1)}$. Then replace $\Delta_2^{(i,j,k)}\Phi_{(n)}$ in Eq. (27d) by

$$\Delta_2^{(i,j,k)}\Phi_{(n)} = B_1\Phi_{(n)}^{(i,j,k)} - B_2\Phi_{(n)}^{(i,j,k+1)} + B_3\Phi_{-(n)}^{(i,j)}, \qquad (3-38)$$

where

$$\Phi_{-(n)}^{(i,j)} = \Phi_{(n)}(\tilde{r}^{(i)}, \zeta^{(j)}, \sin^{-1}(1/\tilde{r}^{(i)}) - 0), \qquad (3-39)$$

and B_1, B_2, and B_3 are chosen in such a way that $\Delta_2^{(i,j,k)}\Phi/(d\theta_\zeta/dk)$ is a difference expression of the 2nd order accuracy for $\partial\Phi/\partial\theta_\zeta$ at $(\tilde{r}^{(i)}, \zeta^{(j)}, \theta_\zeta^{(k)})$.

(ii.b) Let the characteristic pass $\tilde{r} = \tilde{r}^{(i)}$ between $\theta_\zeta = \theta_\zeta^{(k+1)}$ and $\theta_\zeta = \theta_\zeta^{(k)}$. Then replace $\Delta_2^{(i,j,k)}\Phi_{(n)}$ in Eq. (27d) by

$$\Delta_2^{(i,j,k)}\Phi_{(n)} = B_4(\Phi_{(n)}^{(i,j,k)} - \Phi_{-(n)}^{(i,j)}), \qquad (3-40)$$

where B_4 is chosen in such a way that $\Delta_2^{(i,j,k)}\Phi/(d\theta_\zeta/dk)$ is a difference expression of the 1st order accuracy for $\partial\Phi/\partial\theta_\zeta$ at $(\tilde{r}^{(i)}, \zeta^{(j)}, \theta_\zeta^{(k)})$.

The $A_1 \sim A_4$ and $B_1 \sim B_4$ depend on i and k but not on j and n, and are determined once the lattice system is fixed. Therefore, they can be prepared before computation of $\Phi_{(1)}^{(i,j,k)}$.

The new difference formulae (35), (37), (38), and (40) contain $\Phi_+^{(j,k)}$ and $\Phi_-^{(i,j)}$, i.e., the values of Φ on either side of the discontinuity. They are computed as follows. From Eq. (14), the equation for Φ along the characteristic $\tilde{r}\sin\theta_\zeta = 1$, where the discontinuity lies, is written as

$$\zeta\frac{(\tilde{r}^2-1)^{1/2}}{\tilde{r}}\frac{d}{d\tilde{r}}\Phi(\tilde{r}, \zeta, \sin^{-1}(1/\tilde{r})) = \frac{2}{\sqrt{\pi}Kn_w}\tilde{\rho}(\Phi_e - \Phi). \qquad (3-41)$$

The difference equation for Eq. (41) corresponding to the system (26) is

$$\zeta^{(j)}\frac{(\tilde{r}^{(i)2}-1)^{1/2}}{\tilde{r}^{(i)}}\frac{\Delta^{(i,j)}\Phi_{(n)}}{d\tilde{r}/di}=\frac{2}{\sqrt{\pi}Kn_w}\tilde{\rho}^{(i)}_{(n-1)}(\Phi_{e^{(i,j)}_{(n-1)}}-\Phi^{(i,j)}_{(n)}), \qquad (3-42)$$

where $\Delta^{(i,j)}\Phi_{(n)}$ is the expression similar to Eq. (27a) or (27b) with the subscript k being discarded and $\Phi_{e^{(i,j)}_{(n-1)}}$ is $\Phi_{e(n-1)}$ with $\tilde{\rho}=\tilde{\rho}^{(i)}_{(n-1)}$, $\tilde{u}=\tilde{u}^{(i)}_{(n-1)}$, $\tilde{T}=\tilde{T}^{(i)}_{(n-1)}$, $\zeta=\zeta^{(j)}$, and $\theta_\zeta=\sin^{-1}(1/\tilde{r}^{(i)})$. Let $\Phi^{(i,j)}_{R(n)}$ be the solution of Eq. (42) with the initial data given by Eq. (17) † and the data $\tilde{\rho}^{(i)}_{(n-1)}$, $\tilde{u}^{(i)}_{(n-1)}$, and $\tilde{T}^{(i)}_{(n-1)}$ of the previous stage. Then,

$$\Phi^{(i,j)}_{-(n)}=\Phi^{(i,j)}_{R(n)}. \qquad (3-43)$$

Let $\Phi^{(i,j)}_{L(n)}$ be the solution of Eq. (42) with the initial data $\Phi^{(0,j,\hat{K})}_{(n)}$ obtained from the data at $\tilde{r}=1$ by the step (i) of the process of solution in Sec. III A. This is the solution on the other side of the discontinuity. The $\Phi^{(j,k)}_{+(n)}$ is obtained from $\Phi^{(i,j)}_{L(n)}$ by interpolation. (See Fig. 5.)

Now we can obtain the solution describing the discontinuity accurately. We insert the above-mentioned step to obtain $\Phi^{(i,j)}_{-(n)}$ and $\Phi^{(j,k)}_{+(n)}$ between the steps (i) and (ii) in the process (i)–(iv) of solution in Sec. III A and then carry out the step (ii) with the modified difference scheme (see Fig. 2b). The data on the different sides of the discontinuity are computed independently. After the discontinuity decays to be negligibly small, we return to the original scheme (26)–(27d).

---

† We take the limiting value as $\theta_\zeta \to \pi/2-$. From its derivation the value $\Phi^{(0,j,\hat{K})}_{(n)}$, obtained by the step (i) of the process of solution in Sec. III A, is the limiting value as $\theta_\zeta \to \pi/2+$.

IV. ASYMPTOTIC SOLUTION IN THE CONTINUUM LIMIT

Before presenting the results of the numerical analysis, we give the asymptotic solution for $Kn_w \to 0$. The general behavior of steady flows of a slightly rarefied gas past its condensed phase, where (strong) evaporation or condensation is taking place, is studied in Ref. 23. In the limit of the Knudsen number being zero, the flow field is described by the solution of the Euler equation of an ideal gas under an appropriate boundary condition, with local corrections such as Knudsen layer (cf. Chapter II and Ref. 21) or shock layer[47,48]. The condition across the shock layer is the well-known Rankine-Hugoniot relations[47-49]. The boundary condition on the condensed phase at rest where evaporation is taking place is given as follows.

$$\frac{p}{p_w} = h_1(M), \qquad \frac{T}{T_w} = h_2(M), \qquad (M \leq 1), \tag{3-44}$$

where M is the Mach number $(3u_i^2/5RT)^{1/2}$ and we have already obtained the functions $h_1(M), h_2(M)$ in Chapter II ($(M_\infty, p_\infty/p_w, T_\infty/T_w)$ in Table 2–1 corresponds to $(M, h_1(M), h_2(M))$.) In addition, the tangential velocity should be zero. The solution with $M > 1$ is impossible.

The problem of evaporation from a cylinder, therefore, is a simple problem of isentropic flows except for the shock layer, if any. The temperature ratio T_∞/T_w, the nondimensional mass flow rate $Q/(2\pi\rho_w(2RT_w)^{1/2}L)$, and the nondimensional energy flow rate $W/(2\pi p_w(2RT_w)^{1/2}L)$ are easily obtained as functions of the pressure ratio p_∞/p_w as follows.

(i) For $p_\infty/p_w > (4/3)^{5/2}h_1(1)(= 0.4260)$:

The results are expressed with the aid of the parameter M (the Mach number on

the condensed phase).

$$\frac{p_\infty}{p_w} = \left(\frac{M^2}{3} + 1\right)^{\frac{5}{2}} h_1(M), \tag{3-45a}$$

$$\frac{T_\infty}{T_w} = \left(\frac{M^2}{3} + 1\right) h_2(M), \tag{3-45b}$$

$$u_\infty = 0, \tag{3-45c}$$

$$\frac{Q}{2\pi\rho_w(2RT_w)^{1/2}L} = \left(\frac{5}{6}\right)^{\frac{1}{2}} \frac{Mh_1(M)}{\sqrt{h_2(M)}}, \tag{3-45d}$$

$$\frac{W}{2\pi p_w(2RT_w)^{1/2}L} = \frac{1}{\sqrt{3}}\left(\frac{5}{2}\right)^{\frac{3}{2}} \left(\frac{M^2}{3} + 1\right) Mh_1(M)\sqrt{h_2(M)}, \tag{3-45e}$$

where $u_\infty = (u_i^2)^{1/2}$ at infinity.

(ii) For $0 < p_\infty/p_w < (4/3)^{5/2}h_1(1)$:

A shock layer stands between the cylinder and infinity.

$$\frac{T_\infty}{T_w} = \frac{4}{3}h_2(1) = 0.8579, \tag{3-46a}$$

$$u_\infty = 0, \tag{3-46b}$$

$$\frac{Q}{2\pi\rho_w(2RT_w)^{1/2}L} = \left(\frac{5}{6}\right)^{\frac{1}{2}} \frac{h_1(1)}{\sqrt{h_2(1)}} = 0.2361, \tag{3-46c}$$

$$\frac{W}{2\pi p_w(2RT_w)^{1/2}L} = \sqrt{2}\left(\frac{5}{3}\right)^{\frac{3}{2}} h_1(1)\sqrt{h_2(1)} = 0.5065. \tag{3-46d}$$

For this pressure range, the variables at infinity are independent of the pressure ratio p_∞/p_w.

(iii) For $p_\infty/p_w = 0$ (evaporation into vacuum):

$$T_\infty/T_w = 0, \tag{3-47a}$$

$$u_\infty/(2RT_w)^{1/2} = (10h_2(1)/3)^{1/2} = 1.464, \tag{3-47b}$$

$$\frac{Q}{2\pi\rho_w(2RT_w)^{1/2}L} = \left(\frac{5}{6}\right)^{\frac{1}{2}} \frac{h_1(1)}{\sqrt{h_2(1)}} = 0.2361, \tag{3-47c}$$

$$\frac{W}{2\pi p_w(2RT_w)^{1/2}L} = \sqrt{2}\left(\frac{5}{3}\right)^{\frac{3}{2}} h_1(1)\sqrt{h_2(1)} = 0.5065. \tag{3-47d}$$

The dependence of T_∞/T_w, $Q/(2\pi\rho_w(2RT_w)^{1/2}L)$, and $W/(2\pi p_w(2RT_w)^{1/2}L)$ on p_∞/p_w is shown by the curves A in Figs. 6, 7 and 8 and by the data with $Kn_w = 0$ in Tables 1, 2, and 3. It should be noted that the solutions of the cases (ii) and (iii) have infinite derivative with respect to $\tilde{r}$ on the condensed phase, which violates the assumption of the asymptotic analysis in Ref. 23. The case with $M \simeq 1$ on the condensed phase, therefore, should be treated on the basis of kinetic theory, even when the Knudsen number is very small.

V. RESULT OF COMPUTATION

Following the procedure described in Sec. III, we analyzed the problem numerically for a wide range of the pressure ratio and the Knudsen number ($0.05 \leq p_\infty/p_w \leq 0.9$, $0.01 \leq Kn_w \leq 10$). The results are summarized, with their discussions, in this section.

A. Profiles of macroscopic variables

If we look for the solution of the problem for a given pressure ratio p_∞/p_w and a given Knudsen number Kn_w, we find that the solution takes a special temperature ratio T_∞/T_w. That is, for a solution to exist, the temperature ratio should take a value determined by the pressure ratio and the Knudsen number. The relation T_∞/T_w versus p_∞/p_w is shown for various Kn_w in Fig. 6 and Table 1. This is a typical feature of one- and two-dimensional problems of nonfinite domain, common with the classical heat

conduction or convection problem. In these problems the energy flow is large enough to warm up (or cool down) the gas up to infinity. That is, if the temperature at infinity is specified otherwise, a time-dependent process occurs and a new steady state satisfying the preceding relation is established.

The profiles of the macroscopic variables: the flow velocity, the pressure, the temperature, and the Mach number, are shown in Figs. 9–17. Each figure from Fig. 9 to Fig. 14 shows the profiles of the variables at a given pressure ratio p_∞/p_w for various Knudsen numbers ($Kn_w = 0$, 0.01, 0.02, 0.05, 0.1, 0.2, 0.5, 1, 2, 5, and 10). The case with $Kn_w = 0$ is the result by the asymptotic analysis based on Ref. 23 (cf. Sec. IV). The profiles change considerably with the Knudsen number. The variations of the variables with the radial distance, $r = L\tilde{r}$, become more and more moderate as the Knudsen number increases.

In Fig. 9 the profiles at $p_\infty/p_w = 0.8$ (rather weak evaporation) are shown. The flow is accelerated very slightly near the condensed phase and then is decelerated to the stationary state at infinity. The pressure and the temperature for small Kn_w decrease sharply near the condensed phase, overshooting the uniform state at infinity, and then increase gradually to the state at infinity (cf. Ref. 50). As Kn_w becomes larger, their overshoots disappear and they decrease moderately and monotonically to the state at infinity. At $p_\infty/p_w = 0.5$ (Fig. 10), the general features are the same as those at $p_\infty/p_w = 0.8$, but the acceleration of the flow and the overshoots of the pressure and temperature are intensified. At $p_\infty/p_w = 0.4260$ (Fig. 11), the flow (except for the Knudsen-layer correction) with $Kn_w = 0$ reaches sonic ($M = 1$) on the condensed phase, but the flow with $Kn_w \neq 0$ is still subsonic in the entire field. The acceleration and the overshoots are more intensified and extend in a wider region. At $p_\infty/p_w = 0.3$

(Fig. 12), the flows with $Kn_w = 0.01$ and 0.02, as well as that with $Kn_w = 0$, are accelerated to supersonic speed and then are decelerated sharply. As p_∞/p_w decreases, the flow is accelerated up to farther downstream and the acceleration to supersonic state also occurs in larger Kn_w. For $Kn_w \geq 0.2$ in Fig. 13 or $Kn_w \geq 2$ in Fig. 14, however, the flow is still subsonic in the entire field. The deceleration after supersonic region for small Kn_w is very sharp, which corresponds to a shock wave. As Kn_w increases, the acceleration region becomes narrower and the deceleration becomes more moderate even after the supersonic region. In any case, the acceleration near the condensed phase is very sharp, whose local profiles are shown in Fig. 15. In Figs. 16 and 17, the profiles with various p_∞/p_w for given Knudsen numbers are plotted to show the variation of the flow with p_∞/p_w.

B. Mass flow rate and energy flow rate from the cylinder

The variations of the mass flow rate $Q/(2\pi\rho_w(2RT_w)^{1/2}L)$ and the energy flow rate $W/(2\pi p_w(2RT_w)^{1/2}L)$ with the pressure ratio p_∞/p_w are shown for various Knudsen numbers Kn_w in Figs. 7 and 8 and Tables 2 and 3. In the continuum limit, they increase monotonically as p_∞/p_w decreases to 0.4260, and remain constant for smaller p_∞/p_w. The flow becomes sonic at $p_\infty/p_w = 0.4260$ on the condensed phase, and the mass flux is maximum at the sonic condition for a classical ideal fluid. For smaller p_∞/p_w, the flow is expressed by a single supersonic solution starting from the sonic condition on the condensed phase, accompanied by a shock wave and subsonic solution to be adjusted to the pressure at infinity (Figs. 12, 13 and 14). This is the reason of the constancy of T_∞, Q, and W for $p_\infty/p_w \leq 0.4260$. As the Knudsen number increases, this strict feature of the classical ideal gas is relaxed, and T_∞, Q, and W vary more uniformly with p_∞/p_w and exceed the constant values for $Kn_w = 0$.

C. Velocity distribution function

The marginal velocity distribution function $g(= (2RT_w)^2 p_w^{-1} \int_{-\infty}^{\infty} f d\xi_3$; see Eqs. (6) and (13)) at several points in the gas are shown for four typical types of the profiles of macroscopic variables (Sec. III A) in Figs. 18–21. For $p_\infty/p_w = 0.5$ and $Kn_w = 0.01$ (Fig. 18), the distribution is smoothed out by frequent molecular collisions in a short distance with a slight shift of its center corresponding to acceleration of the gas flow ((a) $r/L = 1 \rightarrow$ (b) $r/L = 1.102$). The distribution (b) at $r/L = 1.102$ and that (c) at $r/L = 2.499$ are quite similar. The main difference is the shift of its center toward the origin corresponding to deceleration. The similarity shows that the gas is in the continuum region. For $p_\infty/p_w = 0.5$ and $Kn_w = 1$ (Fig. 19), in a short distance ((a) $r/L = 1 \rightarrow$ (b) $r/L = 1.106$) the distribution on each side of the discontinuity remains almost unchanged except for a shift of the discontinuity and deformation in the small ζ region ($\zeta = (2RT_w)^{-1/2}(\xi_1^2 + \xi_2^2)^{1/2}$). The deformation for small ζ is considerable because slow molecules have many chances of collision; the shift of the discontinuity corresponds to the change of the direction viewing the edge of the cylinder. The distribution is smoothed out in a long distance ((a) $\rightarrow$ (b) $\rightarrow$ (c)), and there remains a discontinuity at $r/L = 2.469$. The deformation is mainly on one side of the discontinuity corresponding to the molecular velocities leaving the cylinder. For $p_\infty/p_w = 0.05$ and $Kn_w = 0.01$ (Fig. 20), the distribution is smoothed out with a shift of its center in a short distance ((a) $r/L = 1 \rightarrow$ (b) $r/L = 1.105$). The center of the distribution is further shifted and its extent shrinks, corresponding to acceleration and temperature drop ((b) $r/L = 1.105 \rightarrow$ (c) $r/L = 10.23$; note the difference in scale between the figures (b) and (c)). Then the peak of the distribution is lowered and another bump appears ((c) $r/L = 10.23 \rightarrow$ (d) $r/L = 12.03$). The peak disappears and a hill around

the bump is established ((d) $r/L = 12.03 \rightarrow$ (e) $r/L = 13.02$). The process (c) $\rightarrow$ (d) $\rightarrow$ (e) corresponds to a shock wave, through which the gas is decelerated and heated. For $p_\infty/p_w = 0.05$ and $Kn_w = 1$ (Fig. 21), the distribution with a big discontinuity on the cylinder ((a) $r/L = 1$) is deformed from the small ζ side, and the peak is formed in positive $\zeta \cos\theta_\zeta$ region, which corresponds to acceleration ((a) $r/L = 1 \rightarrow$ (b) $r/L = 1.106$). Then the peak is lowered gradually and thus the center of mass of the distribution moves toward the origin, corresponding to deceleration ((b) $r/L = 1.106 \rightarrow$ (c) $r/L = 10.15 \rightarrow$ (d) $r/L = 19.98$; note the difference in scale between the figures (b) and (c)). There still remains a discontinuity and big anisotropy of the distribution at $r/L = 19.98$.

We have discussed the discontinuity of the velocity distribution function in a gas around a convex body and proposed a scheme to analyze the discontinuity in Sec. III C. In order to show the decay of the discontinuity with r/L, we present the marginal velocity distribution function $g(r/L, \zeta, \theta_\zeta)$ at a given ζ in Figs. 22 and 23. The discontinuity lies on $(r/L)\sin\theta_\zeta = 1$, which is independent of ζ, p_∞/p_w, and Kn_w. The size of the discontinuity, on the other hand, considerably depends on the Knudsen number and the molecular speed. The discontinuity decays with distance owing to molecular collisions. Therefore it is appreciable only in the neighborhood of the cylinder for $Kn_w = 0.1$ (Fig. 22) and extends far away from the cylinder for $Kn_w = 10$ (Fig. 23(a)), and for a given Kn_w the discontinuity decays more rapidly for smaller ζ since slower molecules have smaller free paths (compare Fig. 23(a) with Fig. 23(b)).

D. Lattice system and the accuracy of computation

Since the behavior of the gas depends considerably on p_∞/p_w and Kn_w, the lattice system (the lattice functions $\tilde{r}(s), \theta_\zeta(s)$, and $\zeta(s)$ defined in Eq. (22); I, J, K, and $\hat{K}$;

$\tilde{r}_D$ and ζ_D) is chosen appropriately depending on the situation. Comparing the data † of T_∞/T_w and $Q/(2\pi\rho_w(RT_w)^{1/2}L)$ obtained with several kinds of lattice systems (half, double, etc. lattices), we confirmed that the data are reliable down to 3 or 4 decimal places shown in Tables 1 and 2. Then for typical cases we examined the difference of the profiles of the macroscopic variables for different lattice systems and checked whether there are enough lattice points for the variation of the variables, especially in the Knudsen layer and the shock wave. If the result was not satisfactory, we recomputed all the cases of similar situations with finer lattice systems.

Some of the data of our lattice system are given here for reference. (i) The lattice function $\tilde{r}(s)$ is given by

$$\frac{d\tilde{r}(s)}{ds} = \frac{f_1(\tilde{r})f_2(\tilde{r})}{f_3(\tilde{r})}, \qquad \tilde{r}(0) = 1, \tag{3-48a}$$

$$f_1 = d_2 + (d_1 - d_2)\exp(-d_3(\tilde{r} - 1)), \tag{3-48b}$$

$$f_2 = 1 + (d_7 - 1)\exp(-d_8(\tilde{r} - 1)), \tag{3-48c}$$

$$f_3 = 1 + d_4\exp(-(\tilde{r} - d_5)^2/d_6), \tag{3-48d}$$

where $d_1, d_2, \ldots, d_8$ are constants chosen properly in each case. The fundamental lattice moderately broadening from the cylinder is expressed by f_1; A finer lattice adjacent to the cylinder for the Knudsen layer and that in the midst of the gas for the shock wave are expressed by f_2 and f_3 respectively. Examples of the lattice data are given in Table 4. The appropriate size of the domain $\tilde{r}_D$ depends considerably on p_∞/p_w and Kn_w, whose examples are given in Table 5. (ii) For $\zeta^{(j)}$ lattice, $\zeta(s) = \alpha s^3$ (α: a constant), $\zeta_D = 8$,

† The data determined in the connecting process with the asymptotic solution in Sec. III B.

and $J = 24$, 48, or 96. Most cases were computed with $J = 24$. (iii) Corresponding to a sharp variation near the cylinder, a finer lattice of $\theta_\zeta^{(k)}$ is required near $\theta_\zeta = \pi/2$; For moderate or large Kn_w, a finer lattice is also required near $\theta_\zeta = 0$ since the discontinuity extends far away from the cylinder. Examples of K and $\hat{K}$ are given in Table 6.

In order to examine the accuracy of our computation, we computed Q and W by Eqs. (19) and (20) at all the lattice points of $\tilde{r}$ and examined their relative errors ((max Q – min Q)/min Q and (max W – min W)/min W). The relative errors of Q and W are less than 0.1% for the values of p_∞/p_w and Kn_w for which the data T_∞/T_w are given down to 4 decimal places in Table 1. For other p_∞/p_w and Kn_w, the errors are 0.1%~0.5% but the cases with 0.4~0.5% are only a few. The data in Tables 2 and 3 are the averages of Q and W over $1 \leq \tilde{r} \leq \tilde{r}_D$ (e.g., $(\tilde{r}_D - 1)^{-1} \int_1^{\tilde{r}_D} Q d\tilde{r}$).

The computation was carried out by Apollo DN 4500, DG AV 310, and MIPS RS 3230 computers at our Laboratory and by FACOM VP-2600 computer at the Data Processing Center of Kyoto University.

VI. EFFECT OF CONDENSATION FACTOR IN KINETIC BOUNDARY CONDITION

As in most works on a gas flow with evaporation and condensation, we considered the problem under the conventional boundary condition (the assumption (ii) in Sec. II), where the velocity distribution of the molecules leaving the condensed phase is independent of the distribution of the incident molecules. Experimental data showing the dependence of the distribution of the molecules on that of the incident molecules on a certain solid surface are reported.[20] A generalization of the conventional boundary condition is reported in Ref. 5, where the conversion formula of the solution of the linearized half-space problem under the conventional condition to that under the generalized one

is also given. The conversion relation is generalized to the two surface and the nonlinear half-space problems in Refs. 23, 26 and Chapter II . The conversion relation can also be derived for the present problem.

The generalized boundary condition given in Ref. 5 is obtained by simply replacing the ρ_w in Eq. (4a) by the following quantity:

$$\alpha_c \frac{p_w}{RT_w} - (1-\alpha_c)(2\pi/RT_w)^{1/2} \int_{\xi_1 x_1 + \xi_2 x_2 < 0} \frac{(\xi_1 x_1 + \xi_2 x_2)}{r} f d\xi_1 d\xi_2 d\xi_3, \qquad (3-49)$$

where α_c is a constant ($0 < \alpha_c \leq 1$) called the condensation factor of the boundary. The case $\alpha_c = 1$ corresponds to the conventional condition. The two problems differ only in the boundary condition (4a) by a factor. We can, therefore, derive a simple conversion formula between the two classes of solutions. Only the result is given here. Let the nondimensional solution ($\tilde{f}$, g, h, $\tilde{u}$, $\tilde{\rho}$, $\tilde{p}$, $\tilde{T}$, $\tilde{Q}(= Q/(2\pi\rho_w(2RT_w)^{1/2}L))$, $\tilde{W}(= W/(2\pi p_w(2RT_w)^{1/2}L))$) under the conventional boundary condition for $\tilde{p}_\infty = P_C$ and $Kn_w = K_C$ be denoted by the subscript C, and let the solution under the generalized boundary condition for $\tilde{p}_\infty = P_G$ and $Kn_w = K_G$ be denoted by the subscript G. The following one-to-one correspondence holds between the two classes of solutions:

$$(\tilde{f}_G,\ P_G,\ K_G) = \Gamma(\tilde{f}_C,\ P_C,\ K_C), \qquad (3-50)$$

where

$$\Gamma = (1 + 2\sqrt{\pi}(1-\alpha_c)\alpha_c^{-1}\tilde{Q}_C)^{-1}. \qquad (3-51)$$

Then,

$$(g_G,\ h_G,\ \tilde{\rho}_G,\ \tilde{p}_G,\ \tilde{Q}_G,\ \tilde{W}_G) = \Gamma(g_C,\ h_C,\ \tilde{\rho}_C,\ \tilde{p}_C,\ \tilde{Q}_C,\ \tilde{W}_C), \qquad (3-52a)$$

$$(\tilde{u}_G,\ \tilde{T}_G,\ M_G) = (\tilde{u}_C,\ \tilde{T}_C,\ M_C). \qquad (3-52b)$$

It is noted that all the ρ_w in Eqs. (6c), (6d), (8b), etc. (except in Eq. (4a)) is the original ρ_w defined by $\rho_w = p_w/RT_w$ but not the quantity (49).

VII. CONCLUDING REMARKS

We considered evaporating flows of a rarefied gas from its cylindrical condensed phase in an infinite expanse of the gas and tried to analyze the problem numerically. First the difficulties in analyzing the problem were resolved: On the basis of the asymptotic analysis, a method to treat infinite domain problems where the approach to the uniform state at infinity is slow as in the present problem is proposed (Sec. III B). The discontinuity of the velocity distribution function in a gas around a convex body is pointed out, and a numerical scheme to analyze this discontinuity is presented (Sec. III C). The discontinuity is not only of theoretical interest but also important in numerical analysis. If the discontinuity is not properly treated, considerable errors are introduced in macroscopic variables, especially for moderate and large Knudsen numbers. With these preparations, we analyzed the problem numerically for a wide range of the pressure ratio ($p_\infty/p_w = 0.05 \sim 0.9$) and the Knudsen number ($Kn_w = 0.01 \sim 10$). The numerical data of the scheme and the accuracy test of the numerical computation are described briefly in Sec. V D. Finally the effect of the condensation factor in the kinetic boundary condition is discussed (Sec. VI).

The comprehensive data of the macroscopic variables over the whole flow field are presented in Figs. 9–17. The profiles of the flow velocity, the pressure, the temperature, and the Mach number of a given pressure ratio for various Knudsen numbers are shown in each of Figs. 9–14 from the pressure ratio 0.8 to 0.05. Comparison of the profiles of various pressure ratios ($0.05 \sim 0.6$) is given in Figs. 16 and 17 for Knudsen numbers 0.01 and 0.2, respectively. The flow, generally, is first accelerated and then decelerated to the state at infinity. The variations of the variables are more moderate for larger Knudsen numbers. Sharp acceleration occurs near the condensed phase (see also Fig. 15). As

the pressure ratio decreases, the region of acceleration extends farther downstream. For the pressure ratio smaller than a certain value, a supersonic region appears in the flow field. The threshold pressure ratio decreases as the Knudsen number increases. For the Knudsen number larger than a certain value, the flow remains subsonic for the entire field (e.g., $Kn_w \geq 2$ for $p_\infty/p_w = 0.05$, $Kn_w \geq 0.2$ for $p_\infty/p_w = 0.2$.). The deceleration from the supersonic flow is very steep for small Knudsen numbers. In most figures the result in the continuum limit obtained by the asymptotic theory[23] is shown for comparison.

The temperature ratio T_∞/T_w, the nondimensional mass flow rate $Q/2\pi\rho_w(2RT_w)^{1/2}L$, and the nondimensional energy flow rate $W/2\pi p_w(2RT_w)^{1/2}L$ versus the pressure ratio for various Knudsen numbers are presented in Figs. 6–8 and in Tables 1–3 with their discussions in Secs. V A and V B. The results in the continuum limit are given in Sec. IV. The choking feature of these three quantities in the continuum limit is seen to relax as the Knudsen number increases. The dependence of the temperature ratio on the pressure ratio is a typical feature of one and two-dimensional problems of nonfinite domain.

The behavior of the velocity distribution function is depicted in Figs. 18–23 with the discussion in Sec. V C. The process of its deformation as going away from the condensed phase is given for four sets of the pressure ratio and the Knudsen number in Figs. 18–21. The discontinuity of the velocity distribution function in the gas is a typical feature of gas flows around a convex body. It extends far away from the cylinder and the distribution function shows a strong anisotropy for small pressure ratio and moderate or large Knudsen numbers (Fig. 21). The process of deceleration through a shock wave is clearly seen in Fig. 20.

The case with zero pressure ratio (evaporation into vacuum), however, was not computed although the case with small pressure ratio $p_\infty/p_w = 0.05$ was computed. The recent experiment [28] of Faubel *et al.* arose new interest in analysis of the problem. For comprehensive understanding of the problem, further extensive study is required although some works have been done (e.g., Refs. 8 and 27).

ACKNOWLEDGMENTS

The author wishes to express his special thanks to Professor Yoshio Sone, Department of Aeronautical Engineering, Kyoto University, for suggesting this problem and guiding carefully throughout the course of this investigation. The author wishes to express his thanks also to Associate Professor Kazuo Aoki, Department of Aeronautical Engineering, Kyoto University, for his advice in various aspects in his research study. Discussion with Dr. Taku Ohwada, Department of Aeronautical Engineering, Kyoto University, is gratefully acknowledged.

REFERENCES

1 M. N. Kogan and N. K. Makashev, Fluid Dyn. **6**, 913 (1971).

2 Y. P. Pao, Phys. Fluids **14**, 306, 1340 (1971).

3 C. E. Siewert and J. R. Thomas, Jr., Phys. Fluids **16**, 1557 (1973).

4 Y. Sone and Y. Onishi, J. Phys. Soc. Jpn. **35**, 1773 (1973).

5 J. W. Cipolla, Jr., H. Lang, and S. K. Loyalka, J. Chem. Phys. **61**, 69 (1974).

6 P. Gajewski, A. Kulicki, A. Wiśniewski, and M. Zgorelski, Phys. Fluids **17**, 321 (1974).

7 T. Matsushita, Phys. Fluids **19**, 1712 (1976).

8 C. J. Knight, J. Fluid Mech. **75**, 469 (1976).

9 T. Ytrehus, in *Rarefied Gas Dynamics*, edited by J. L. Potter (AIAA, New York, 1977), p. 1197.

10 Y. Sone and Y. Onishi, J. Phys. Soc. Jpn. **44**, 1981 (1978).

11 Y. Sone, J. Phys. Soc. Jpn. **45**, 315 (1978).

12 Y. Onishi and Y. Sone, J. Phys. Soc. Jpn. **47**, 1976 (1979).

13 D. A. Labuntsov and A. P. Kryukov, Int. J. Heat Mass Transfer **22**, 989 (1979).

14 S. M. Yen, in *Rarefied Gas Dynamics*, edited by S. S. Fisher (AIAA, New York, 1981), p. 356.

15 M. D. Arthur and C. Cercignani, Z. Angew. Math. Phys. **31**, 634 (1980).

16 A. A. Abramov and M. N. Kogan, Sov. Phys. Dokl. **29**, 763 (1984).

17 A. P. Kryukov, Fluid Dyn. **20**, 487 (1985).

18 Y. Sone, K. Aoki, and I. Yamashita, in *Rarefied Gas Dynamics*, edited by V. C. Boffi and C. Cercignani (Teubner, Stuttgart, 1986), Vol. 2, p. 323.

19 Y. Sone, T. Ohwada, and K. Aoki, Phys. Fluids A **1**, 1398 (1989).

20 R. Mager, G. Adomeit, and G. Wortberg, in *Rarefied Gas Dynamics: Physical Phenomena*, Progress in Astronautics and Aeronautics, edited by E. P. Muntz, D. C. Weaver, and D. H. Campbell (AIAA, Washington, DC, 1989), Vol. 117, p. 460.

21 K. Aoki, Y. Sone, and T. Yamada, Phys. Fluids A **2**, 1867 (1990).

22 M. N. Kogan and A. A. Abramov, in *Rarefied Gas Dynamics*, edited by A. E. Beylich (VCH, Weinheim, 1991), p. 1251.

23 K. Aoki, and Y. Sone, in *Advances in Kinetic Theory and Continuum Mechanics*, edited by R. Gatignol and Soubbaramayer (Springer, Berlin, 1991), p. 43.

24 Y. Sone, in *Advances in Kinetic Theory and Continuum Mechanics*, edited by R. Gatignol and Soubbaramayer (Springer, Berlin, 1991), p. 19.

25 Y. Sone, in *Rarefied Gas Dynamics*, edited by A. E. Beylich (VCH, Weinheim, 1991), p. 489.

26 Y. Sone, T. Ohwada, and K. Aoki, in *Mathematical Aspects of Fluid and Plasma Dynamics, Proceedings*, edited by G. Toscani, V. Boffi, and S. Rionero, Lecture Notes in Mathematics Vol. 1460 (Springer, Berlin, 1991), p. 186.

27 D. Sibold and H. M. Urbassek, Phys. Fluids A **3**, 870 (1991).

28 M. Faubel, S. Schlemmer, and J. P. Toennis, Z. Phys. D **10**, 269 (1988).

29 Soubbaramayer, *Lecture notes on Uranium enrichment* (at Tsinghua University, Pekin, 1984) Fasciule 2.

30 Y. Sone, in Rarefied Gas Dynamics, edited by L. Trilling and H. Y. Wachman (Academic Press, New York, 1969), p. 243.

31 Y. Sone, in Rarefied Gas Dynamics, edited by D. Dini (Editrice Tecnico Scientifica, Pisa, 1971), p. 737.

32 Y. Sone and H. Sugimoto, J. Vac. Soc. Jpn. **31**, 420 (1988) (in Japanese).

33 Y. Sone, K. Aoki, H. Sugimoto, and T. Yamada, Theor. Appl. Mech. (Bulgaria) **19**, No. 3, 89 (1988).

34 H. Sugimoto and Y. Sone, J. Vac. Soc. Jpn. **32**, 214 (1989) (in Japanese).

35 Y. Sone and H. Sugimoto, in *Adiabatic Waves in Liquid-Vapor Systems*, IUTAM Symposium, Göttingen, 1989, edited by G. E. A. Meier and P. A. Thompson (Springer, Berlin, 1990), p. 293.

36 P. L. Bhatnagar, E. P. Gross, and M. Krook, Phys. Rev. **94**, 511 (1954).

37 P. Welander, Ark. Fys. **7**, 507 (1954).

38 F. Reif, *Fundamentals of Statistical and Thermal Physics* (McGraw-Hill, New York, 1965), p. 304.

39 C. K. Chu, Phys. Fluids **8**, 12 (1965).

40 H. Grad, Phys. Fluids **6**, 147 (1963).

41 H. Sugimoto and Y. Sone, J. Vac. Soc. Jpn. **34**, 387 (1991) (in Japanese).

42 H. Sugimoto and Y. Sone, Phys. Fluids A (to be published)

43 Y. Sone, Phys. Fluids **16**, 1422 (1973).

44 Y. Sone and K. Aoki, Transp. Theory Stat. Phys. **16**, 189 (1987); Mem. Fac. Eng. Kyoto Univ. **49**, 237 (1987).

45 Y. Sone, *Lecture Notes on Molecular Gas Dynamics* (Department of Aeronautical Engineering, Kyoto University, Kyoto, 1990) Chap. III (in Japanese).

46 K. Aoki, Y. Sone, K. Nishino, and H. Sugimoto, in *Rarefied Gas Dynamics*, edited by A. E. Beylich (VCH, Weinheim, 1991), p. 222.

47 H. Grad, in *Transport Theory*, edited by R. Bellman, G. Birkhoff, and I. Abu-Shumays (American Mathematical Society, Providence, RI, 1969), p. 269.

48 C. Cercignani and C. Lancellotti, in *Rarefied Gas Dymanics*, edited by A. E. Beylich

(VCH, Weinheim, 1991), p. 153.

49 H. W. Liepmann and A. Roshko, *Elements of Gasdynamics* (Wiley, New York, 1960), p. 56.

50 Y. Onishi and Y. Sone, Phys. Fluids **26**, 659 (1983).

FIGURES

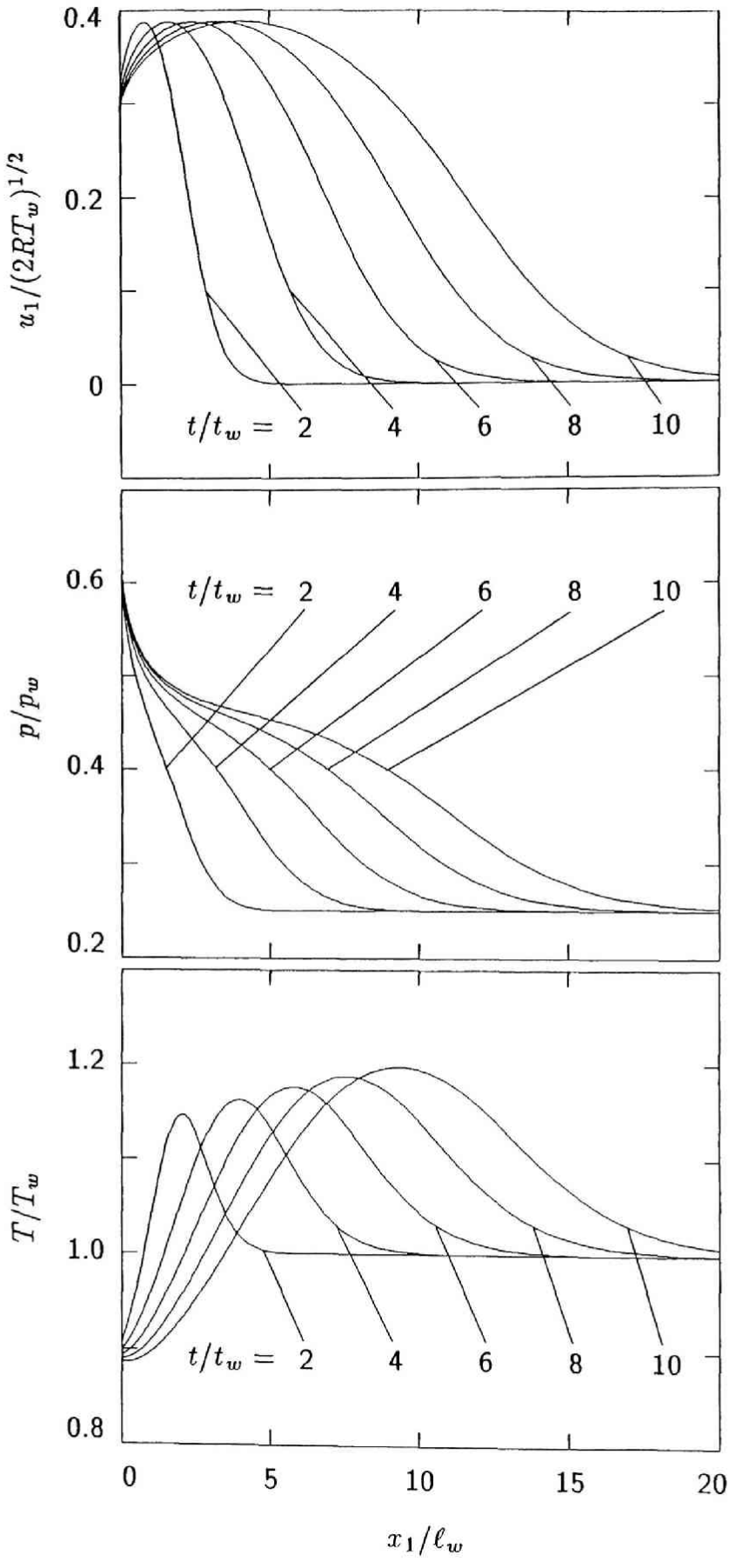

Fig. 2–1. Transient behavior Ia ($M_\infty = 0$, $p_\infty/p_w = 1/4$, $T_\infty/T_w = 1$).

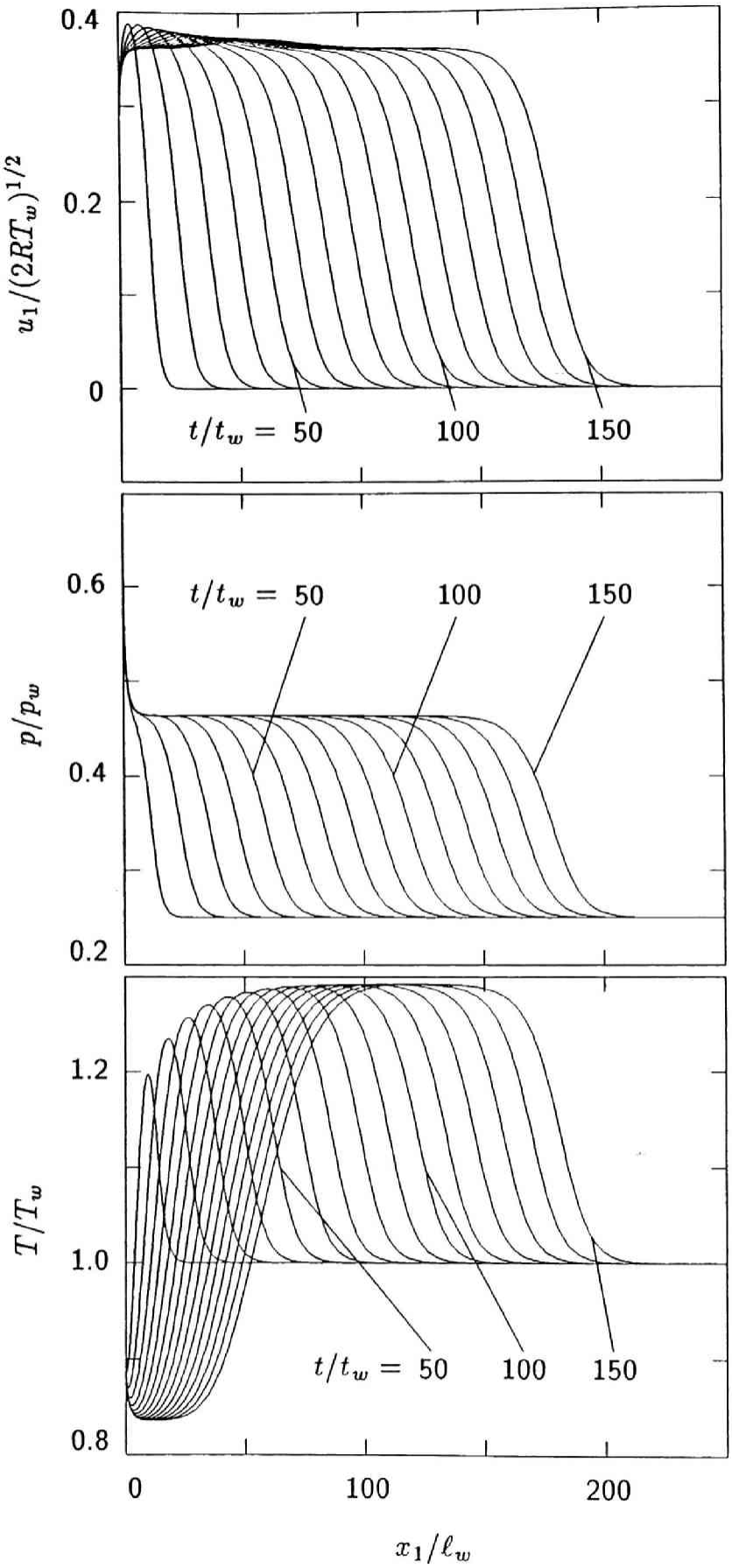

Fig. 2–2. Transient behavior Ib ($M_\infty = 0$, $p_\infty/p_w = 1/4$, $T_\infty/T_w = 1$).

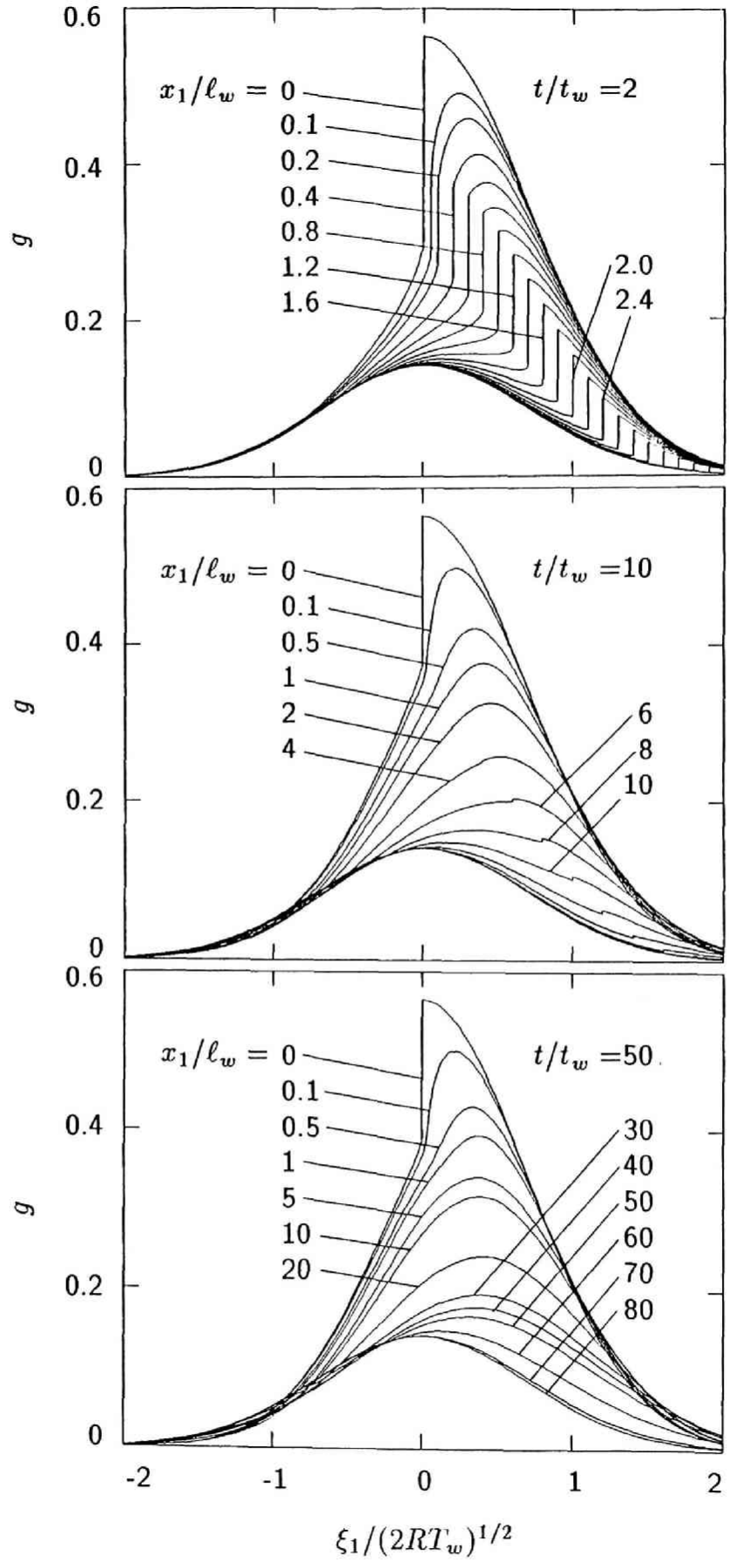

Fig. 2–3. Transient behavior Ic ($M_\infty = 0$, $p_\infty/p_w = 1/4$, $T_\infty/T_w = 1$).

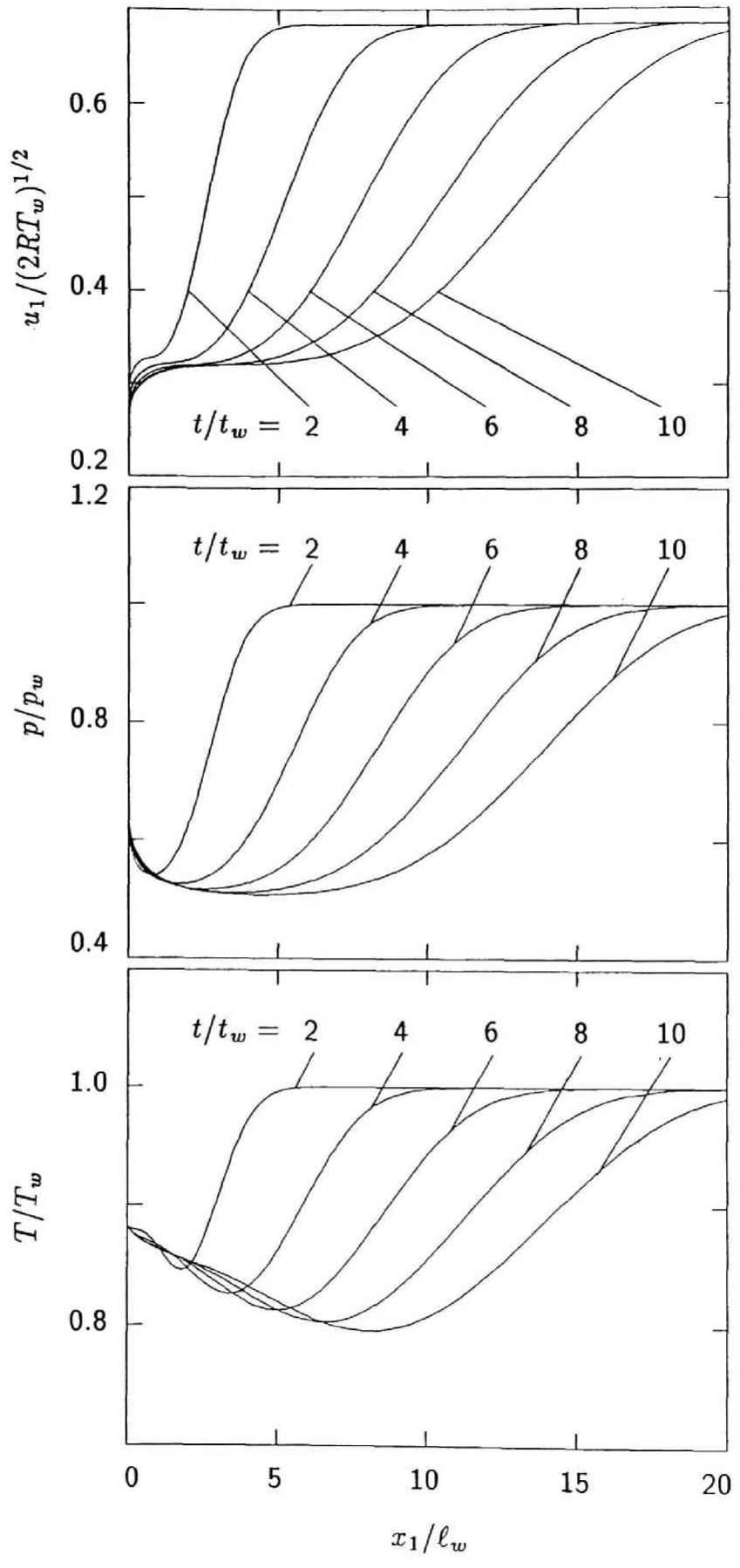

Fig. 2–4. Transient behavior IIa ($M_\infty = 0.75$, $p_\infty/p_w = 1$, $T_\infty/T_w = 1$).

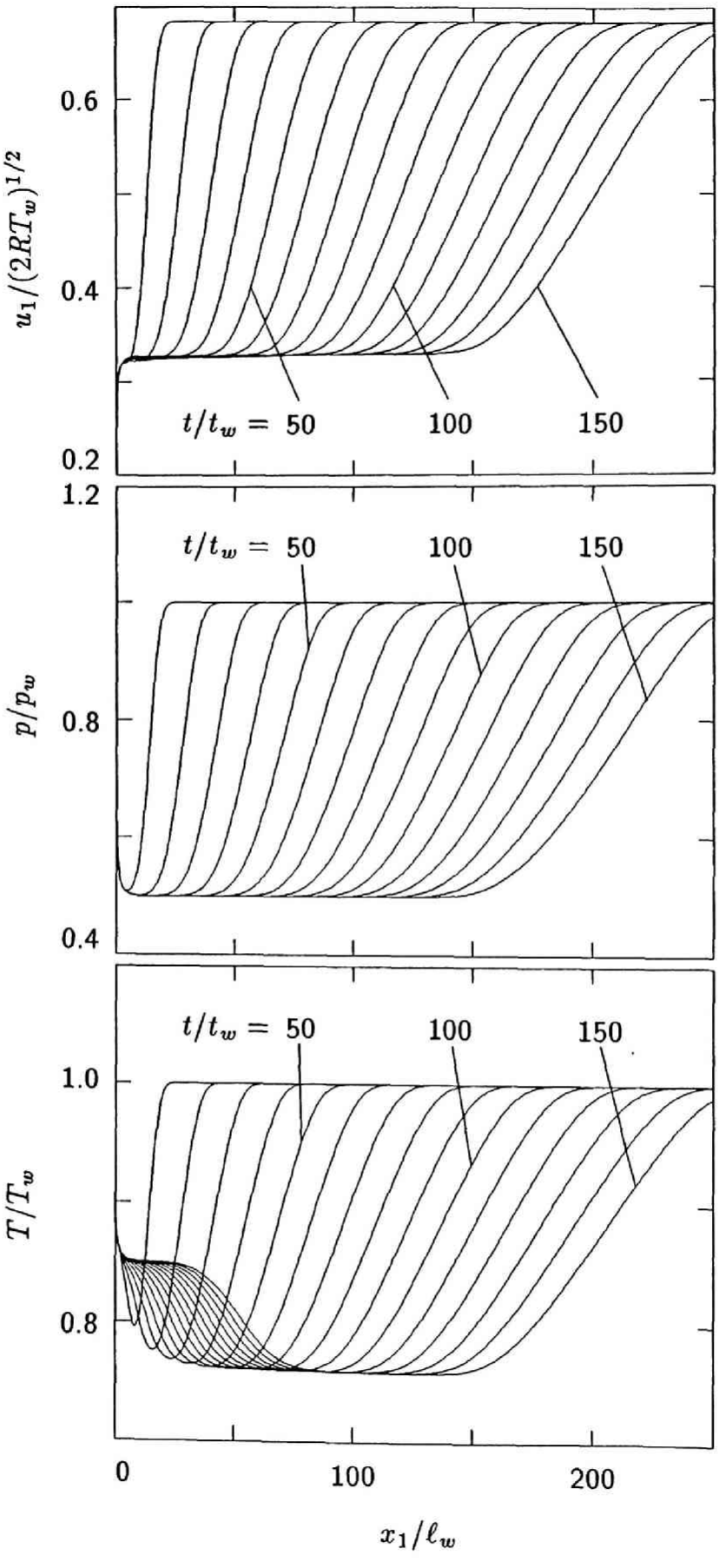

Fig. 2–5. Transient behavior IIb ($M_\infty = 0.75$, $p_\infty/p_w = 1$, $T_\infty/T_w = 1$).

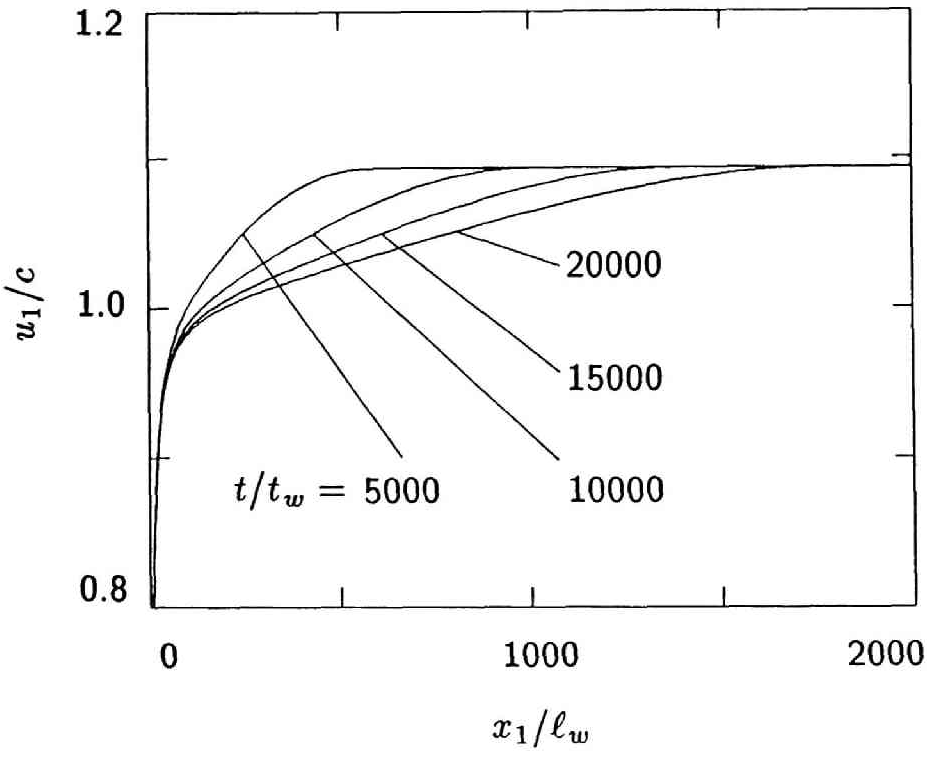

Fig. 2–6. Shift of the supersonic region ($M_\infty = 1.0924$, $p_\infty/p_w = 0.1850$, $T_\infty/T_w = 0.6152$).

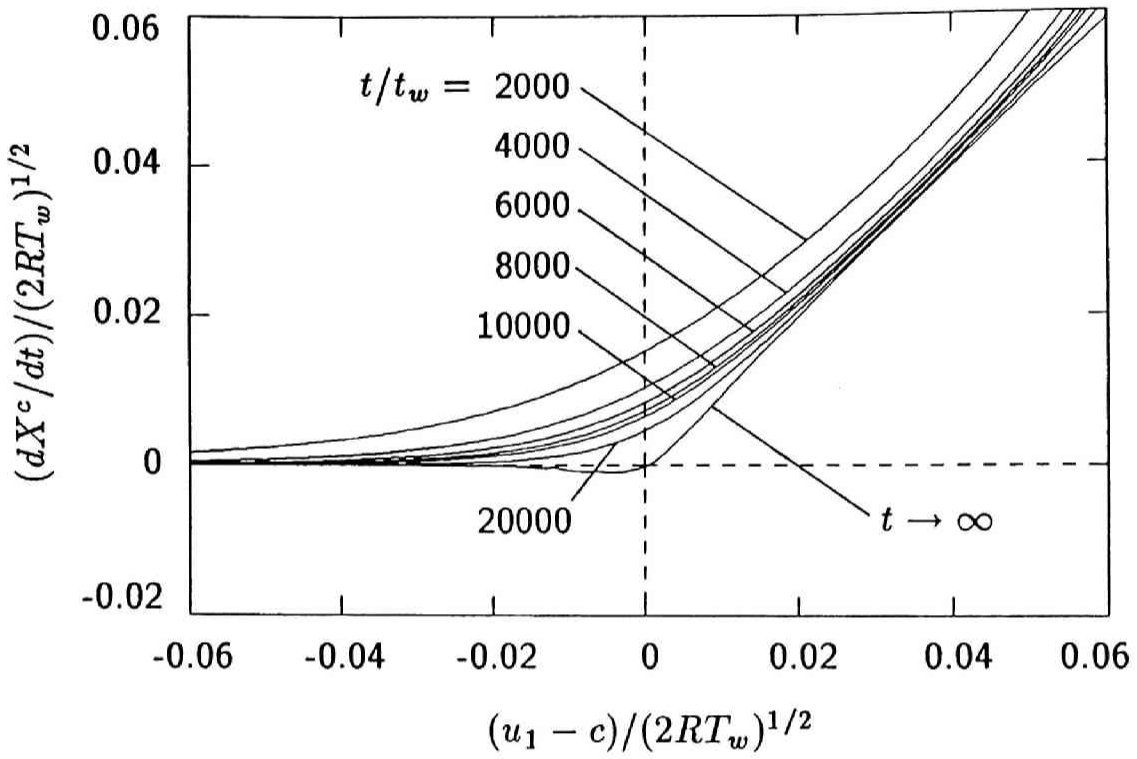

Fig. 2–7. dX^c/dt vs. $u_1 - c$ in the case of Fig. 2–6.

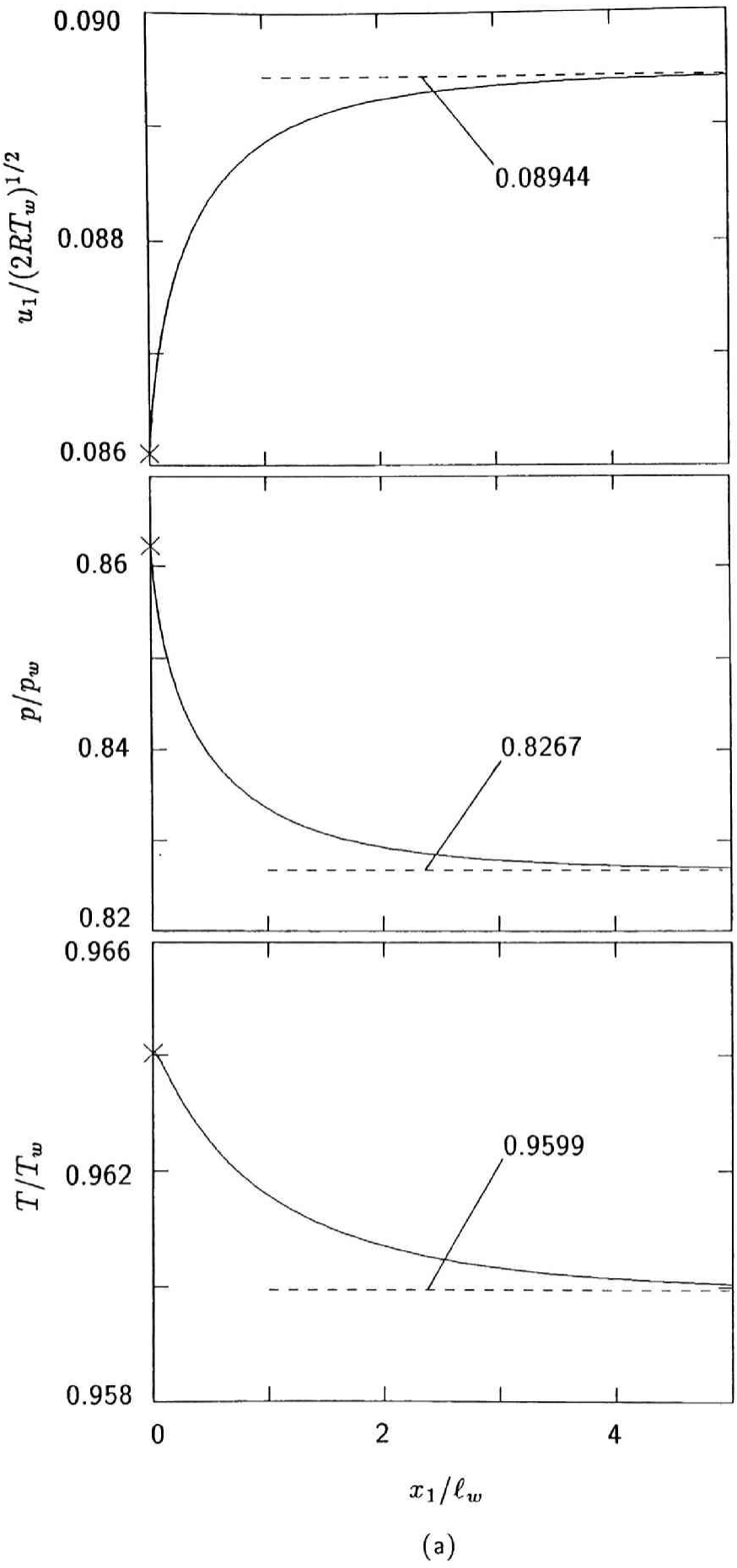

Fig. 2–8. Transition region in the steady evaporation. Here, × indicates the value at $x_1 = 0$. (a) : M_∞=0.1, (b) : M_∞=0.5001, (c) : M_∞=0.9897.

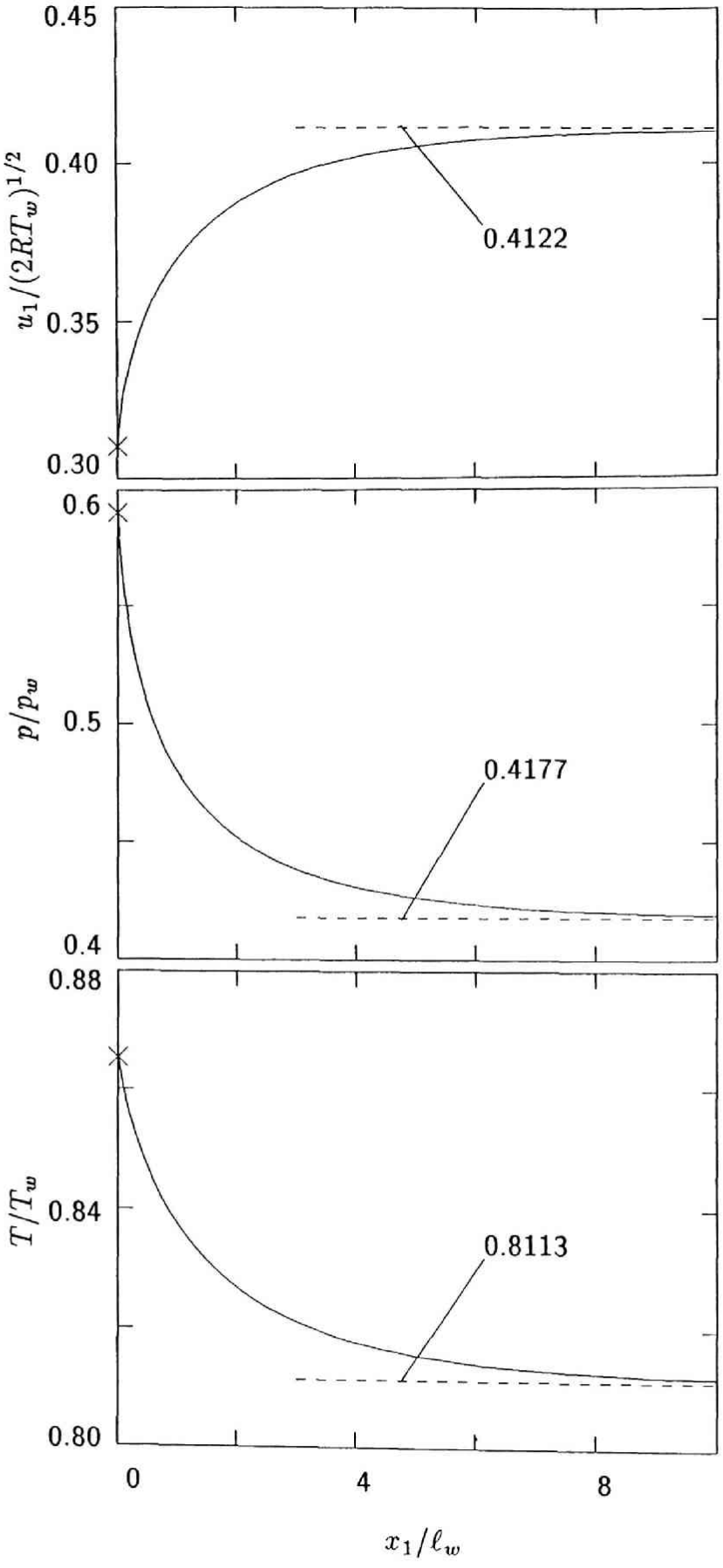
0.45
0.40
0.35
0.30
$u_1/(2RT_w)^{1/2}$
0.4122
0.6
0.5
0.4
p/p_w
0.4177
0.88
0.84
0.80
T/T_w
0.8113
0
4
8
x_1/ℓ_w

(b)

Fig. 2–8. (cont.)

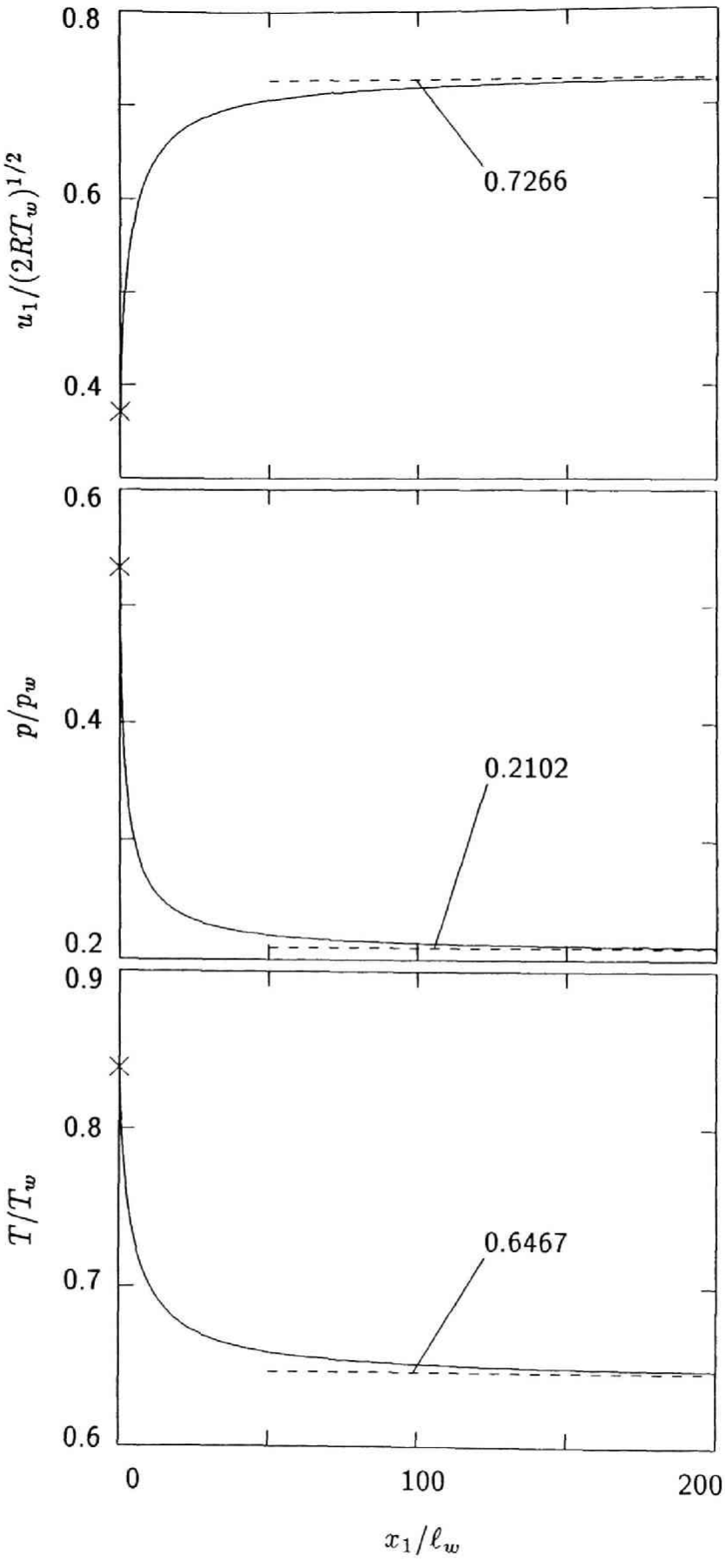
0.8
0.6
0.4
$u_1/(2RT_w)^{1/2}$
0.7266
0.6
0.4
0.2
p/p_w
0.2102
0.9
0.8
0.7
0.6
T/T_w
0.6467
0
100
200
x_1/ℓ_w

(c)

Fig. 2–8. (cont.)

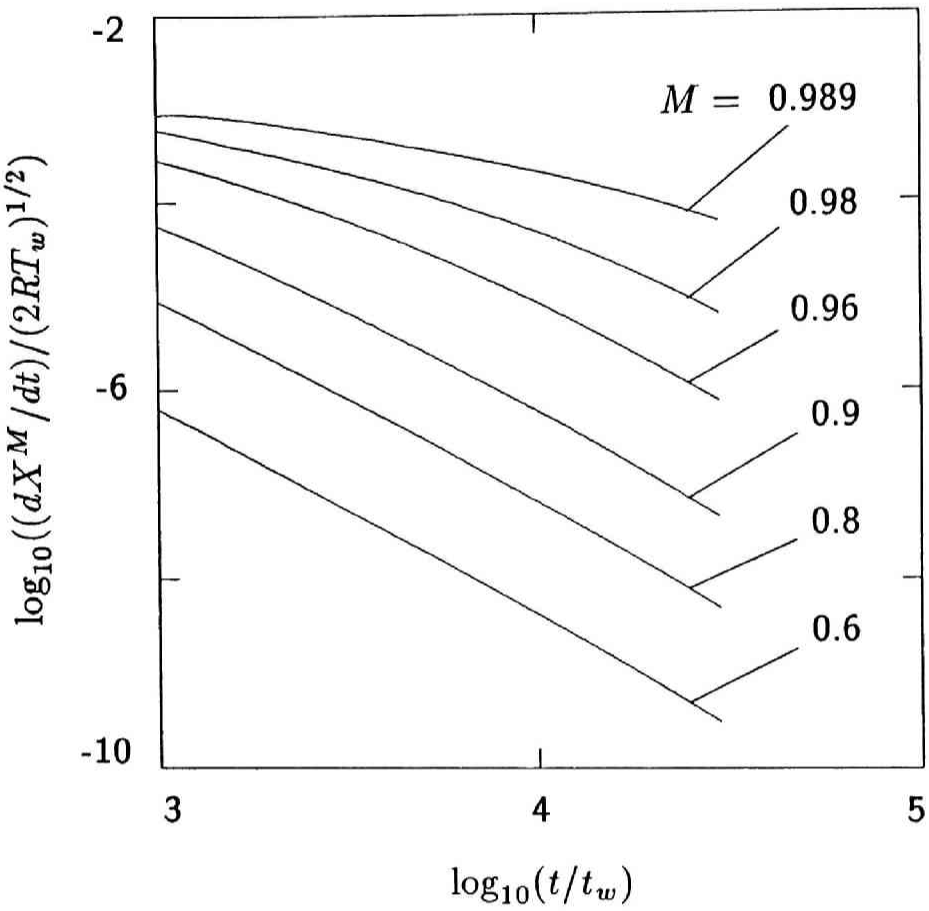

Fig. 2–9. Convergence test to the steady profile $M_\infty = 0.9897$.

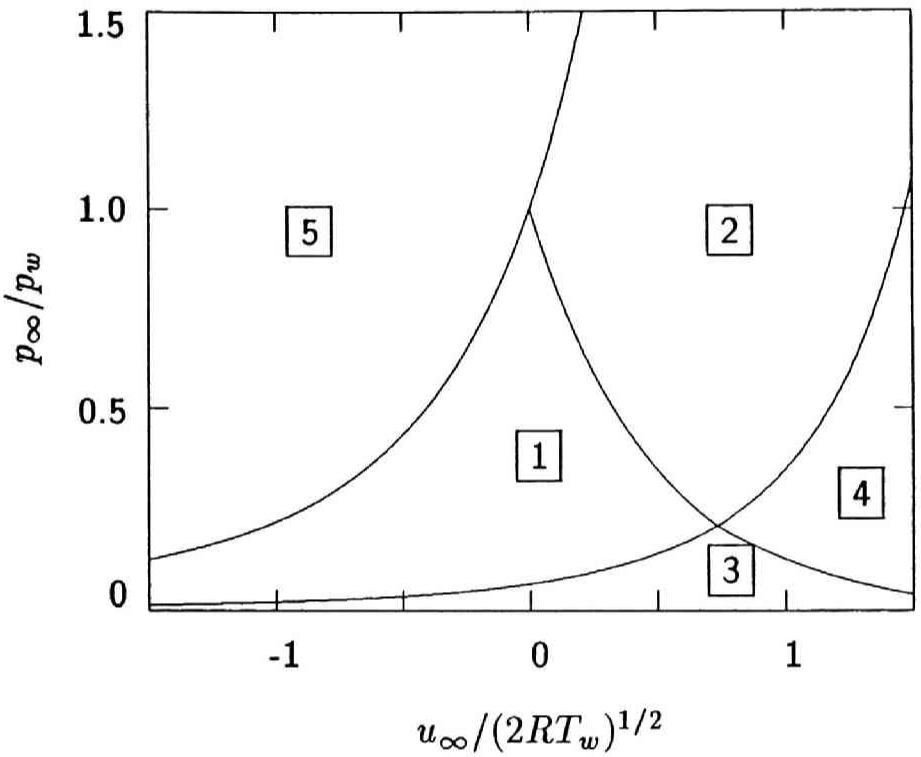

Fig. 2–10. Classification of the asymptotic behavior (cf. Chap. II Sec. IV C).

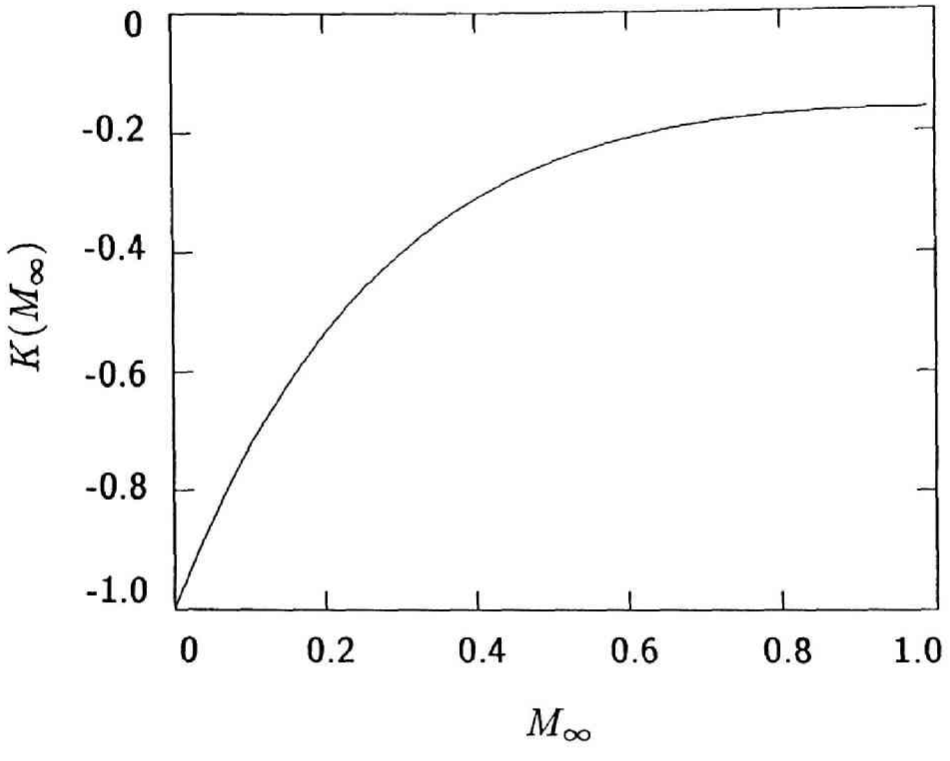

Fig. 2–11. $K(M_\infty)$ vs. M_∞ [Eq. (2–15)].

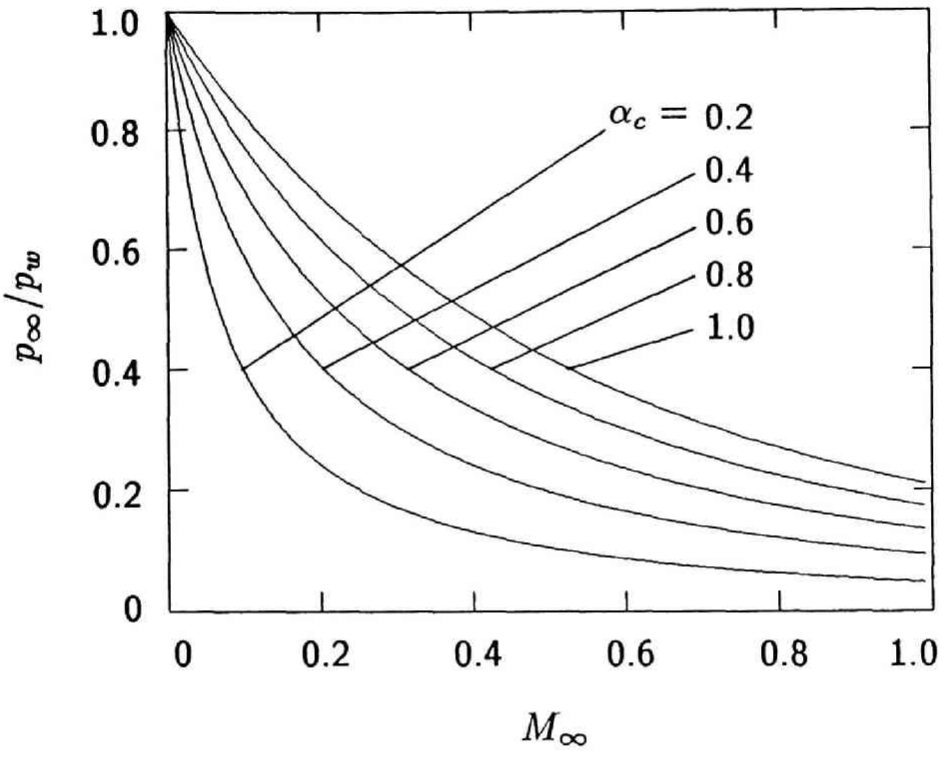

Fig. 2–12. p_∞/p_w^G vs. M_∞ [Eq. (2–14b)].

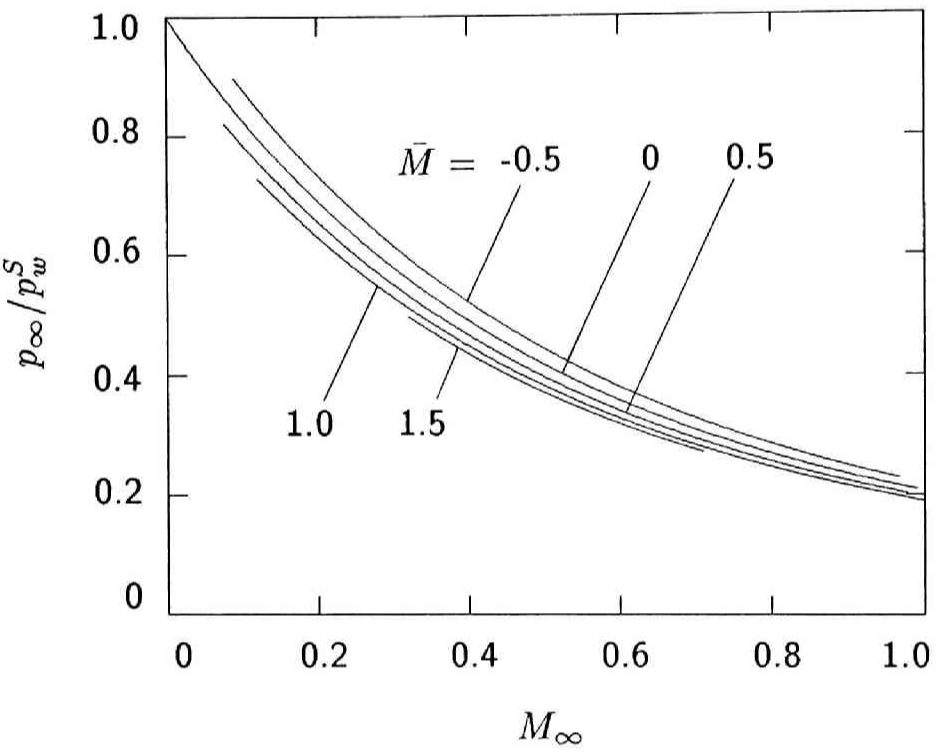

Fig. 2–13. p_∞/p_w^S vs. M_∞ [cf. Eq. (2–16a)].

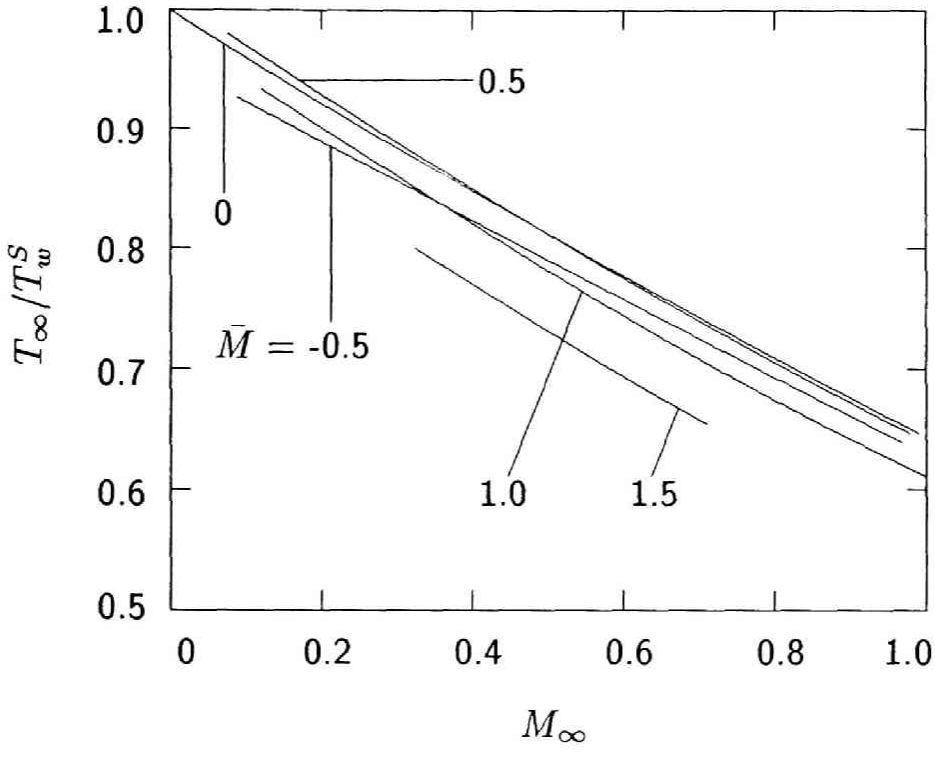

Fig. 2–14. T_∞/T_w^S vs. M_∞ [cf. Eq. (2–16b)].

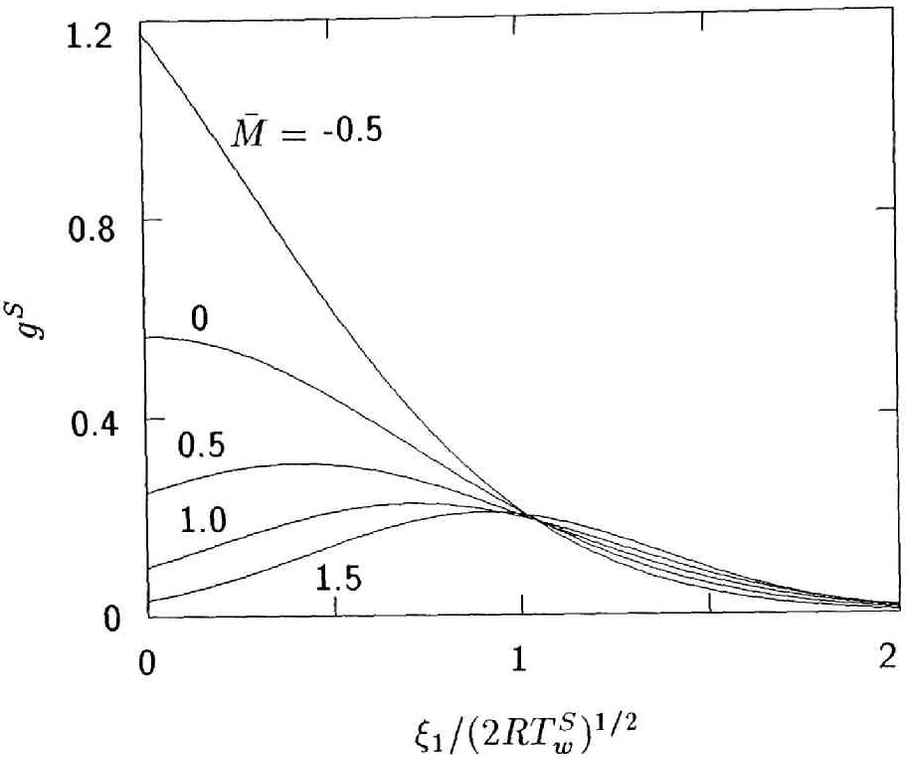

Fig. 2–15. Reduced distribution g^S $[g^S = (2RT_w^S)^{3/2}(2p_w^S)^{-1} \int \bar{f} d\xi_2 d\xi_3]$.

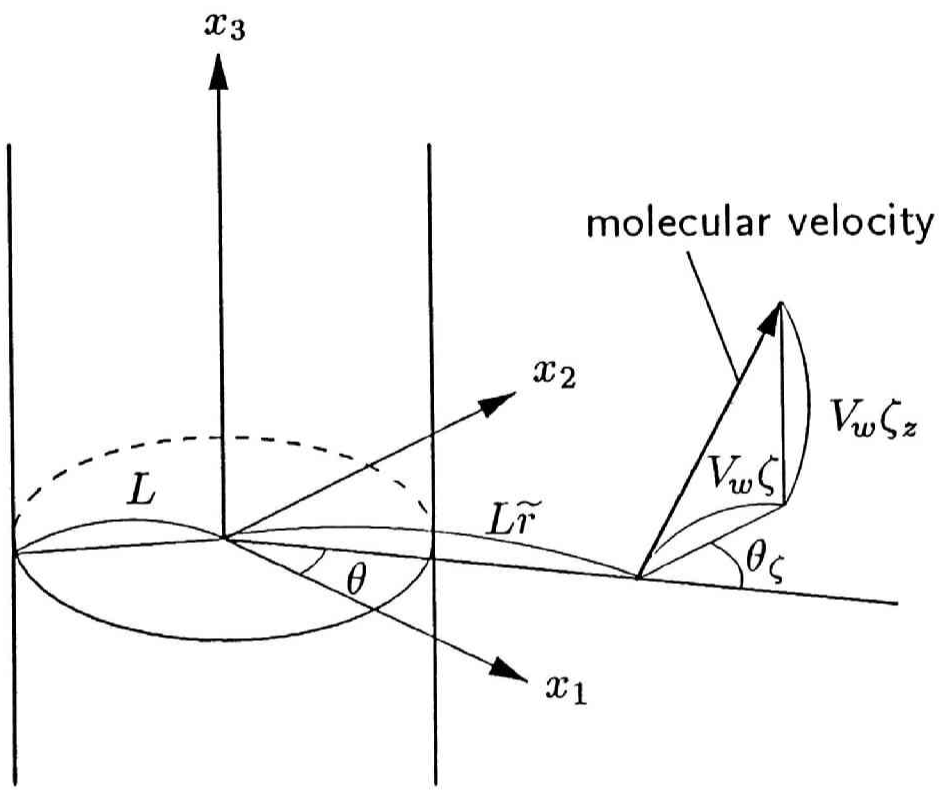

Fig. 3–1. Coordinate system. The variables (r, θ, x_3), where $r = L\tilde{r}$, are cylindrical coordinates for the physical space, and the variables $(V_w\zeta, \theta_\zeta, V_w\zeta_z)$ are local cylindrical coordinates for the molecular velocity.

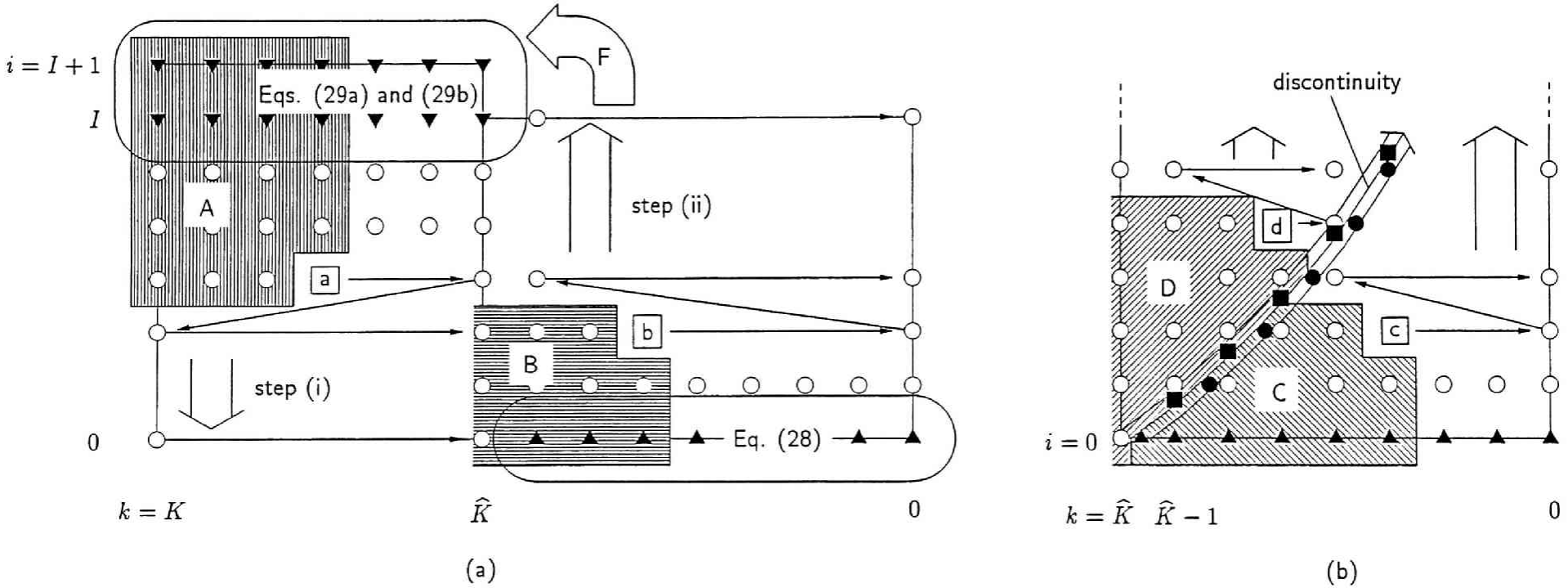

Fig. 3–2. Diagram of the process of solution: (a) the general process without taking the discontinuity of Φ into account (the process (i)–(iv) in Chap.III Sec. III A); (b) a modified process of obtaining the solution with discontinuity. The data $\Phi^{(i,j,k)}_{(n)}$ at [a], [b], [c], and [d] are computed from the data in A, B, C, and D respectively. Computation is carried out in the direction of the arrow $\rightarrow$; the arrow $\Rightarrow$ represents the global direction of process. The symbols $\bullet$ and $\blacksquare$ on each side of the arrow along the discontinuity represent $\Phi^{(i,j)}_{-(n)}$ and $\Phi^{(j,k)}_{+(n)}$, respectively, which are computed by the integral along the discontinuity (Chap. III Sec. III C). In each iteration, the data on the different sides of the discontinuity are computed independently. After the discontinuity decays to be negligibly small, we return to the general process (a). The arrow with the mark F is the feedback process to the boundary data (3–29a) and (3–29b) (Chap. III Sec. III B).

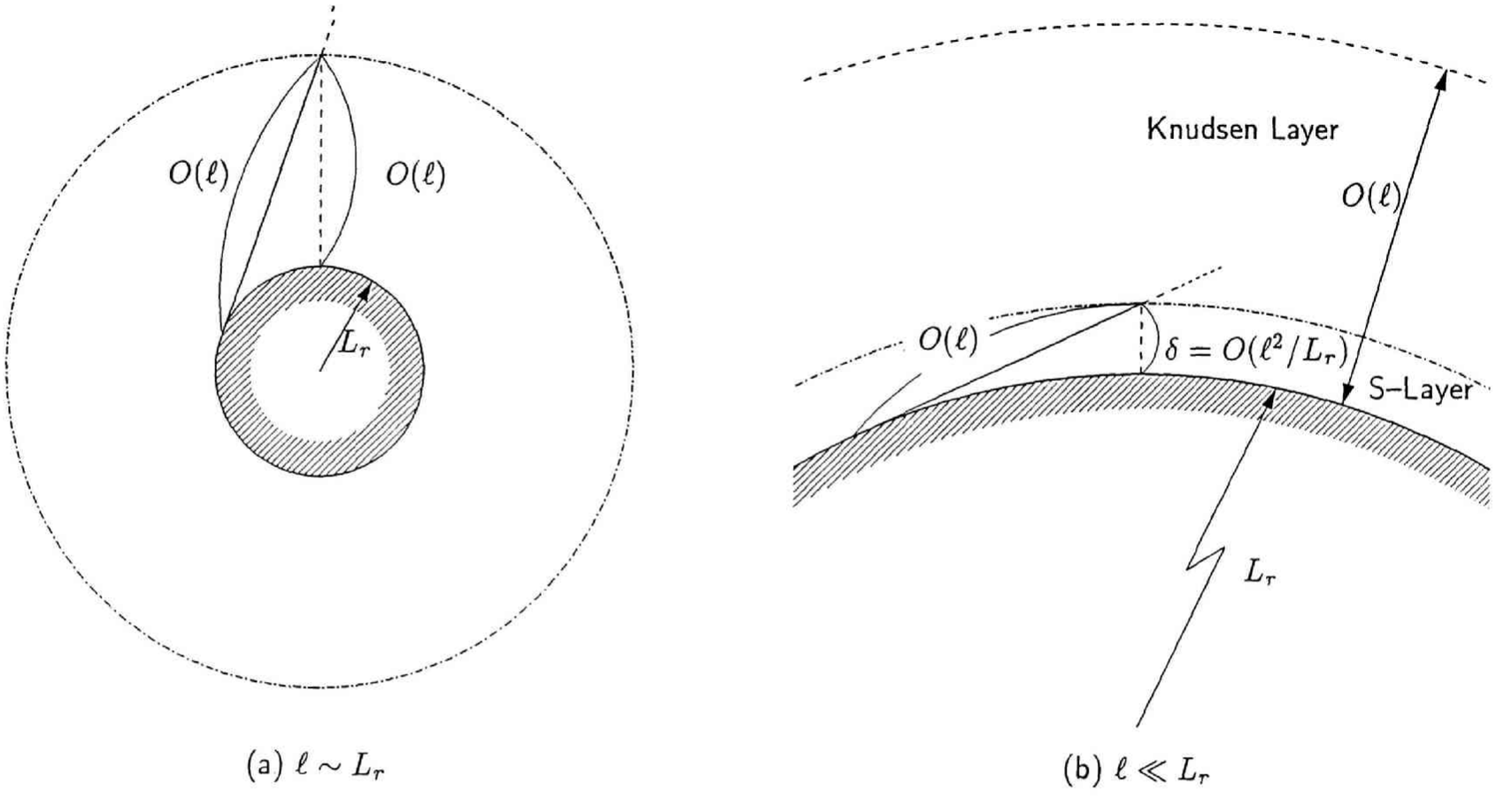

(a) $\ell \sim L_r$ (b) $\ell \ll L_r$

Fig. 3–3. Discontinuity of the velocity distribution function and the S-layer: (a) $\ell \sim L_r$; (b) $\ell \ll L_r$. The discontinuity is on a line tangent to the boundary at the velocity of the molecules leaving the boundary along this line. The discontinuity is appreciable on the solid line with length of $O(\ell)$, but it decays with distance from the boundary owing to molecular collisions and is negligible on the fine dashed line. For $\ell \sim L_r$ (a), the discontinuity extends to a region, shown by the chain line, of $O(\ell)$ from the boundary. For small ℓ/L_r (b), the discontinuity is in a thin layer, shown by the chain line, with thickness $\delta = O(\ell^2/L_r)$; the region, bounded by the dashed line, of $O(\ell)$ from the boundary is the Knudsen layer.

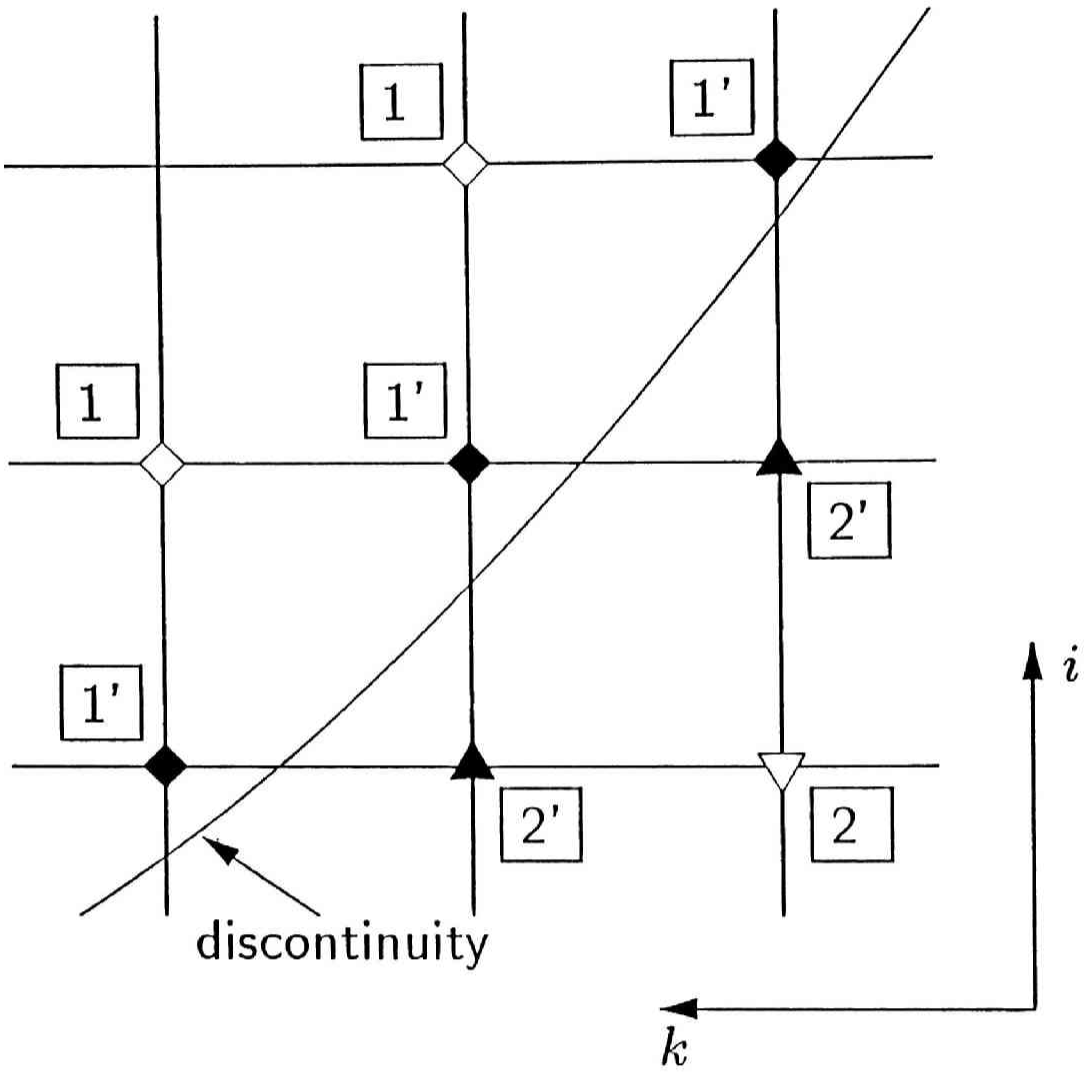

Fig. 3–4. Difference formulae at points near the discontinuity. When the lattice point (i, j, k) is at $\boxed{1}$, the difference formula (3–35) is used; $\boxed{1'}\rightarrow$ Eq. (3–37); $\boxed{2}\rightarrow$ Eq. (3–38); $\boxed{2'}\rightarrow$ Eq. (3–40).

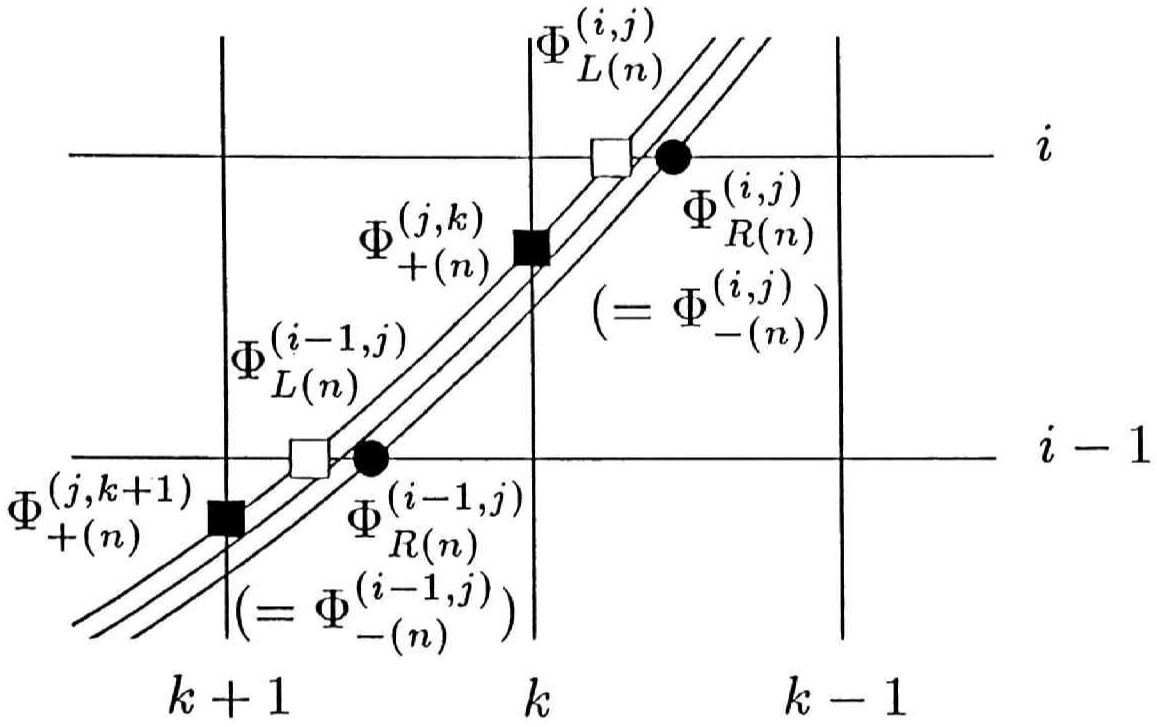

Fig. 3–5. The velocity distribution function $\Phi^{(i,j)}_{R(n)}$, $\Phi^{(i,j)}_{L(n)}$, $\Phi^{(i,j)}_{-(n)}$, and $\Phi^{(j,k)}_{+(n)}$ along the discontinuity. The $\Phi^{(i,j)}_{R(n)}$ and $\Phi^{(i,j)}_{L(n)}$ are the solutions of Eq. (3–42) under the initial conditions Eq. (3–17) and $\Phi^{(0,j)}_{L(n)} = \Phi^{(0,j,\hat{K})}_{(n)}$ respectively. Then, $\Phi^{(i,j)}_{-(n)} = \Phi^{(i,j)}_{R(n)}$, and $\Phi^{(j,k)}_{+(n)}$ is obtained by interpolation of $\Phi^{(i,j)}_{L(n)}$, $\Phi^{(i-1,j)}_{L(n)}$ (and $\Phi^{(i-2,j)}_{L(n)}$).

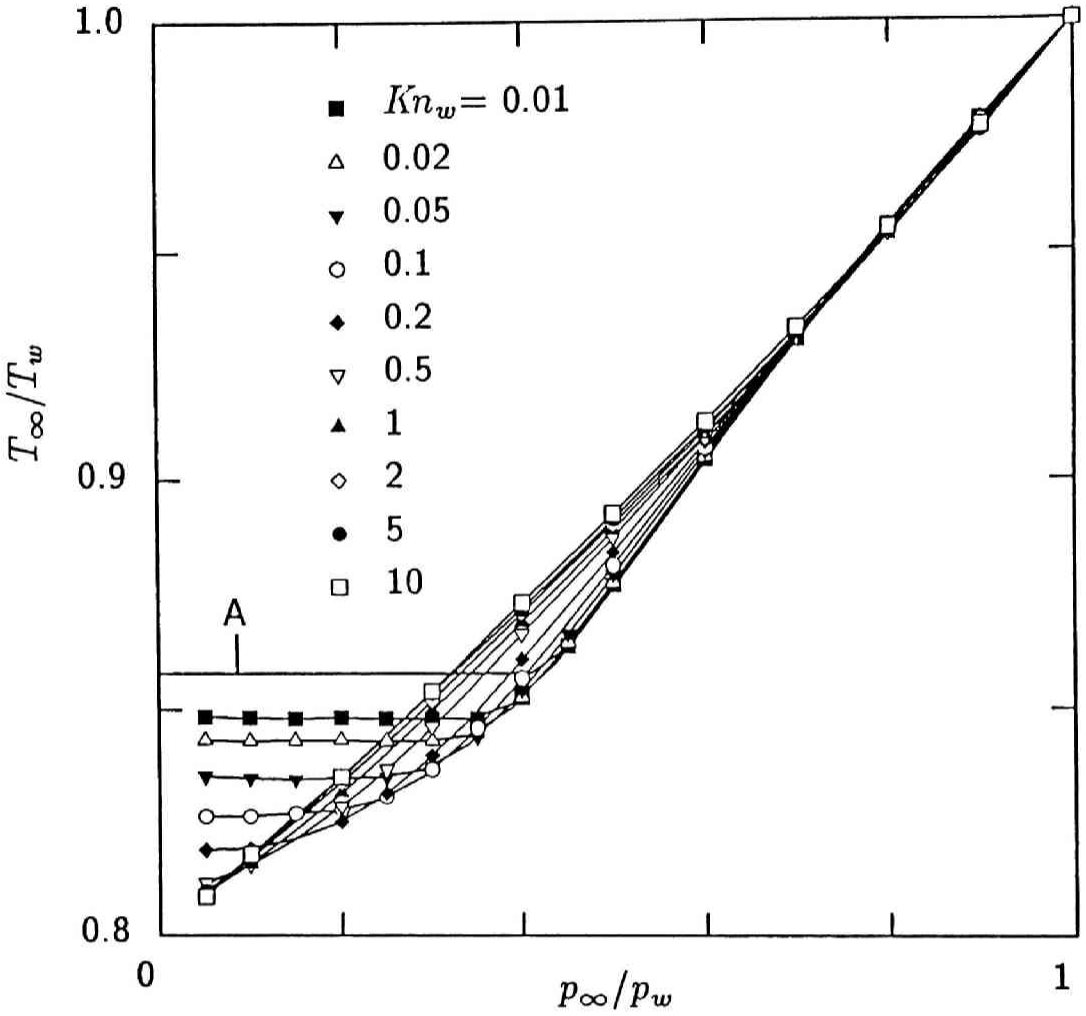

Fig. 3–6. The temperature ratio T_∞/T_w versus the pressure ratio p_∞/p_w for various Knudsen numbers Kn_w. The curve with the mark A is the asymptotic solution ((3–45a), (3–45b), and (3–46a)).

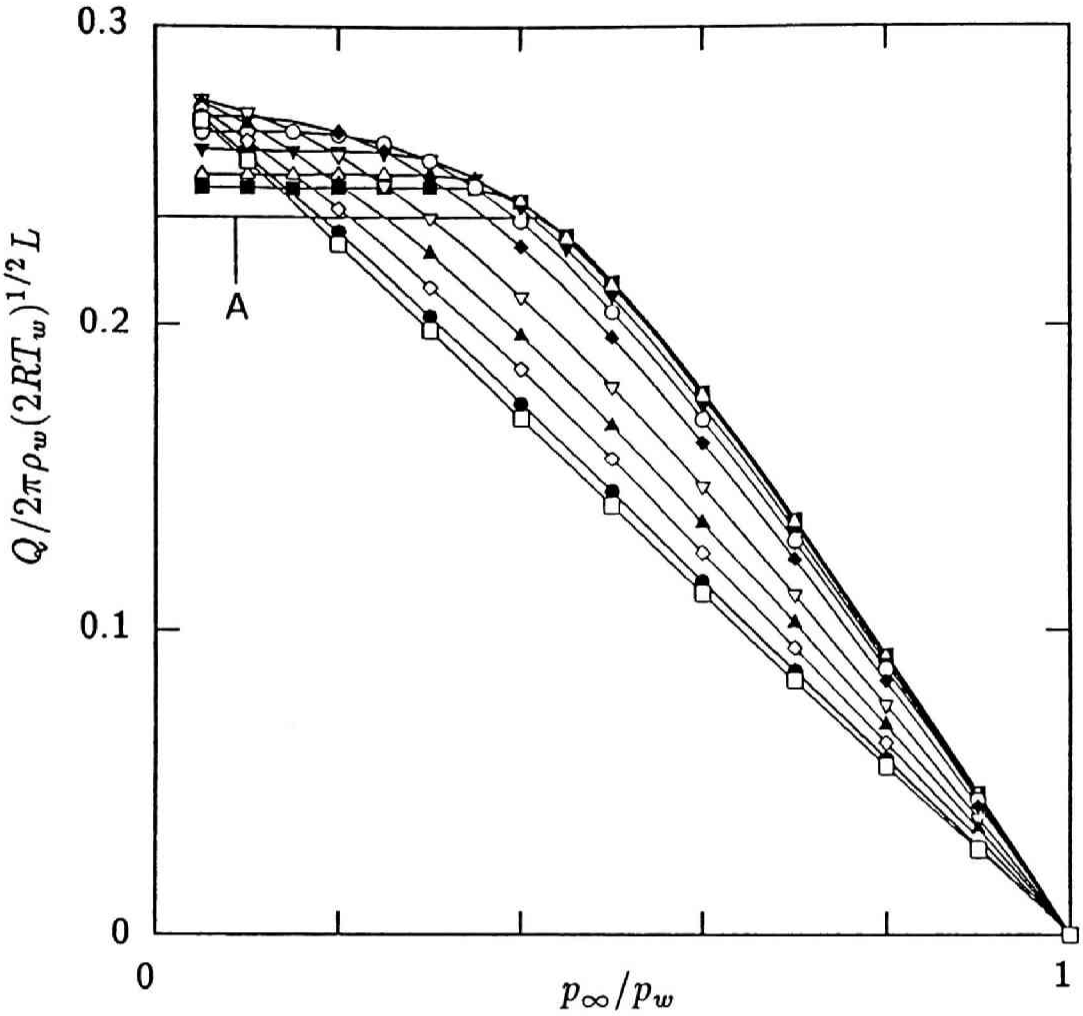

Fig. 3–7. The nondimensional mass flow rate $Q/(2\pi\rho_w(2RT_w)^{1/2}L)$ versus the pressure ratio p_∞/p_w for various Knudsen numbers Kn_w. The same symbols as in Fig. 3–6 are used to indicate the Knudsen number. The curve with the mark A is the asymptotic solution ((3–45a), (3–45d), (3–46c), and (3–47c)).

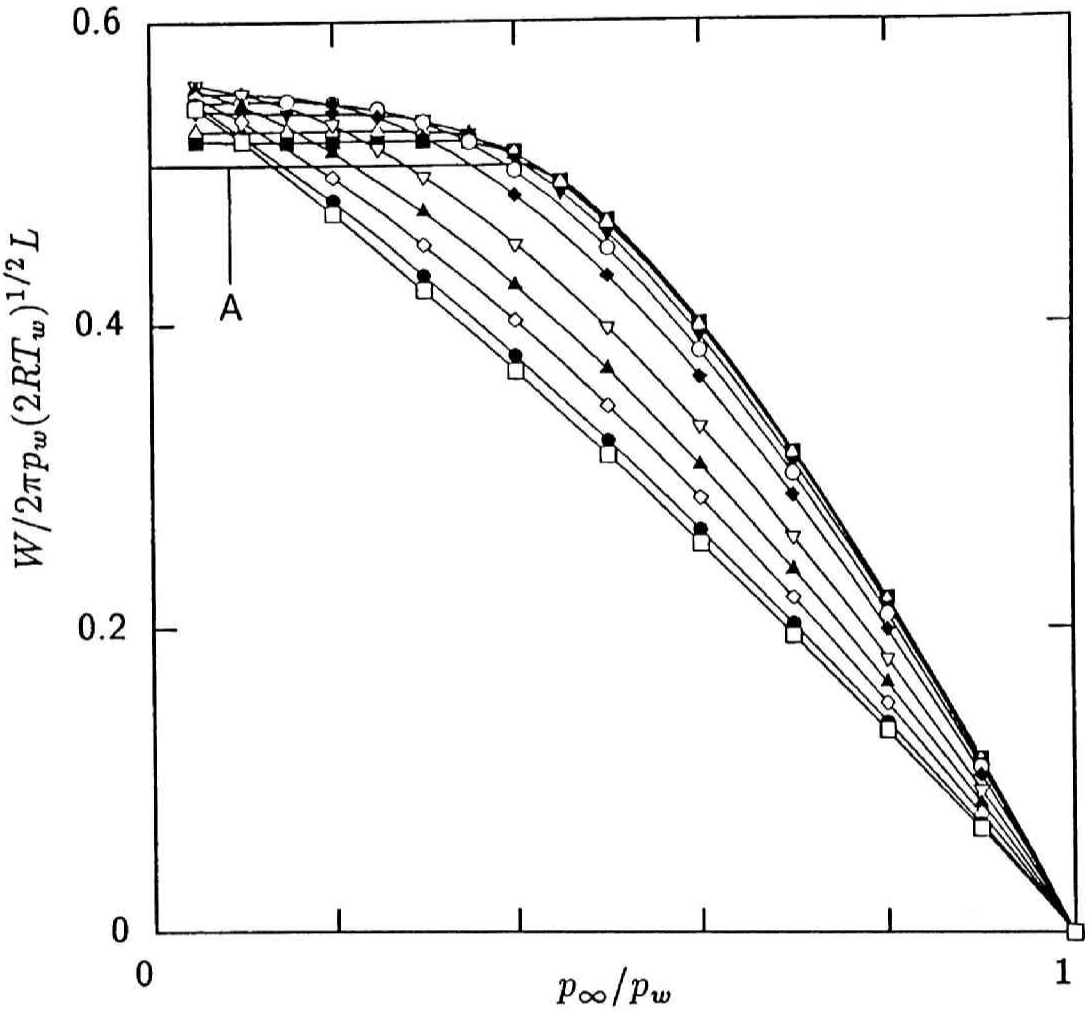

Fig. 3–8. The nondimensional energy flow rate $W/(2\pi p_w(2RT_w)^{1/2}L)$ versus the pressure rate p_∞/p_w for various Knudsen number Kn_w. The same symbols as in Fig. 3–6 are used to indicate the Knudsen number. The curve with the mark A is the asymptotic solution ((3–45a), (3–45e), (3–46d), and (3–47d)).

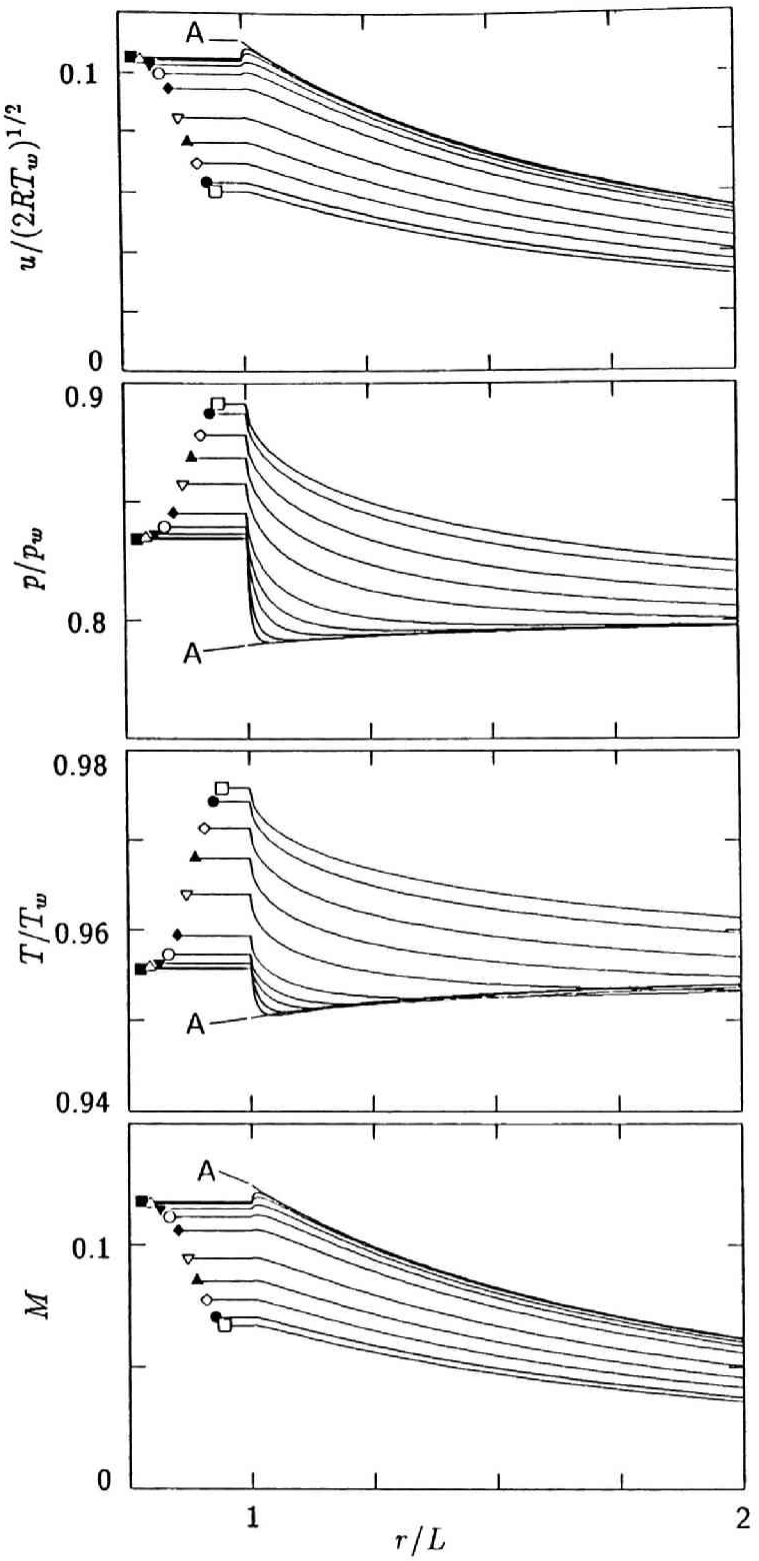

Fig. 3–9. The distributions of the nondimensional macroscopic variables, the flow velocity $u/(2RT_w)^{1/2}$, the pressure p/p_w, the temperature T/T_w, and the Mach number $M(= u/(5RT/3)^{1/2})$, for various Knudsen numbers Kn_w I: Case $p_\infty/p_w = 0.8$. The curves for $Kn_w = 0$, 0.01, 0.02, 0.05, 0.1, 0.2, 0.5, 1, 2, 5, and 10 are shown in the figure. They lie in the order (or the reverse order) of the Knudsen number near the cylinder, but in Figs. 10~14 they are not necessarily monotonically arranged on, or very near, the cylinder, where the curves can not be distinguished. The values on the cylinder are marked by ■ for $Kn_w = 0.01$, △ for 0.02, ▼ for 0.05, ○ for 0.1, ◆ for 0.2, ▽ for 0.5, ▲ for 1, ◇ for 2, ● for 5, and □ for 10. These are the same symbols as those in Fig. 3–6. The curves for $Kn_w = 0$, denoted by A, are obtained by the asymptotic theory[23], but their Knudsen layer corrections, which are flattened on the ordinates, are not shown here.

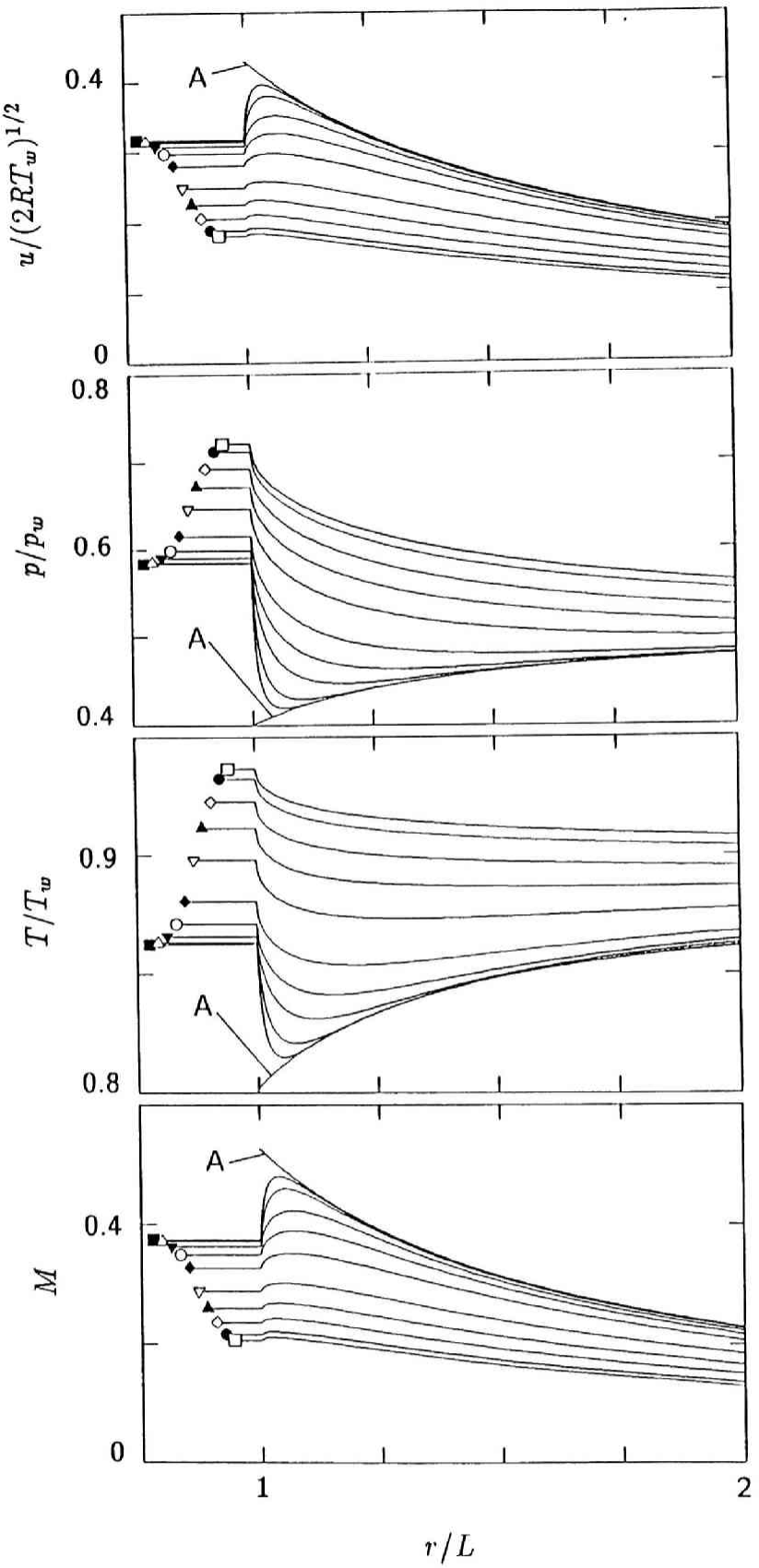

Fig. 3–10. The distributions of the nondimensional macroscopic variables, the flow velocity $u/(2RT_w)^{1/2}$, the pressure p/p_w, the temperature T/T_w, and the Mach number $M(= u/(5RT/3)^{1/2})$, for various Knudsen numbers Kn_w II: Case $p_\infty/p_w = 0.5$. (See the caption of Fig. 3–9.)

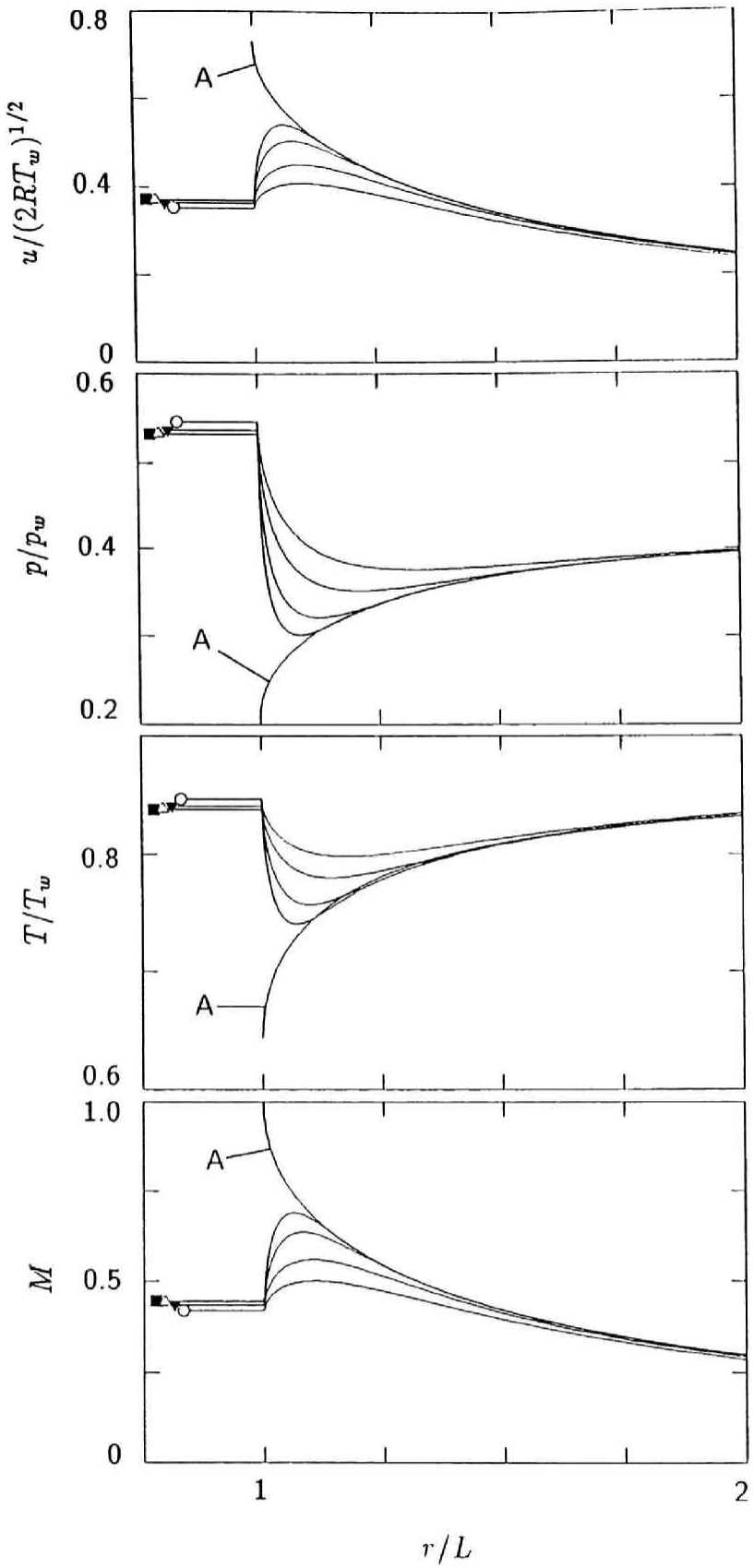

Fig. 3–11. The distributions of the nondimensional macroscopic variables, the flow velocity $u/(2RT_w)^{1/2}$, the pressure p/p_w, the temperature T/T_w, and the Mach number $M(= u/(5RT/3)^{1/2})$, for various Knudsen numbers Kn_w III: Case $p_\infty/p_w = 0.4260$, which is the branch point of supersonic or subsonic solutions for $Kn_w = 0$. (See the caption of Fig. 3–9.) Only the cases $Kn_w = 0$, 0.01, 0.02, 0.05, and 0.1 are given here.

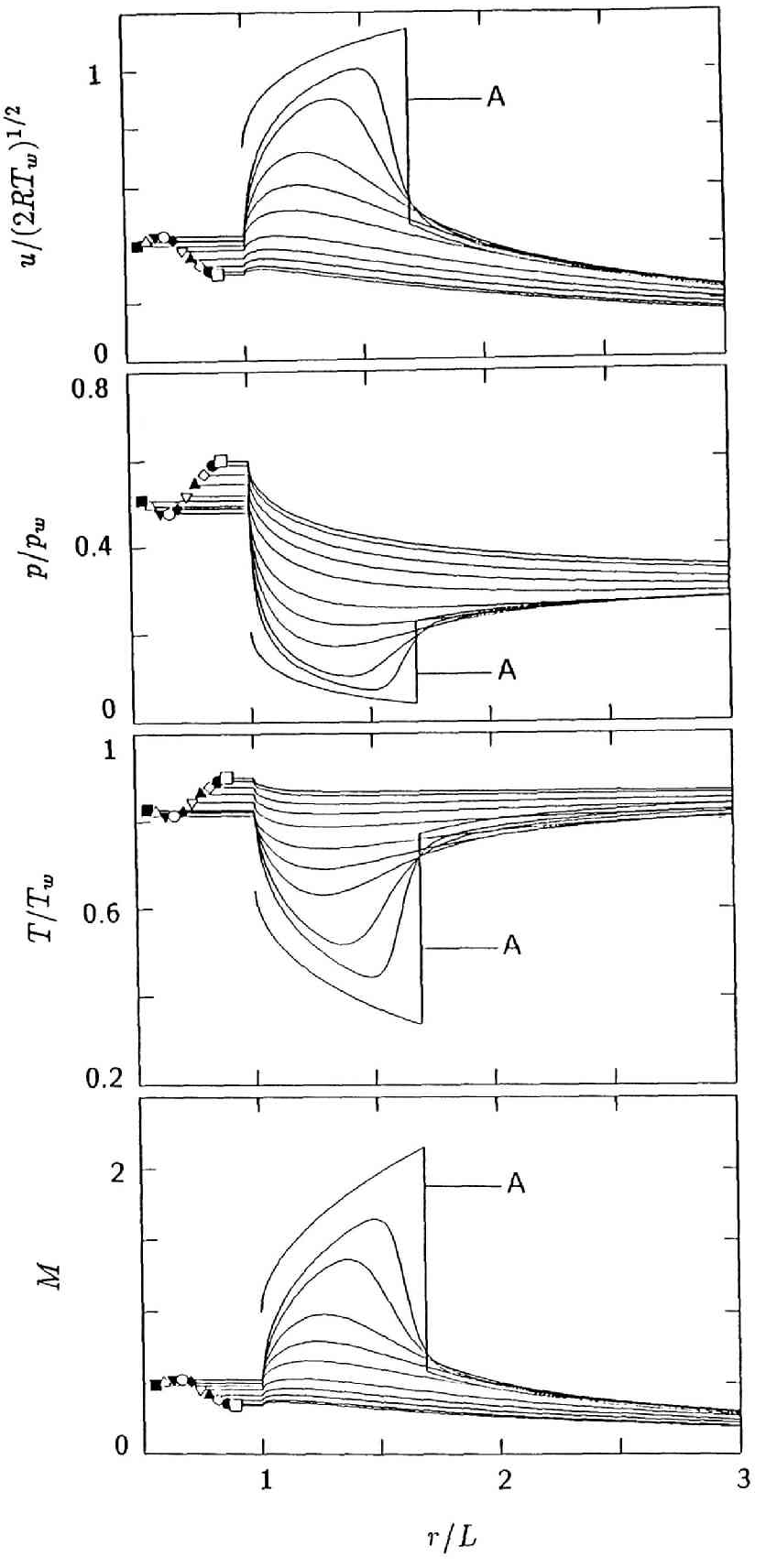

Fig. 3–12. The distributions of the nondimensional macroscopic variables, the flow velocity $u/(2RT_w)^{1/2}$, the pressure p/p_w, the temperature T/T_w, and the Mach number $M(= u/(5RT/3)^{1/2})$, for various Knudsen numbers Kn_w IV: Case $p_\infty/p_w = 0.3$. (See the caption of Fig. 3–9.)

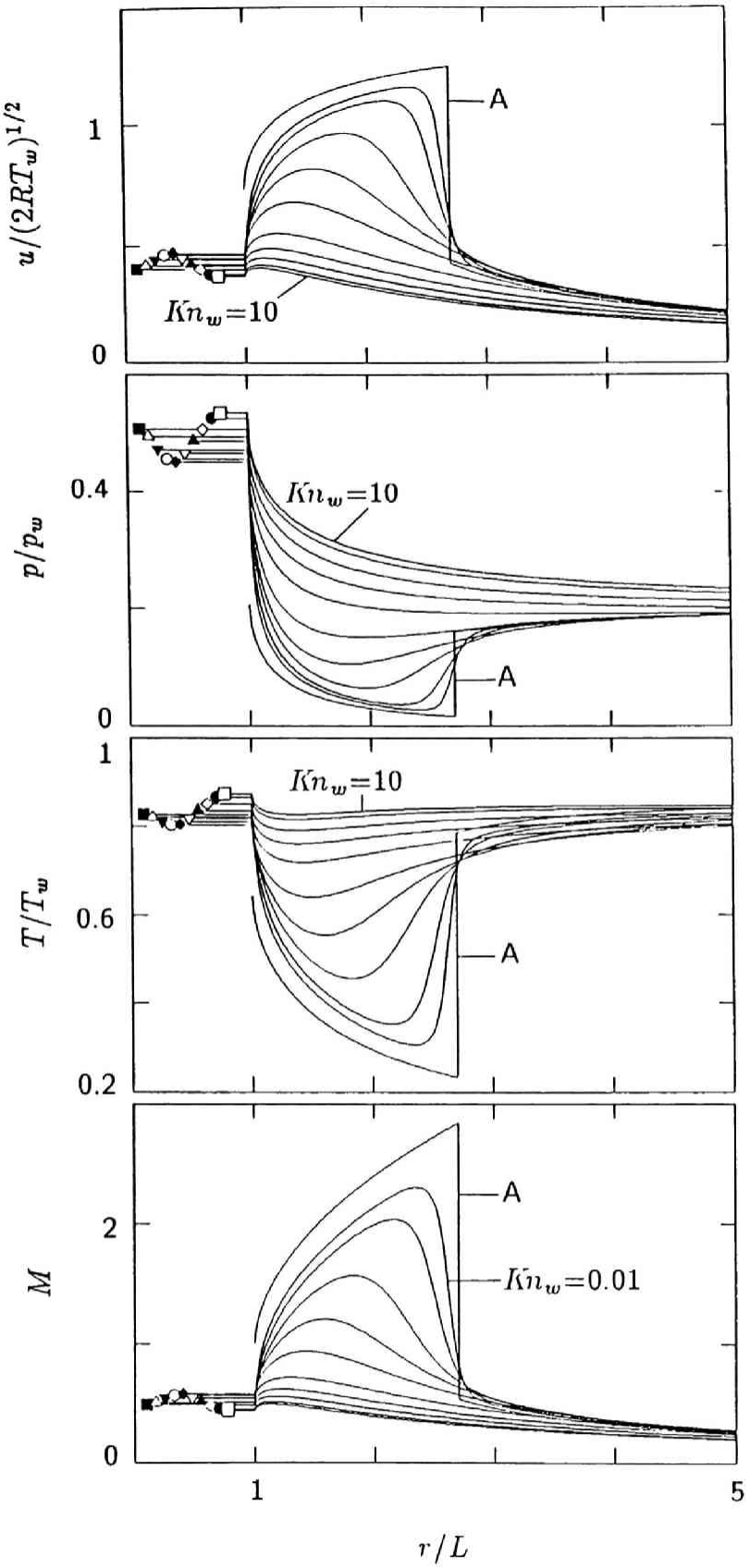

Fig. 3–13. The distributions of the nondimensional macroscopic variables, the flow velocity $u/(2RT_w)^{1/2}$, the pressure p/p_w, the temperature T/T_w, and the Mach number $M(= u/(5RT/3)^{1/2})$, for various Knudsen numbers Kn_w V: Case $p_\infty/p_w = 0.2$. (See the caption of Fig. 3–9.)

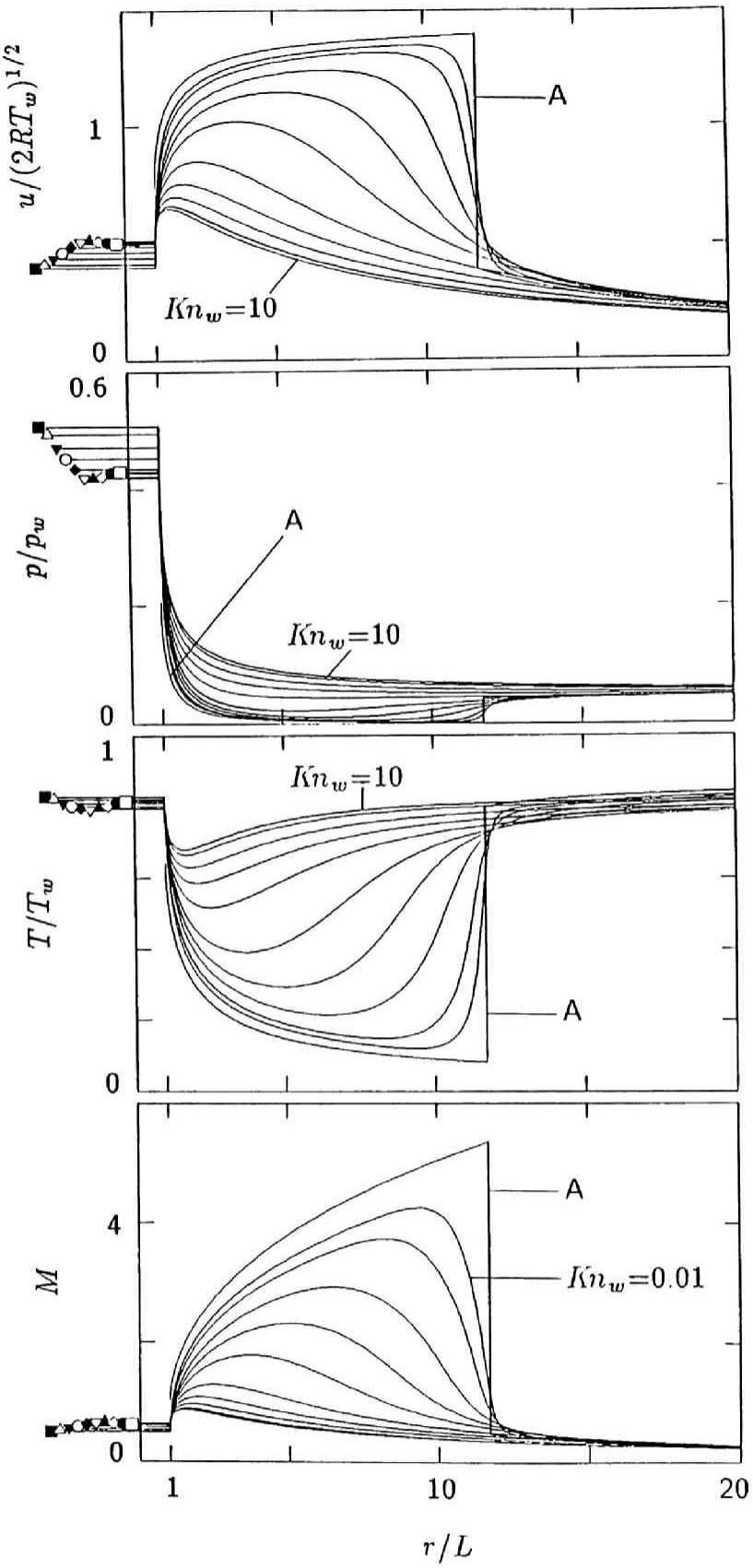

Fig. 3–14. The distributions of the nondimensional macroscopic variables, the flow velocity $u/(2RT_w)^{1/2}$, the pressure p/p_w, the temperature T/T_w, and the Mach number $M(= u/(5RT/3)^{1/2})$, for various Knudsen numbers Kn_w VI: Case $p_\infty/p_w = 0.05$. (See the caption of Fig. 3–9.)

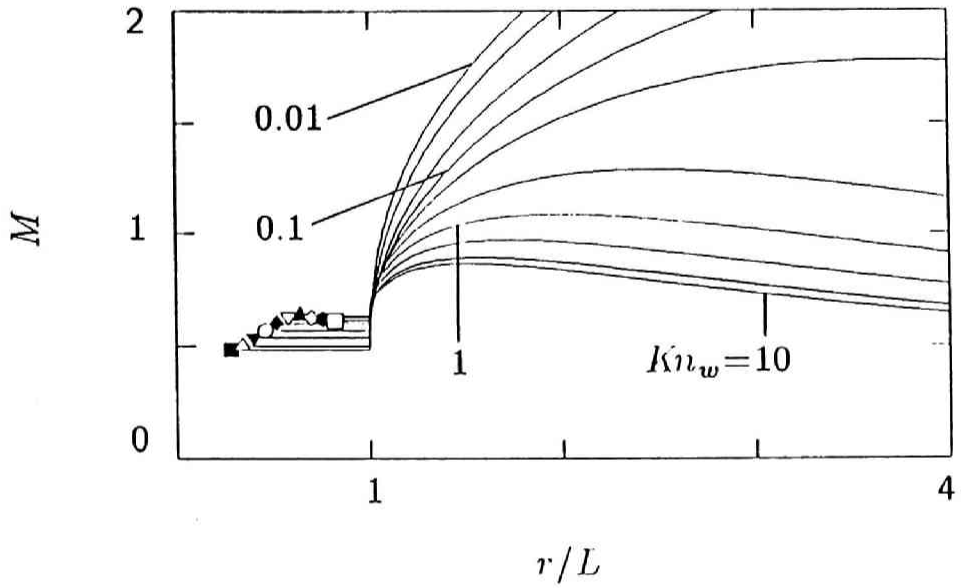

Fig. 3–15. Sharp acceleration to supersonic flows near the condensed phase (p_∞/p_w =0.05). The curves for Kn_w = 0.01, 0.02, 0.05, 0.1, 0.2, 0.5, 1, 2, 5, and 10 are shown. This is an enlarged figure around the cylinder of Fig. 3–14. The values on the cylinder are shown by the same symbols as in Fig. 3–9 (see the caption of Fig. 3–9).

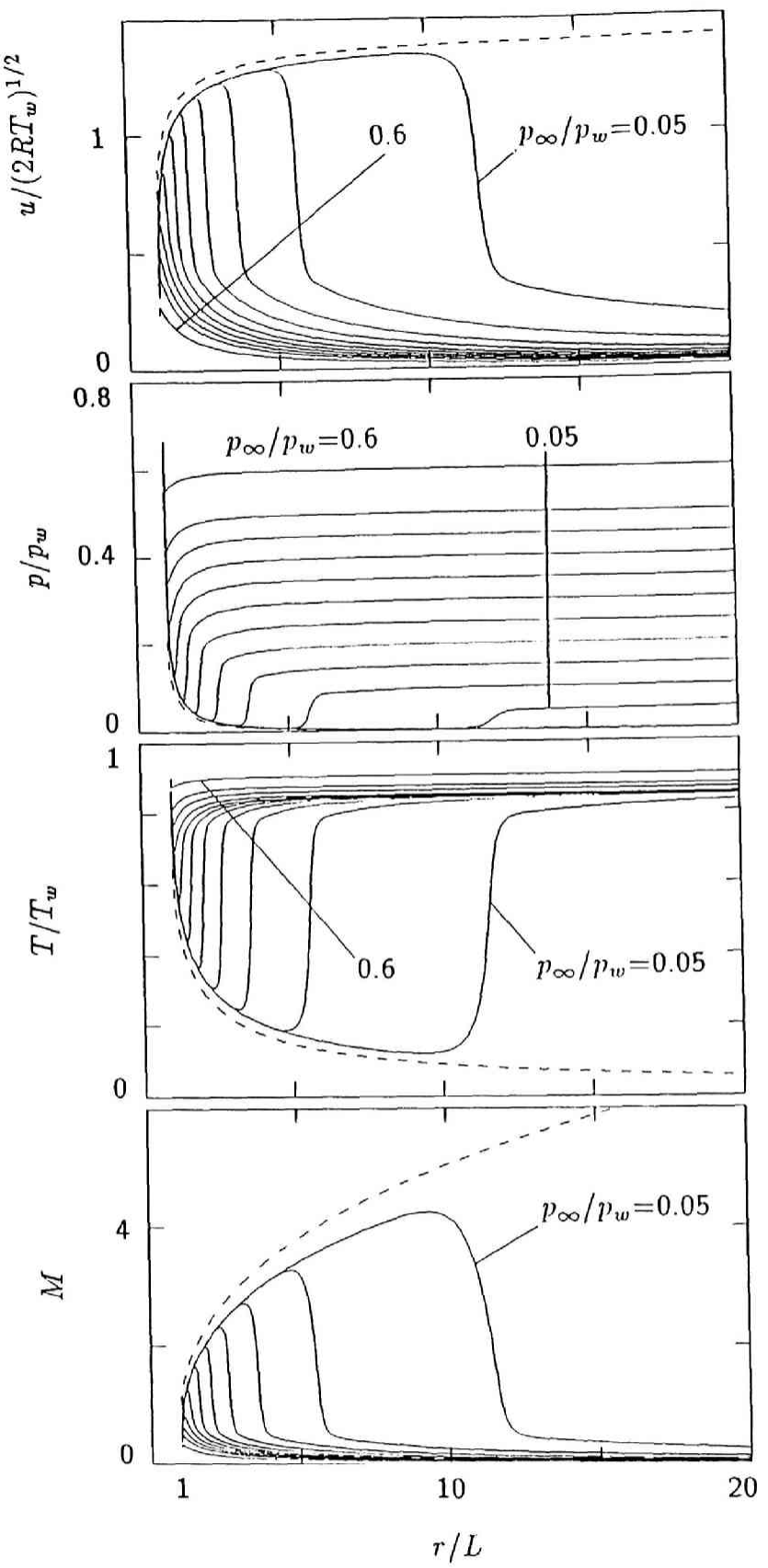

Fig. 3–16. Comparison of the distributions of the nondimensional macroscopic variables of different pressure ratios I: Case $Kn_w = 0.01$. The curves for $p_\infty/p_w = 0.05$, 0.1, 0.15, 0.2, 0.25, 0.3, 0.35, 0.4, 0.45, 0.5, and 0.6 are shown. They are lined in the order of p_∞/p_w. The supersonic branch of the continuum solution ($Kn_w = 0$) is shown by dashed lines for reference.

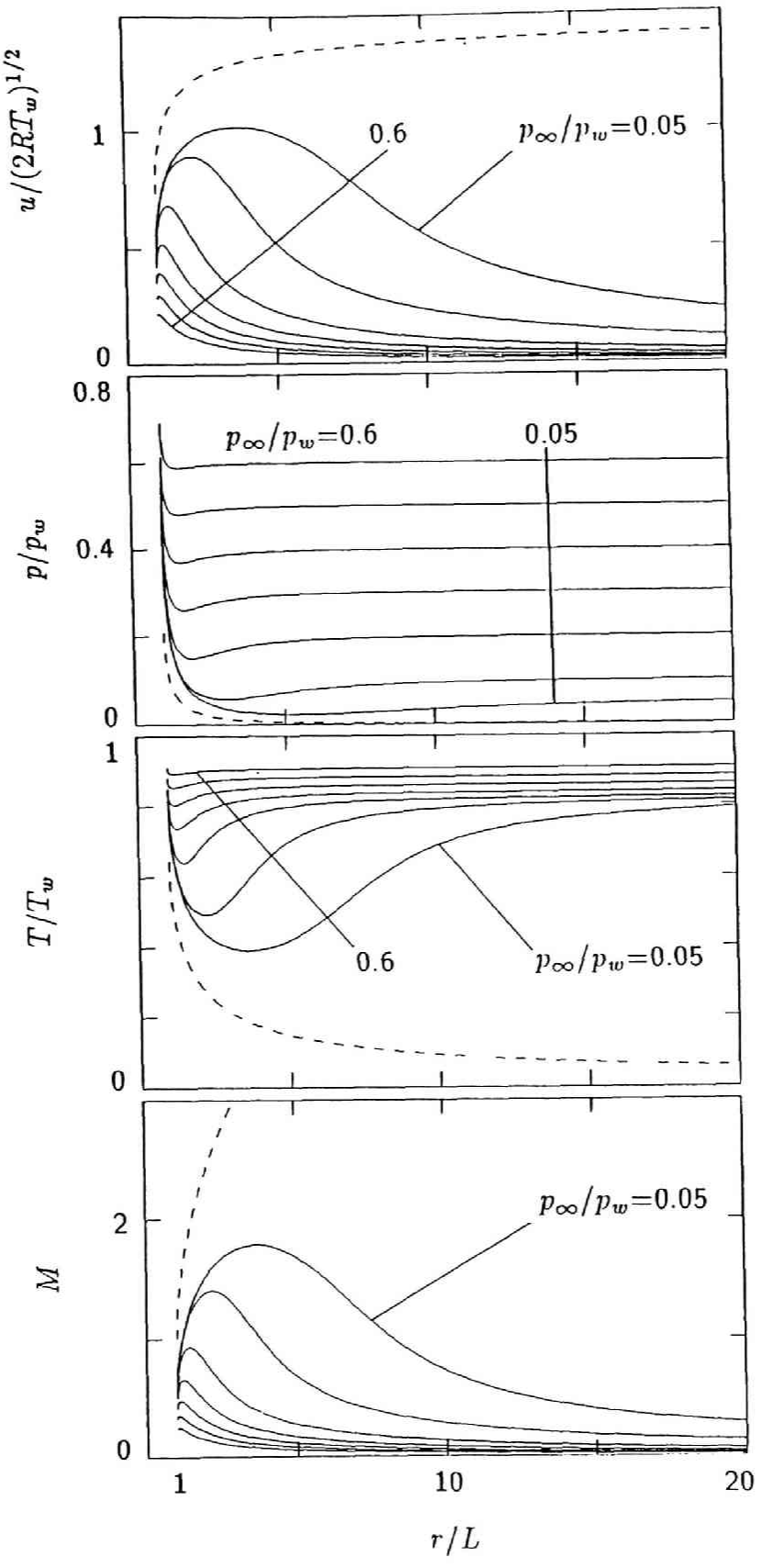

Fig. 3–17. Comparison of the distributions of the nondimensional macroscopic variables of different pressure ratios II: Case $Kn_w = 0.2$. The curves for $p_\infty/p_w = 0.05$, 0.1, 0.2, 0.3, 0.4, 0.5, and 0.6 are shown. They are lined in the order of p_∞/p_w. The supersonic branch of the continuum solution ($Kn_w = 0$) is shown by dashed lines for reference.

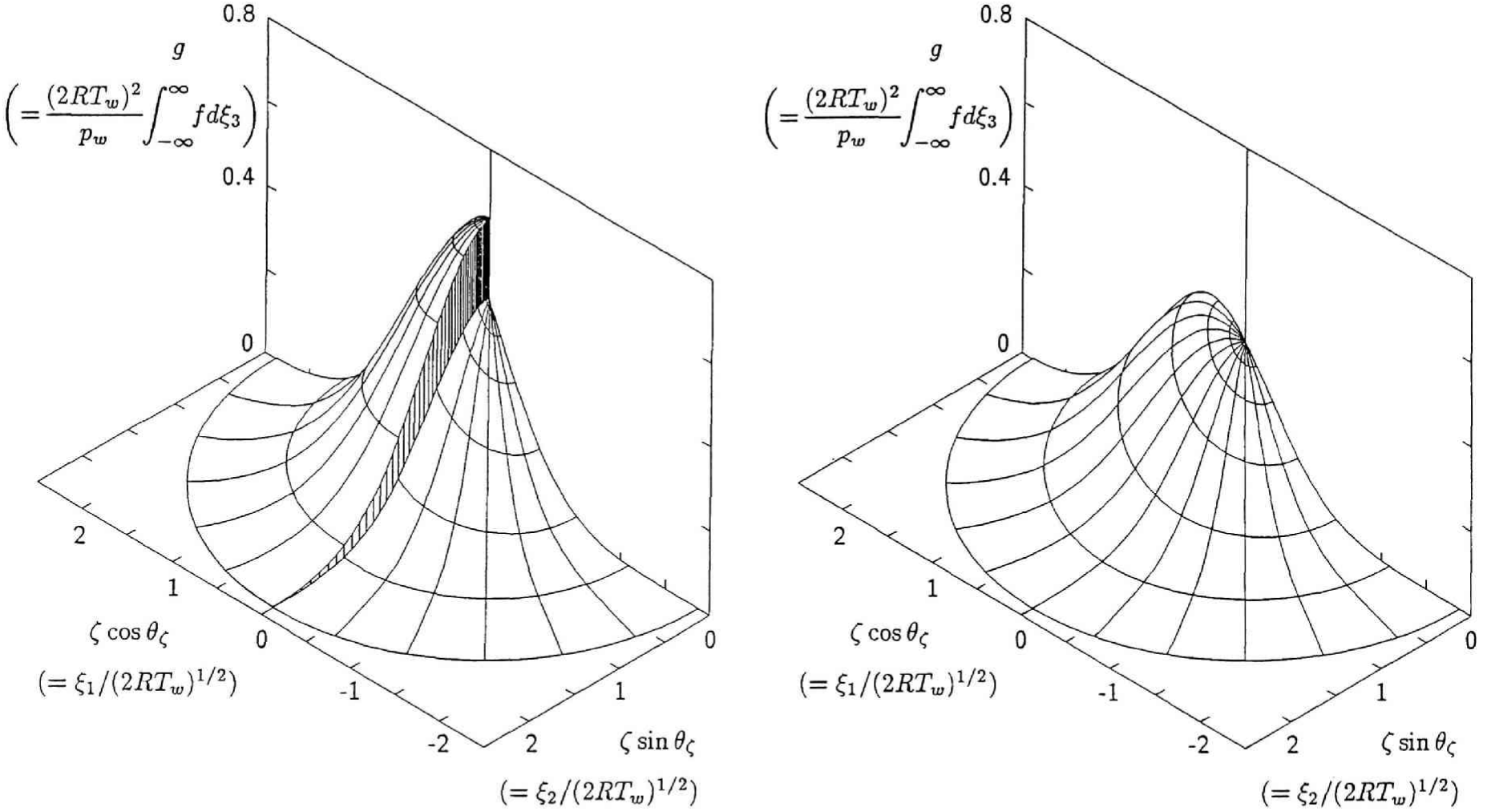

Fig. 3–18. The marginal velocity distribution function $g(=(2RT_w)^2 p_w^{-1}\int_{-\infty}^{\infty} f d\xi_3)$ at three points in the gas for $p_\infty/p_w = 0.5$ and $Kn_w = 0.01$. (a) $r/L = 1$, (b) $r/L = 1.102$, and (c) $r/L = 2.499$. The surface g is shown by some (not all) of the lattice lines ζ =const and θ_ζ =const. The vertical stripes show the discontinuity of g. The $\xi_1/(2RT_w)^{1/2}$ and $\xi_2/(2RT_w)^{1/2}$ in the parentheses are these coordinates of the case where the point under consideration lies on the positive x_1 axis.

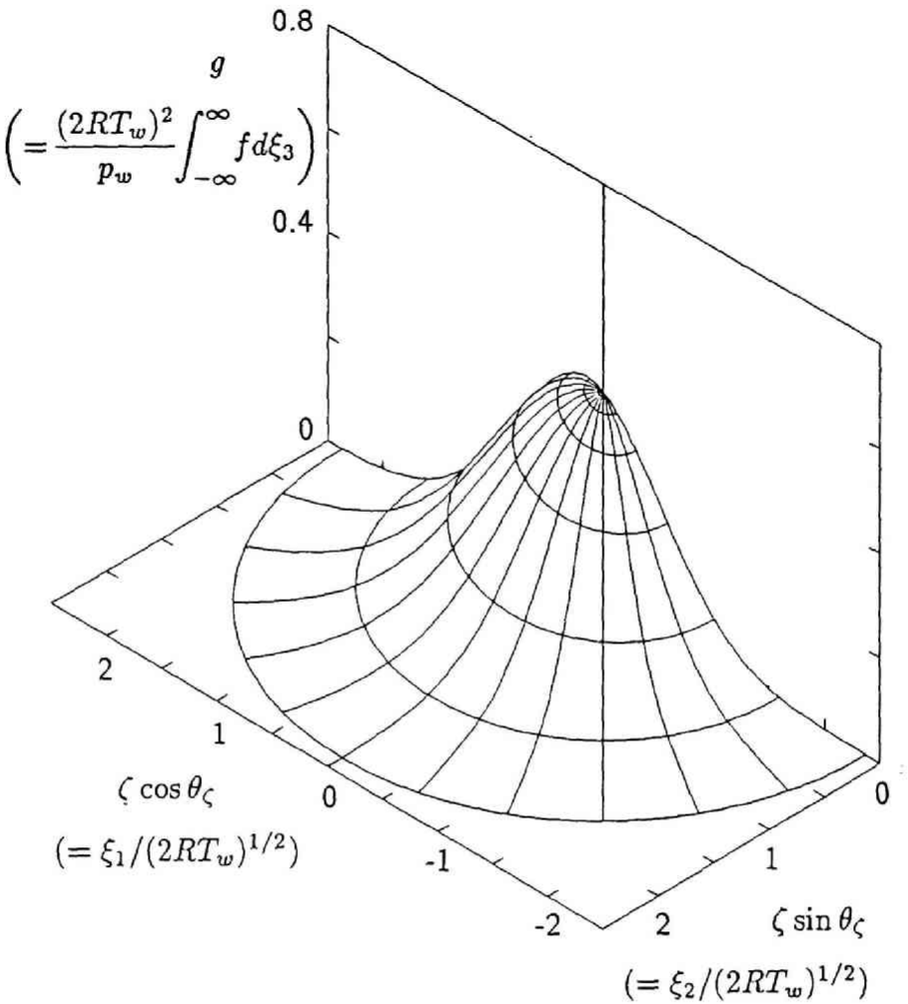

(c) $r/L = 2.499$

Fig. 3–18. (cont.)

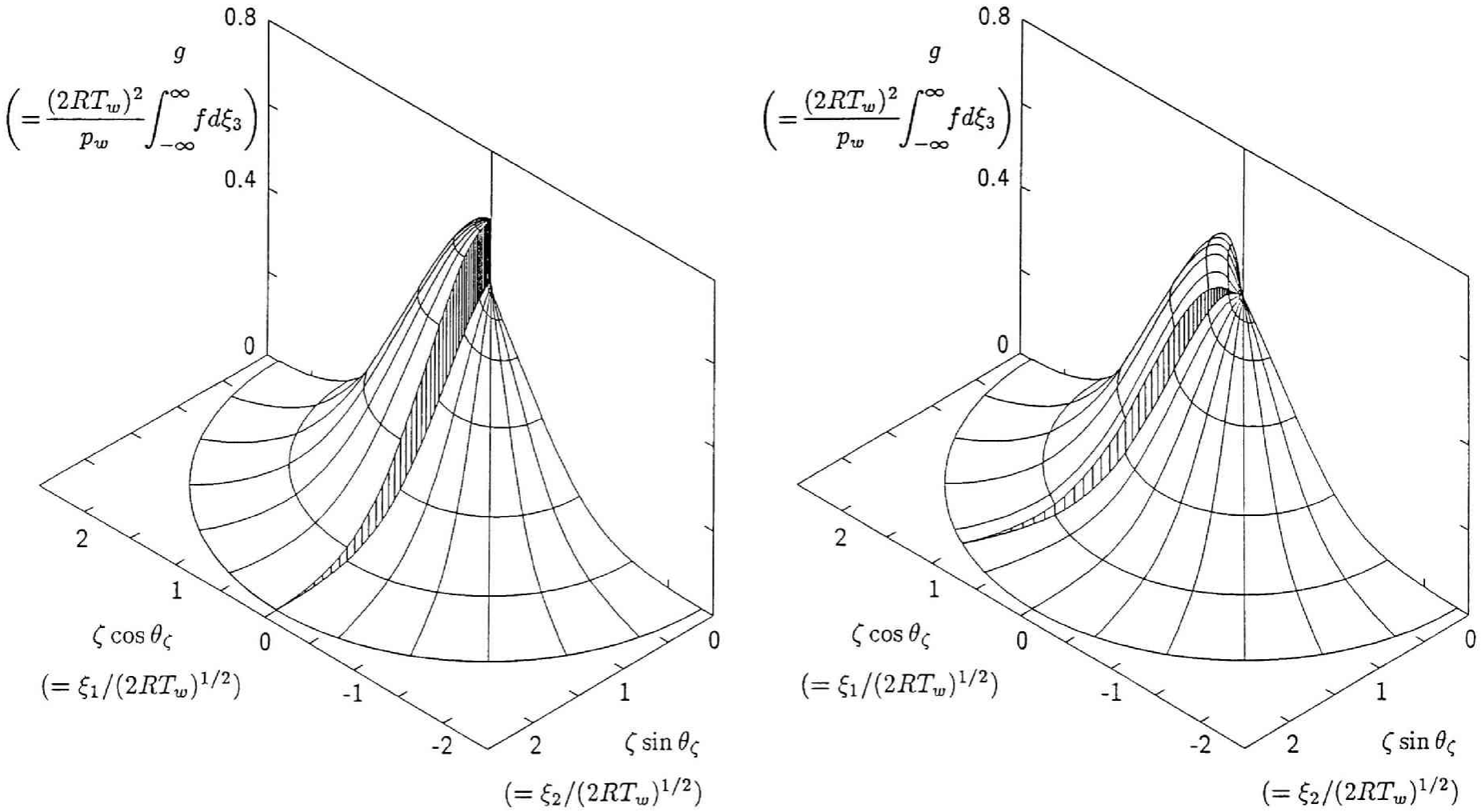

(a) $r/L = 1$

(b) $r/L = 1.106$

Fig. 3–19. The marginal velocity distribution function g at three points in the gas for $p_\infty/p_w = 0.5$ and $Kn_w = 1$. (a) $r/L = 1$, (b) $r/L = 1.106$, and (c) $r/L = 2.469$. (See the caption of Fig. 3–18.)

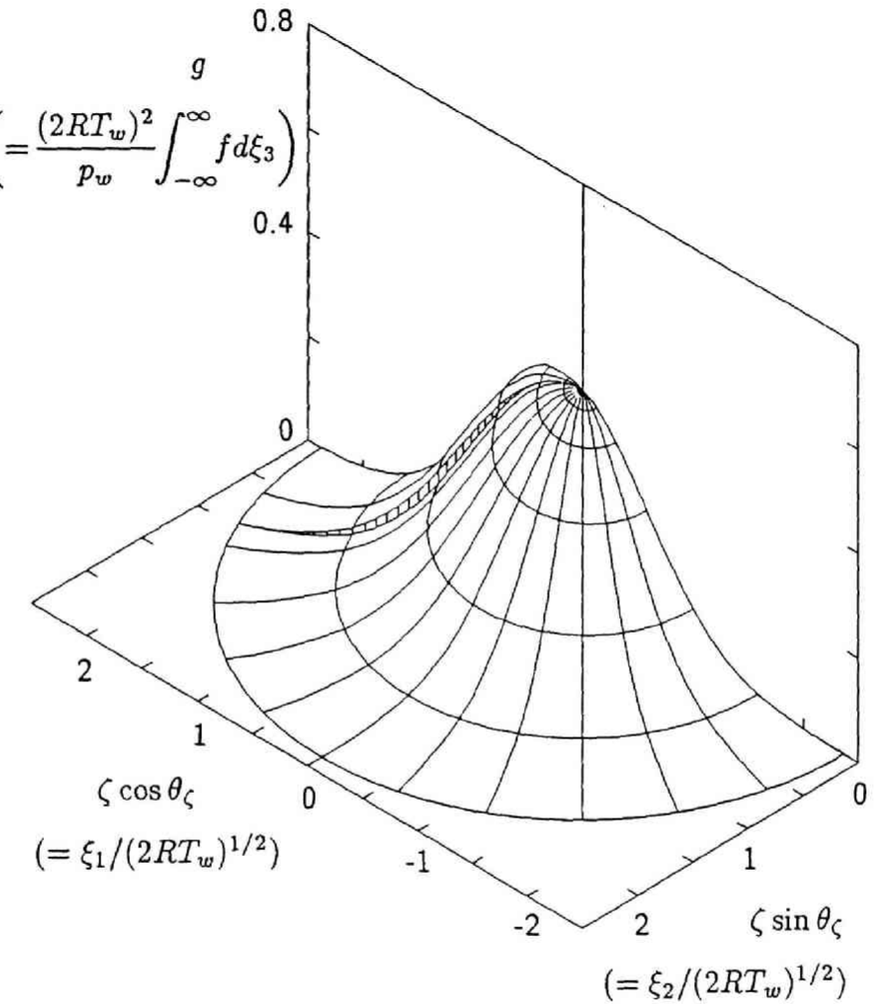

(c) $r/L = 2.469$

Fig. 3–19. (cont.)

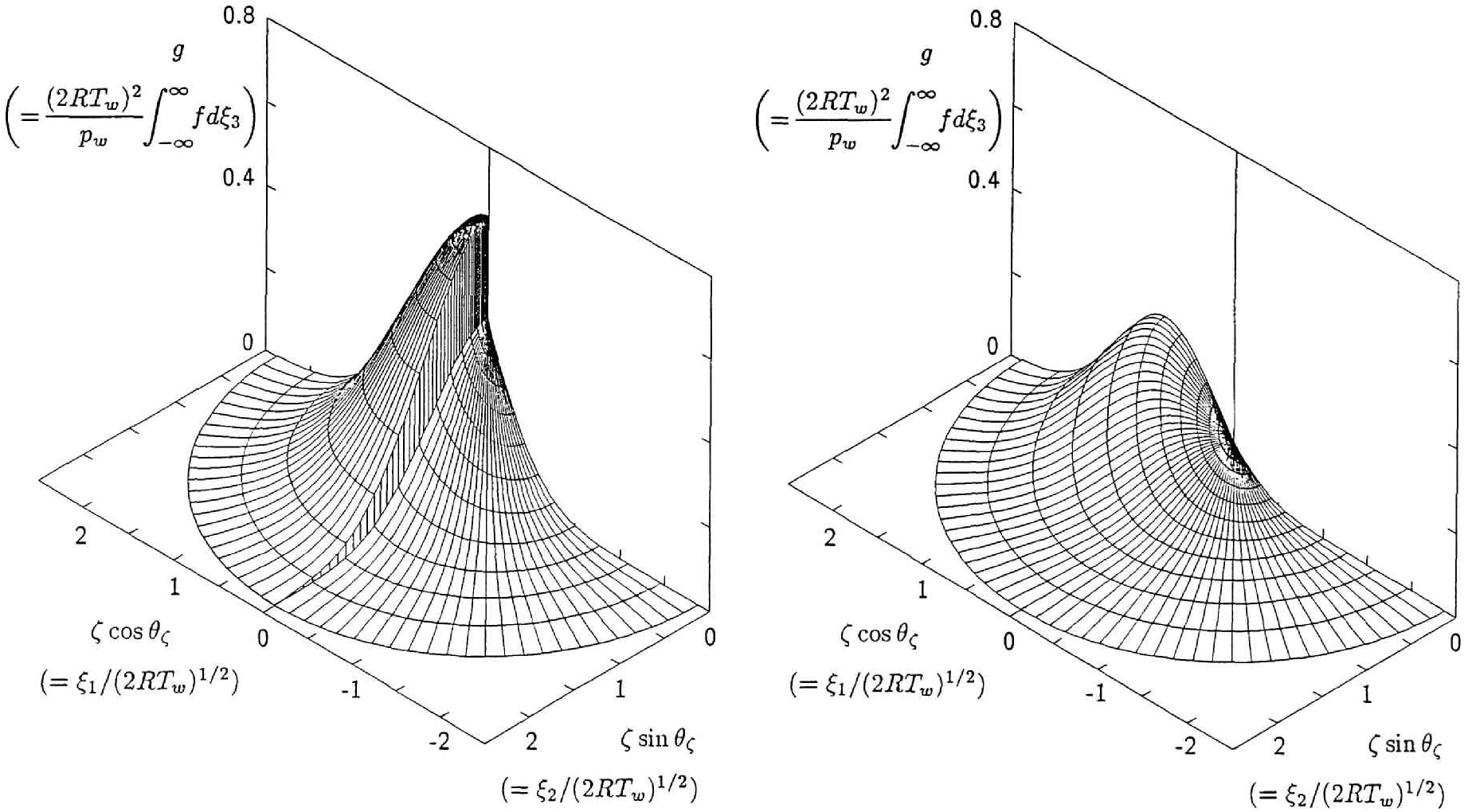

Fig. 3–20. The marginal velocity distribution function g at five points in the gas for $p_\infty/p_w = 0.05$ and $Kn_w = 0.01$. (a) $r/L = 1$, (b) $r/L = 1.105$, (c) $r/L = 10.23$, (d) $r/L = 12.03$, and (e) $r/L = 13.02$. (See the caption of Fig. 3–18.) Note the difference in scale between the first two figures ((a) and (b)) and the rest ((c), (d), and (e)).

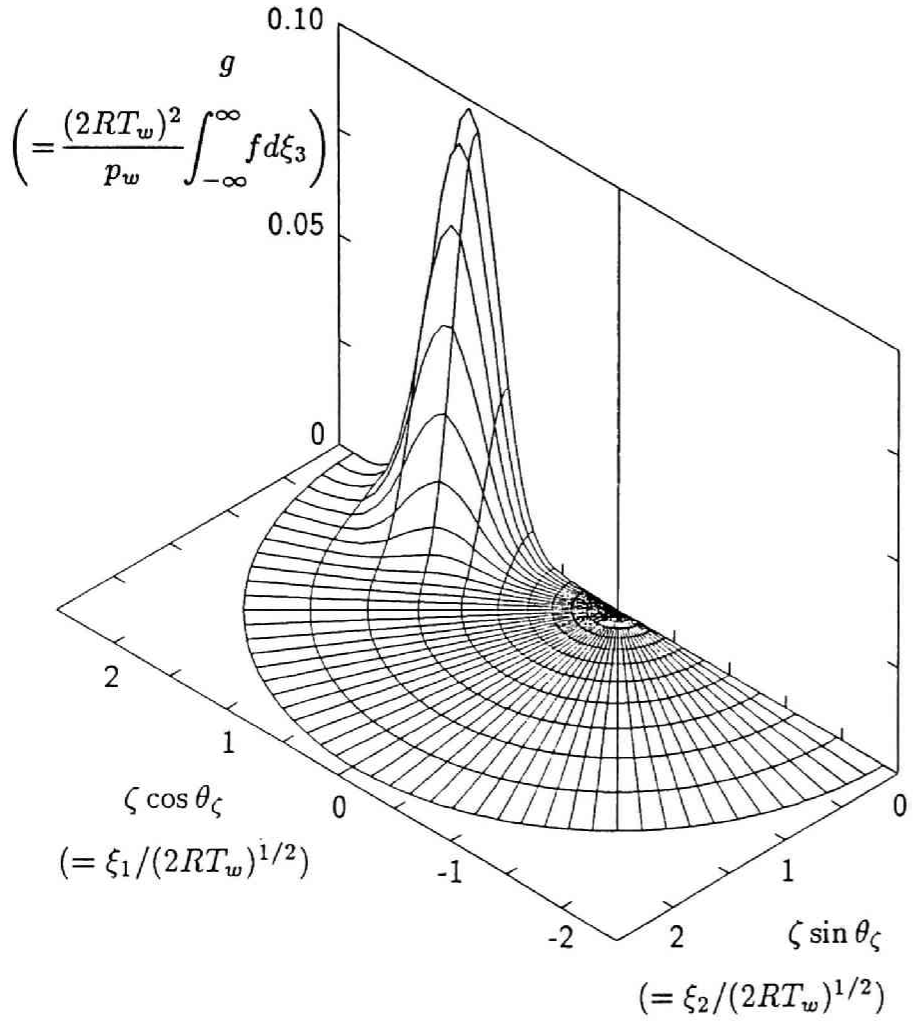

(c) $r/L = 10.23$

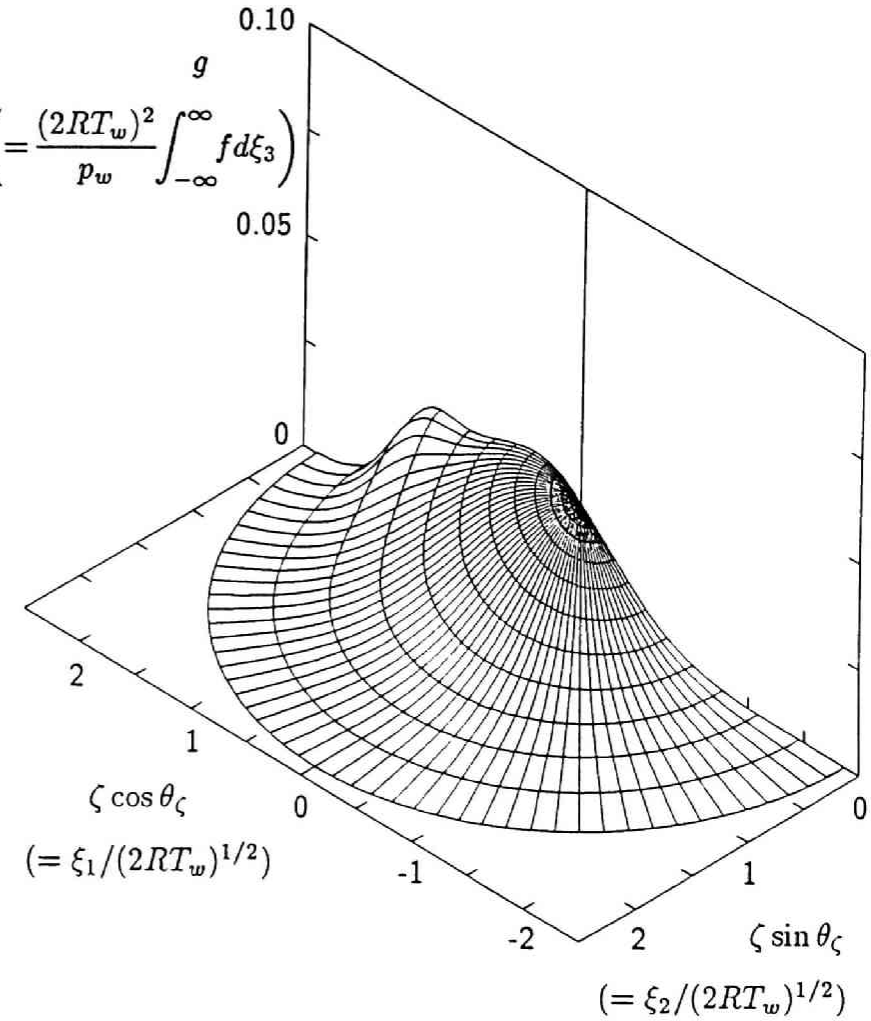

(d) $r/L = 12.03$

Fig. 3–20. (cont.)

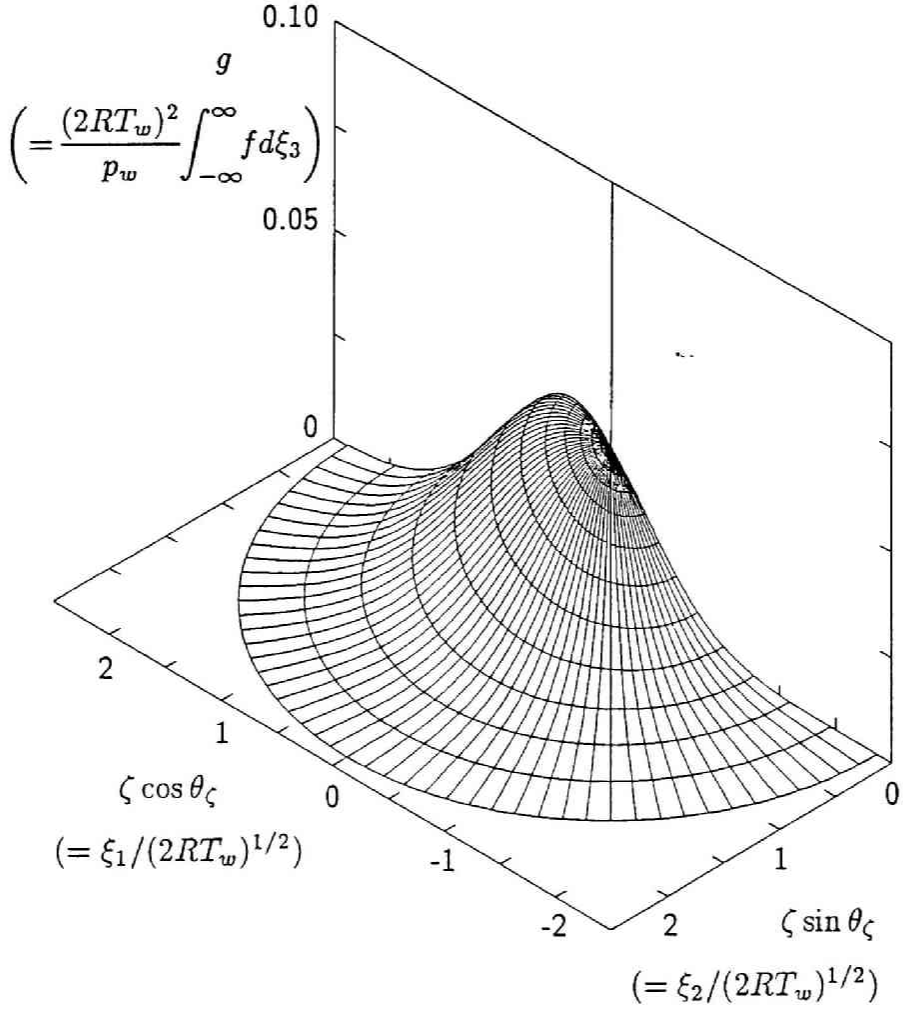

(e) $r/L = 13.02$

Fig. 3–20. (cont.)

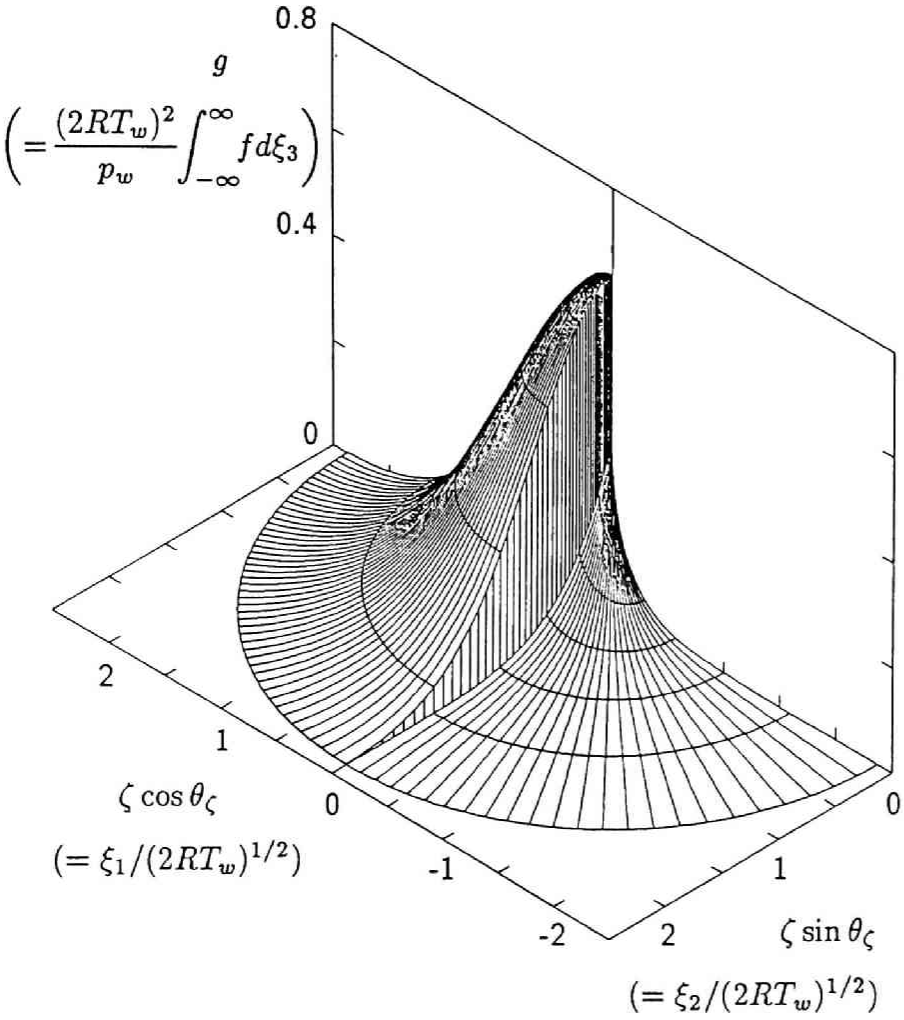

(a) $r/L = 1$

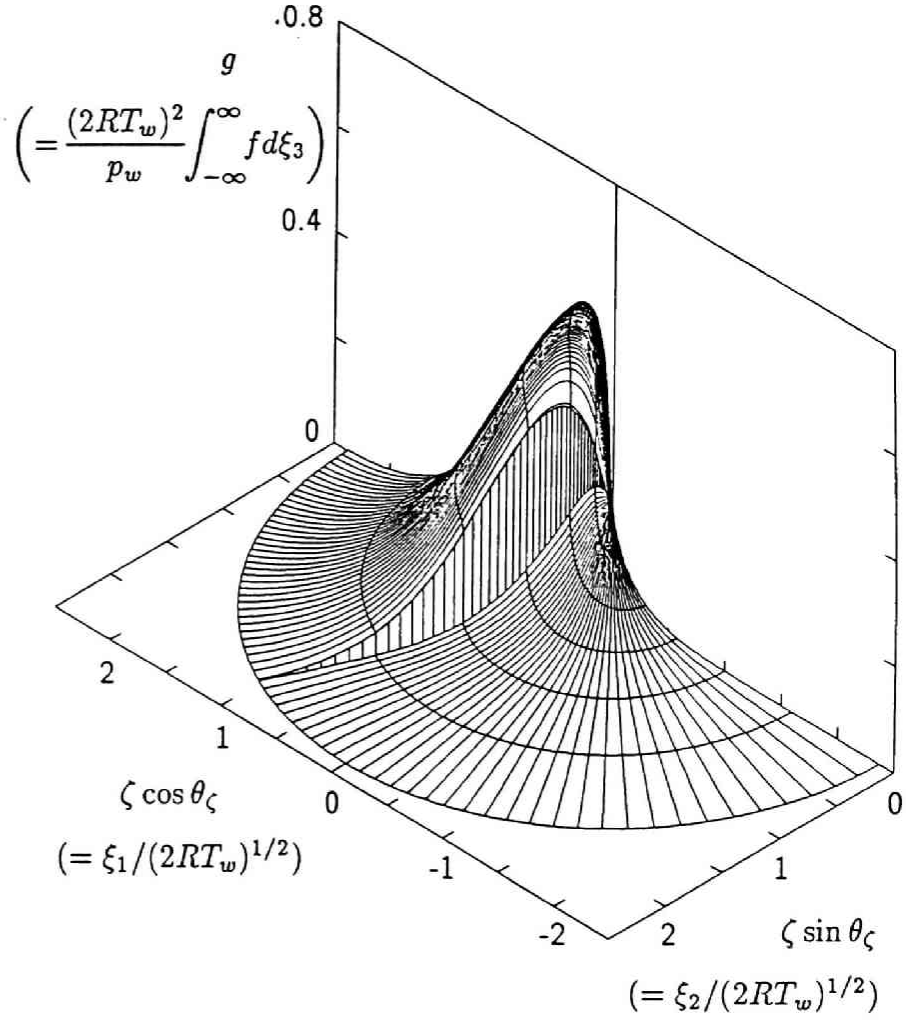

(b) $r/L = 1.106$

Fig. 3–21. The marginal velocity distribution function g at four points in the gas for $p_\infty/p_w = 0.05$ and $Kn_w = 1$. (a) $r/L = 1$, (b) $r/L = 1.106$, (c) $r/L = 10.15$, and (d) $r/L = 19.98$. (See the caption of Fig. 3–18.) Note the difference in scale between the first two figures ((a) and (b)) and the rest ((c) and (d)).

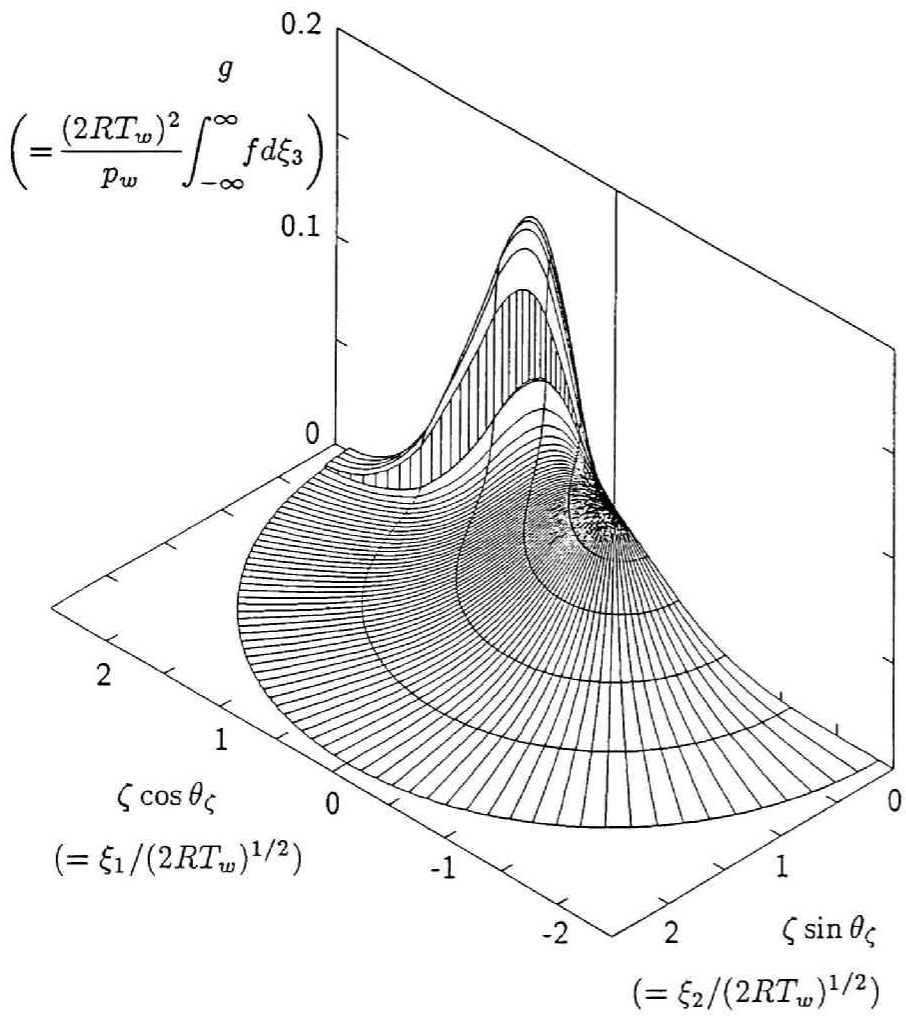

(c) $r/L = 10.15$

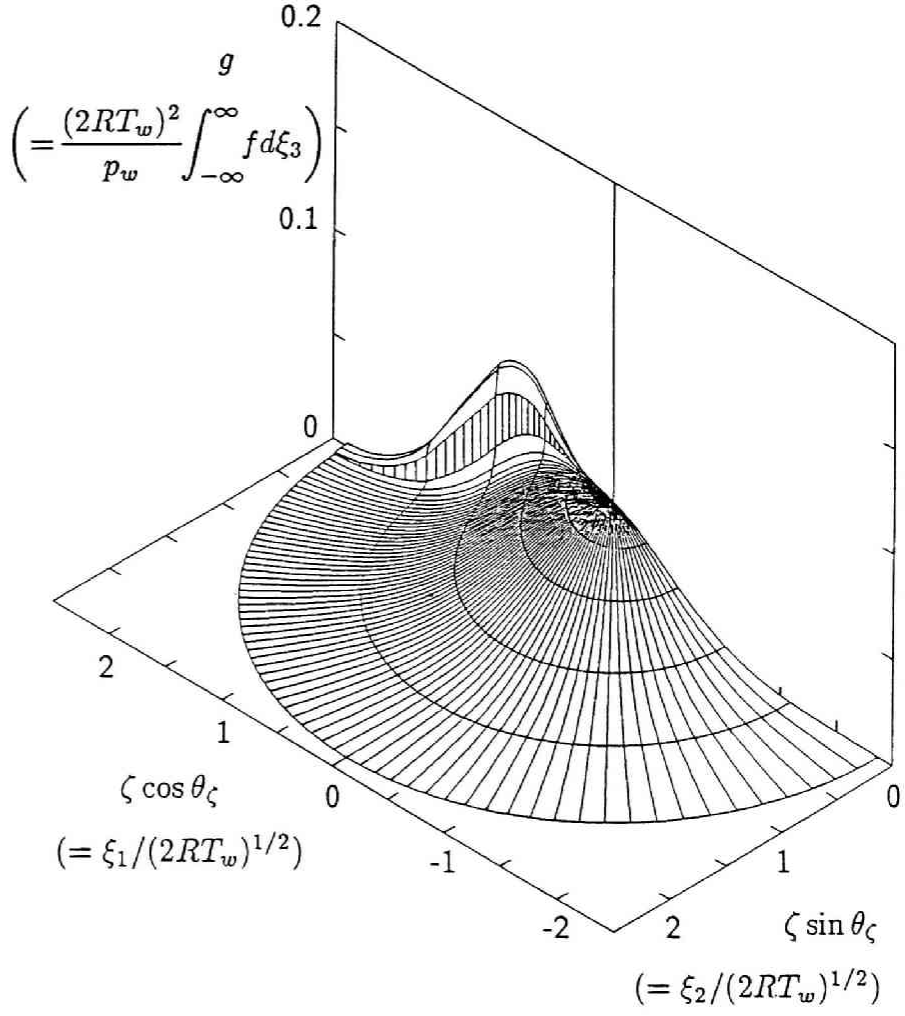

(d) $r/L = 19.98$

Fig. 3–21. (cont.)

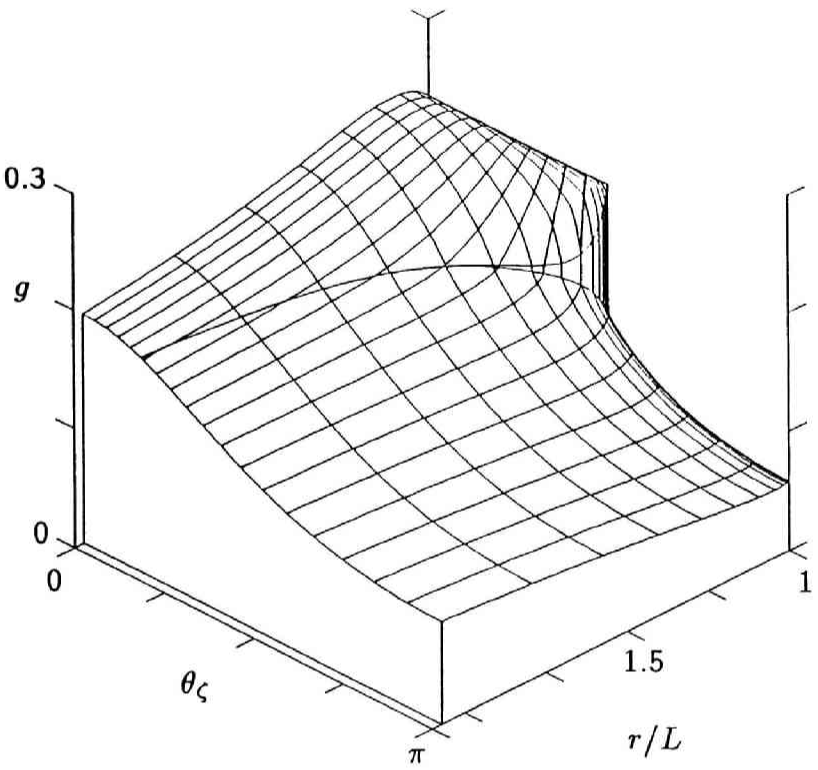

$\zeta = 1$

Fig. 3–22. The marginal velocity distribution function g at $\zeta = 1$ for $p_\infty/p_w = 0.5$ and $Kn_w = 0.1$. The surface g is shown by some (not all) of the lattice lines r/L =const and θ_ζ =const. The vertical lines show the discontinuity of g.

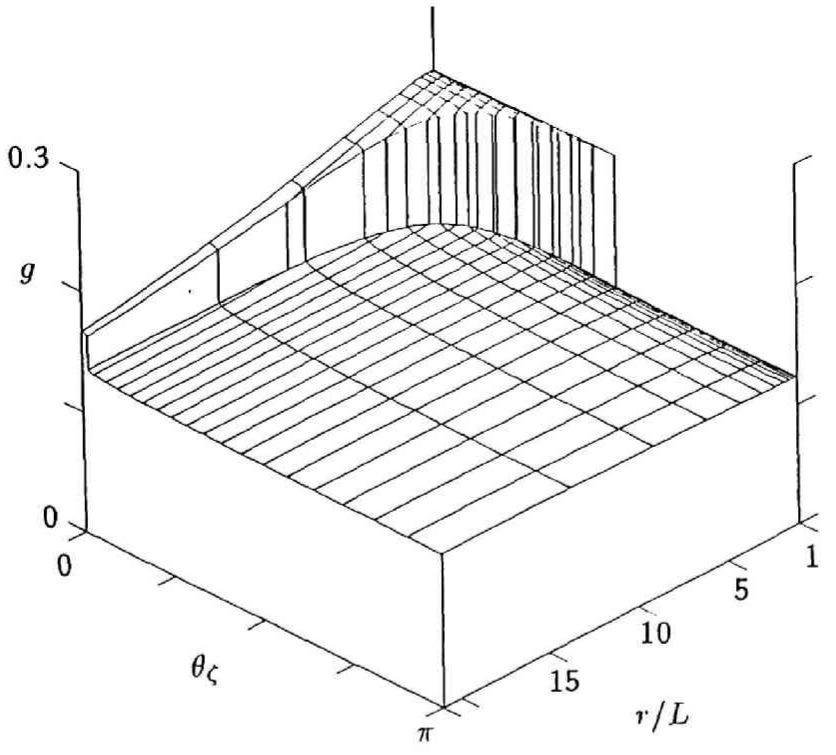

(a) $\zeta = 1$

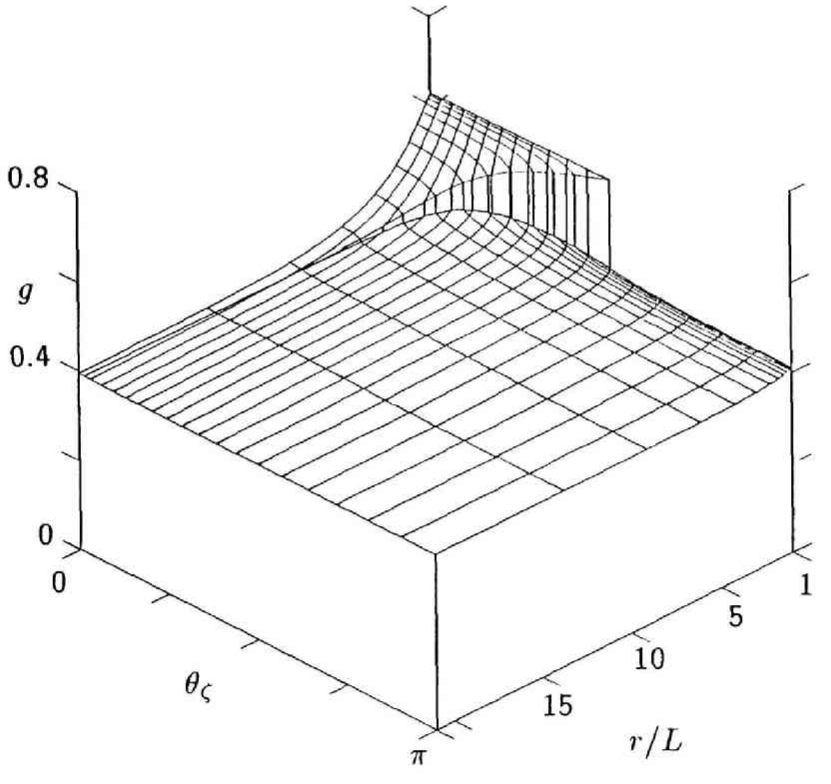

(b) $\zeta = 0.125$

Fig. 3–23. The marginal velocity distribution function g at $\zeta = 1$ and $\zeta = 0.125$ for $p_\infty/p_w = 0.5$ and $Kn_w = 10$. (a) $\zeta = 1$ and (b) $\zeta = 0.125$. (See the caption of Fig. 3–22.)

TABLES

Table 2–1 p_∞/p_w and T_∞/T_w versus M_∞ in the steady evaporation.

M_∞	p_∞/p_w	T_∞/T_w	M_∞	p_∞/p_w	T_∞/T_w
0.0000	1.0000	1.0000	0.5200	0.4050	0.8043
0.04999	0.9083	0.9798	0.5400	0.3927	0.7973
0.05998	0.8912	0.9758	0.5600	0.3809	0.7904
0.07998	0.8582	0.9679	0.5800	0.3695	0.7834
0.1000	0.8267	0.9599	0.6000	0.3586	0.7765
0.1200	0.7966	0.9521	0.6200	0.3481	0.7696
0.1400	0.7679	0.9443	0.6400	0.3380	0.7628
0.1600	0.7404	0.9365	0.6600	0.3283	0.7560
0.1800	0.7142	0.9288	0.6800	0.3189	0.7492
0.2000	0.6891	0.9212	0.7000	0.3099	0.7424
0.2200	0.6651	0.9136	0.7200	0.3012	0.7356
0.2400	0.6421	0.9060	0.7400	0.2928	0.7289
0.2600	0.6201	0.8985	0.7600	0.2848	0.7222
0.2800	0.5991	0.8910	0.7800	0.2770	0.7155
0.3000	0.5789	0.8835	0.8000	0.2695	0.7088
0.3200	0.5596	0.8761	0.8200	0.2622	0.7022
0.3400	0.5411	0.8688	0.8400	0.2553	0.6956
0.3600	0.5233	0.8615	0.8600	0.2485	0.6890
0.3800	0.5063	0.8542	0.8800	0.2420	0.6824
0.4000	0.4900	0.8470	0.9000	0.2358	0.6758
0.4200	0.4743	0.8398	0.9200	0.2297	0.6693
0.4400	0.4593	0.8326	0.9400	0.2239	0.6628
0.4600	0.4449	0.8255	0.9600	0.2182	0.6563
0.4800	0.4310	0.8184	0.9800	0.2128	0.6498
0.5000	0.4177	0.8113	0.9900	0.2101	0.6466

Table 3–1 The temperature ratio T_∞/T_w versus the pressure ratio p_∞/p_w for various Knudsen numbers.

	T_∞/T_w										
p_∞/p_w	$Kn_w = 0$[a]	0.01	0.02	0.05	0.1	0.2	0.5	1	2	5	10
0.90	0.9783	0.9784	0.9784	0.9783	0.9779	0.9773	0.9764	0.976	0.976	0.976	0.977
0.80	0.9552	0.9553	0.9554	0.9555	0.9552	0.9546	0.9535	0.953	0.954	0.954	0.955
0.70	0.9304	0.9306	0.9309	0.9313	0.9316	0.9316	0.9311	0.931	0.932	0.932	0.933
0.60	0.9038	0.9043	0.9049	0.9060	0.9069	0.9080	0.9091	0.910	0.911	0.911	0.913
0.50	0.8761	0.8769	0.8775	0.8793	0.8814	0.8842	0.887	0.889	0.890	0.891	0.893
0.45	0.8631	0.8637	0.8644	0.8662	–	–	–	–	–	–	–
0.40	0.8579	0.8525	0.8527	0.8541	0.8568	0.861	0.866	0.869	0.871	0.872	0.873
0.35	0.8579	0.8480	0.8447	0.8439	0.846	–	–	–	–	–	–
0.30	0.8579	0.8480	0.8431	0.8373	0.837	0.840	0.846	0.850	0.852	0.854	0.854
0.25	0.8579	0.848	0.843	0.835	0.831	0.831	0.837	–	–	–	–
0.20	0.8579	0.848	0.843	0.835	0.828	0.825	0.829	0.832	0.834	0.835	0.835
0.15	0.8579	0.848	0.843	0.835	0.827	–	–	–	–	–	–
0.10	0.8579	0.848	0.843	0.835	0.826	0.819	0.816	0.816	0.817	0.817	0.818
0.05	0.8579	0.848	0.843	0.835	0.826	0.819	0.812	0.809	0.809	0.810	0.809

[a] The data for $Kn_w = 0$ are taken from Eqs. (3–45a), (3–45b) and (3–46a).

Table 3–2 The nondimensional mass flow rate $Q/2\pi\rho_w(2RT_w)^{1/2}L$ from the cylinder versus the pressure ratio p_∞/p_w for various Knudsen numbers.

	$Q/2\pi\rho_w(2RT_w)^{1/2}L$										
p_∞/p_w	Kn_w =0[a]	0.01	0.02	0.05	0.1	0.2	0.5	1	2	5	10
0.90	0.0466	0.0463	0.0461	0.0453	0.0442	0.0421	0.0380	0.035	0.031	0.029	0.027
0.80	0.0922	0.0917	0.0912	0.0897	0.0874	0.0833	0.0753	0.069	0.063	0.058	0.055
0.70	0.1364	0.1357	0.1349	0.1326	0.1290	0.1231	0.1116	0.102	0.094	0.087	0.083
0.60	0.1780	0.1772	0.1763	0.1733	0.1685	0.1608	0.1465	0.135	0.125	0.116	0.112
0.50	0.2152	0.2141	0.2130	0.2096	0.2044	0.1956	0.179	0.166	0.156	0.145	0.140
0.45	0.2305	0.2297	0.2288	0.2256	–	–	–	–	–	–	–
0.40	0.2361	0.2416	0.2415	0.2394	0.2346	0.226	0.209	0.196	0.185	0.174	0.169
0.35	0.2361	0.2463	0.2493	0.2498	0.247	–	–	–	–	–	–
0.30	0.2361	0.2464	0.2509	0.2560	0.256	0.250	0.236	0.224	0.213	0.203	0.198
0.25	0.2361	0.2464	0.2510	0.258	0.261	0.259	0.247	–	–	–	–
0.20	0.2361	0.2464	0.2510	0.259	0.264	0.265	0.257	0.248	0.239	0.231	0.227
0.15	0.2361	0.246	0.251	0.259	0.265	–	–	–	–	–	–
0.10	0.2361	0.246	0.251	0.259	0.265	0.270	0.271	0.268	0.262	0.257	0.255
0.05	0.2361	0.246	0.251	0.259	0.265	0.270	0.276	0.275	0.272	0.270	0.269

[a] The data for $Kn_w = 0$ are taken from Eqs. (3–45a), (3–45d) and (3–46c).

Table 3–3 The nondimensional energy flow rate $W/2\pi p_w(2RT_w)^{1/2}L$ from the cylinder versus the pressure ratio p_∞/p_w for various Knudsen numbers.

	$W/2\pi p_w(2RT_w)^{1/2}L$										
p_∞/p_w	Kn_w =0[a]	0.01	0.02	0.05	0.1	0.2	0.5	1	2	5	10
0.90	0.1140	0.1133	0.1127	0.1109	0.1080	0.1029	0.0928	0.084	0.077	0.070	0.067
0.80	0.2202	0.2190	0.2178	0.2143	0.2086	0.1988	0.1796	0.164	0.150	0.138	0.132
0.70	0.3172	0.3156	0.3138	0.3086	0.3005	0.2866	0.2598	0.238	0.220	0.203	0.195
0.60	0.4023	0.4005	0.3986	0.3924	0.3819	0.3651	0.3329	0.307	0.285	0.265	0.255
0.50	0.4714	0.4693	0.4672	0.4608	0.4503	0.4324	0.398	0.370	0.346	0.324	0.314
0.45	0.4972	0.4959	0.4943	0.4886	–	–	–	–	–	–	–
0.40	0.5065	0.5149	0.5147	0.5111	0.5025	0.487	0.454	0.426	0.403	0.379	0.369
0.35	0.5065	0.5221	0.5265	0.5270	0.521	–	–	–	–	–	–
0.30	0.5065	0.5222	0.5289	0.5358	0.535	0.525	0.499	0.475	0.453	0.433	0.423
0.25	0.5065	0.5222	0.5289	0.539	0.543	0.538	0.516	–	–	–	–
0.20	0.5065	0.5222	0.5290	0.540	0.547	0.547	0.533	0.515	0.499	0.483	0.474
0.15	0.5065	0.522	0.529	0.540	0.548	–	–	–	–	–	–
0.10	0.5065	0.522	0.529	0.541	0.548	0.553	0.553	0.546	0.535	0.526	0.523
0.05	0.5065	0.522	0.529	0.542	0.547	0.553	0.559	0.556	0.551	0.547	0.544

[a] The data for $Kn_w = 0$ are taken from Eqs. (3–45a), (3–45e) and (3–46d).

Table 3–4 Examples of the lattice of $\tilde{r}$.

$(Kn_w, p_\infty/p_w)$	(0.01, 0.05)		(0.1, 0.4)		(10, 0.05)	
i	$\tilde{r}^{(i)}$	$d\tilde{r}/di$	$\tilde{r}^{(i)}$	$d\tilde{r}/di$	$\tilde{r}^{(i)}$	$d\tilde{r}/di$
0	1	5×10^{-8}	1	5×10^{-6}	1	7.29×10^{-3}
10	1.0006	3.73×10^{-4}	1.00009	1.36×10^{-5}	1.12	0.0185
50	1.067	3.86×10^{-3}	1.007	6.90×10^{-4}	9.05	0.743
100	1.93	0.0466	1.27	0.0117	351	16.7
144	9.13	0.389	–	–	–	–
176	12.0	0.0325	–	–	–	–
200	13.0	0.0902	6.43	0.139	11800	160
210	17.4	0.755	–	–	–	–
230	40.4	1.63	–	–	–	–
236	51.2 $(=\tilde{r}_D)$	1.97	–	–	–	–
250			–	–	19800 $(=\tilde{r}_D)$	160
252			20.7 $(=\tilde{r}_D)$	0.475		

Table 3–5 Examples of the outer limit $\tilde{r}_D$ of the numerical computation.

Kn_w	p_∞/p_w =0.1	0.2	0.4	0.6	0.8
0.01	20	10	10	5	2.5
0.1	100	50	20	10	5
1	200	100	50	50	50
10	10000	2000	2000	1000	1000

Table 3-6 Examples of $(K,\ \hat{K})$

Kn_w	p_∞/p_w =0.1	0.2	0.6	0.8
0.01	96, 48	96, 48	96, 48	96, 48
0.1	144, 96	96, 48	72, 48	72, 48
1	144, 96	144, 96	96, 48	72, 48
10	240, 192	240, 192	144, 96	144, 96